RZESZOW UNIVERSITY OF TECHNOLOGY

Łukasiewicz
Warsaw Institute of Technology

CONTENTS

COMPARISON OF ASSEMBLY HOLES QUALITY AFTER DRILLING AND HELICAL MILLING OF THE AL/CFRP STACKS

PORÓWNANIE JAKOŚCI OTWORÓW MONTAŻOWYCH PO WIERCENIU I FREZOWANIU SPIRALNYM KONSTRUKCJI PRZEKŁADKOWEJ TYPU AL/CFRP

Elżbieta DOLUK[1] (iD)

[1] Department of Production Computerisation and Robotisation, Faculty of Mechanical Engineering, Lublin University of Technology, Nadbystrzycka 36, 20-618 Lublin, Poland

* Corresponding author: e.doluk@pollub.pl, tel.: (+48 507 666 485)

Abstract

Hybrid sandwich structures composed of aluminium alloys and CFRP (Carbon Fibre Reinforced Polymer) are now frequently used in the aerospace industry. One of the factors inhibiting their application is the difficult processing resulting from the anisotropic nature of this type of construction. These materials are often joined by screws or rivets requiring mounting holes. One of the main problems is ensuring the quality of the holes after machining. The aim of this study is to assess the hole quality (dimensional and shape accuracy) and the occurrence of delamination after machining of a Al 2024/CFRP sandwich structure. In this experiment drilling and helical milling results were compared. A traditional HSS twist drill and a PCD milling cuter with a straight cut were used. The machining was carried out with a variable cutting speed. The tests were performed for two strategy of the machining – Al/CFRP (Al 2024 T3 – Carbon Fibre Reinforced Polymer) and CFRP/Al (Carbon Fibre Reinforced Polymer – Al 2024 T3).

Keywords: Al/CFRP stacks, drilling, helical milling, hole quality

Streszczenie

Hybrydowe konstrukcje przekładkowe składające się ze stopów aluminium i kompozytów epoksydowo-węglowych (CFRP) są obecnie często stosowane w przemyśle lotniczym. Jednym z czynników hamujących ich zastosowanie jest trudna obróbka wynikająca z dużej anizotropowości tego typu materiałów. Konstrukcje te są często łączone za pomocą połączeń śrubowych lub nitowych wymagających otworów montażowych. Jednym z głównych problemów jest zapewnienie jakości otworów po obróbce. Celem artykułu jest ocena jakości otworów (dokładności wymiarowo-kształtowej) oraz występowania delaminacji po obróbce konstrukcji przekładkowej Al 2024/CFRP. W eksperymencie porównano wyniki wiercenia i frezowania spiralnego. Zastosowano tradycyjne wiertło kręte wykonane ze stali szybkotnącej oraz frez węglikowy o prostych zębach pokrytych powłoką diamentową (PKD). Obróbka została przeprowadzona ze zmienną prędkością skrawania. Testy przeprowadzono dla dwóch strategii obróbki – Al/CFRP (stop aluminium/kompozyt epoksydowo-węglowy) i CFRP/Al (kompozyt epoksydowo-węglowy/stop aluminium).

Słowa kluczowe: konstrukcja przekładkowa Al/CFRP, wiercenie, frezowania spiralne, jakość otworów

1. Introduction

The constant search for lighter constructions and faster means of transport led to dynamic technological developments. The search began for engineering materials that could meet the demands placed on them.

Efforts have been made to develop a construction with adequate strength properties, while at the same time allowing the weight of the construction to be reduced. One such material is a sandwich structure.

One of the increasingly used constructions is a combination of metal alloys and fibre composites,

especially CFRPs (Carbon Fibre Reinforced Polymers). Unlike metallic materials, CFRP is a heterogeneous material consisting of two phases: matrix and reinforcement. These phases have different structures and arrangements (Leprete et al., 2018). Such a structure leads to the occurrence of many post-process defects (e.g. delamination, debonding) and a different directionality of the material and surface roughness than after metal machining (Doluk & Rudawska, 2022; Karataş & Gökkaya, 2018) The combination of aluminium alloys and CFRPs enables the creation of a construction with less weight, high strength and corrosion resistance compared to an equivalent solid construction made of metal. These and other advantages of hybrid sandwich structures have contributed to their frequent use in the aerospace industry (Hegde et al., 2019). Machining of Al/CFRP structures presents even more difficulties than machining CFRP. The tool simultaneously machines materials with significantly different properties and different machinability. This results in rapid wear of the cutting tool and problems in achieving the desired machined surface quality (Poutord et al., 2013; Doluk et al., 2022). One way of joining sandwich structures is through the use of mechanical connections. In most cases, these require assembly holes, which are usually made in a drilling process. Nowadays, in order to increase the efficiency of the assembly and machining process, the aim is to make these holes in a single process operation desirable to obtain holes with the highest possible dimensional and shape accuracy. Surface quality is one of the determinants of accuracy and verification of manufacturing performance. Machining performance is closely related to the proper planning and management of the production system, including the appropriate selection of machining conditions (Kuczmaszewski et al., 2019; Matuszak et al., 2022; Gola, 2018). The determination of cutting conditions for highly anisotropic materials, which include Al/CFRP stacks, is extremely important from the point of view of reducing assembly errors, production time, as well as joint aesthetics.

Many of the problems encountered in the machining of hybrid sandwich structures are due to improperly selected machining conditions (Caggiano, 2018; Fleischer et al., 2018). In (Angelone et al., 2019) the influence of spindle speed (n = 300 – 6000 rpm) and feed rate (f = 0.05 – 0.15 mm/rev) on the damages of a hole diameter after drilling with two-flute twist drills (WC) was studied. The temperature in the cutting zone was also recorded. The results showed that using a feed rate of f = 0.15 mm/rev and spindle speed of n = 4500 rpm produced the highest hole quality. The use of lower values led to less dimensional parameters (roundness, delamination, smoothness). Zitoune et al.,

2010, studied the influence of drill diameter and cutting conditions on hole quality, thus force, torque and circularity after machining. They presented the appearance of chips depending on the cutting parameters adopted. They noted that better results were obtained for lower drill diameters (< 6 mm). They showed that drill diameter and feed rate have the highest influence on the chip formation mechanism. In (Zitoune et al., 2016) the effect of cutting parameters during drilling with a traditional twist drill and a double cone drill was evaluated. Cutting forces, hole accuracy and CFRP/Al interface were recorded. It was noted that the double cone drill produced lower thus force values than the traditional twist drill. In (Shyha et al., 2011) an experiment was performed to determine the effect of cutting tool type (uncoated and coated drill) on burr height, delamination, hole edge and roughness after drilling in the Ti/CFRP/Al stacks. The entry and exit zones of cutting tool were investigated after flood cutting fluid and mist-spray. It was shown that the cutting environment had a highest effect on hole quality than the type of tool used. Bunting & Bunting, 2020, presented the influence of drill type (PCD drill vs. WC drill) and cutting parameters on hole drilling performance in the CFRP/Ti stacks. The cutting force values, dimensional and shape hole accuracy and burr height obtained with the drills analysed were compared. It was found that the use of a PCD drill increased the efficiency of the process due to the possibility of increasing the depth of cut. In addition, the holes made with the PCD drill had higher dimensional and shape accuracy. In (Torres et al., 2009) a prototype drill bit for drilling holes in carbon fibre/epoxy laminates was proposed. It was also shown that the use of a low cutting speed (v_c = 53 m/min) and a low feed rate (f = 0.025 mm/rev) could counteract excessive delamination of the tested material during machining. In the paper (Ciecieląg & Zaleski, 2022) the influence of material stiffness on cutting force and surface roughness after the milling of three types of materials: aluminium alloy, titanium alloy and CFRP was studied. It was shown that the investigated parameters of hole surface quality are influenced not only by the stiffness of the component, but also by their different properties (Young's modulus). In (Ciecieląg, 2023) the influence of cutting tool type on the cutting force and deformation of thin-walled components made of fibre composites (CFRP and GFRP) after the milling process was determined. It was shown that low feed rates should be used when machining thin-walled fibre composites, as this allows the lowest value of permanent deformation to be obtained.

Much research to date has focused on drilling holes in sandwich structures (Ciecieląg, 2023; Ahn et

al., 2023; Wang et al., 2020; Kuoa & Sooa, 2014; An et al., 2020). However, most of these focus on drilling holes using specialised drills or those designed to machine one of the materials forming the sandwich structure (usually to a material with poorer machinability). There is a lack of studies focusing on the potential use and effectiveness of helix milling when machining holes in this type of material.

The aim of this study was to compare the holes quality (dimensional and shape accuracy) machined with a traditional uncoated twist drill and a straight-blade PCD cutter. An additional objective was to determine the influence of machining strategy (sample orientation during process) and cutting speed on the holes quality in the Al/CFRP stack.

2. Materials and methods

In this study a II-layered sandwich structure consisting of metal and composite was used. The research object was formed from Al 2024-T3 (Al) (EN 515:2017) and CFRP (Carbon Fibre Reinforced Plastics). Both materials were chosen because of their frequent use in aircraft constructions (Hegde et al., 2019; Labidi, 2020). The main properties of the alloy are presented in Table 1.

Table 1. Properties of 2024-T3 aluminum alloy

Density	2.78 g/cm^3
Young's Modulus	73 GPa
Tensile Yield Strength	345 MPa
Fatigue Strength	138 MPa

The content of the main alloying elements in the alloy is: Al 93.5%, Cu 4.5%, Mg 1.5%, Mn 0.5%. The composite material was composed of 20 unidirectional prepregs CM-Preg TI02/1000 manufactured by Mitsubishi Chemical Group (Heinsberg, Germany). The plies sequence was [0/90]. The thickness of each layer was about 0.3 mm (epoxy tissue prepregs). The CFRP was made of CP006 epoxy matrix and high strength carbon fibres (about 60%). The laminate was fabricated by hand lay-up process and autoclave curing (for 60 minutes at 130°C under pressure of 0.4 MPa). The main properties of the composite material are: density 1.75 g/cm^3, Young's Modulus E = 135 GPa, Tensile Yield Strength 1900 MPa.

The materials forming the sandwich structure were bonded using a two-part epoxy adhesive 3M DP460 (3M, Minnesota, USA) with a 2:1 mix ratio. The adhesive exhibits high peel and shear strength, which is why it has found applications in the aerospace industry. The adhesive composition was applied evenly to both surfaces to be joined using an applicator. The thickness of the adhesive was approximately 0.1 mm. Polymerisation process was carried out in vacuum bag at a pressure of 0.1 MPa for 24 hours. The samples were seasoned for 7 days under ambient conditions (at 23°C and approximately 35% humidity). Fig. 1 shows a schematic of the sample after the bonding process.
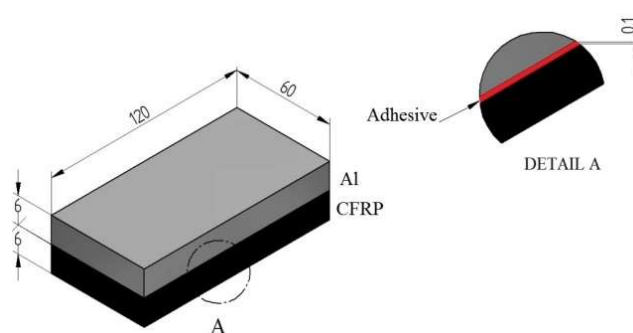
Fig. 1. Geometry and dimensions of the sample

The drilling and helical milling processes were performed on a CNC FV-580A vertical machining centre (AVIA, Warsaw, Poland). A schematic representation of the drilling and milling processes, including the location of the holes on the sample, is shown in Fig. 2. The drilling and milling tests were conducted on 6 consecutive holes with different cutting speed (3 holes after drilling and 3 holes after milling – Fig. 2b). The drilling and milling processes were carried out three times for each machining variant. Experiment was performed without coolant.

Two tools were used in the experiment. The first tool is a traditional twist drill made of HSS steel with a point angle 135° (Hoffman Group, Munich, Germany). The second one is a two-blade diamond (PCD) milling cutter with a straight cut (Hoffman Group, Munich, Germany). The shape and detailed dimensions of the tools are presented in Fig. 3.

The experiment also investigated the effect of cutting speed on the holes quality after machining. Three cutting speeds were selected for each of the two tools. As the tools used differed in geometry and material, different cutting speeds were selected for each tool. Table 1 summarises the values of the v_c parameter, depending on the machining process.
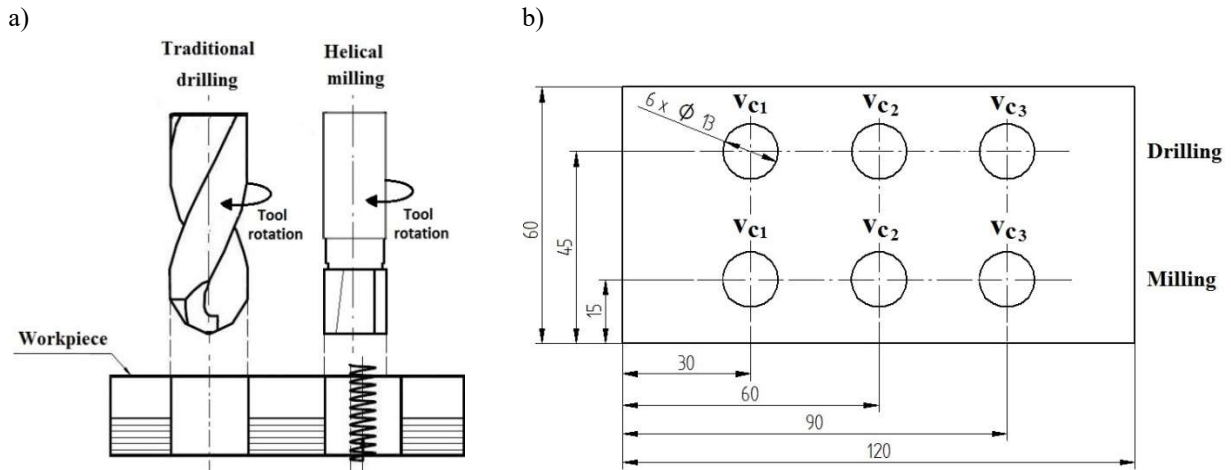
a)   b)

Fig. 2. Experimental setup: a) scheme of traditional drilling and helical milling, b) location of the holes on the sample

a)   b)
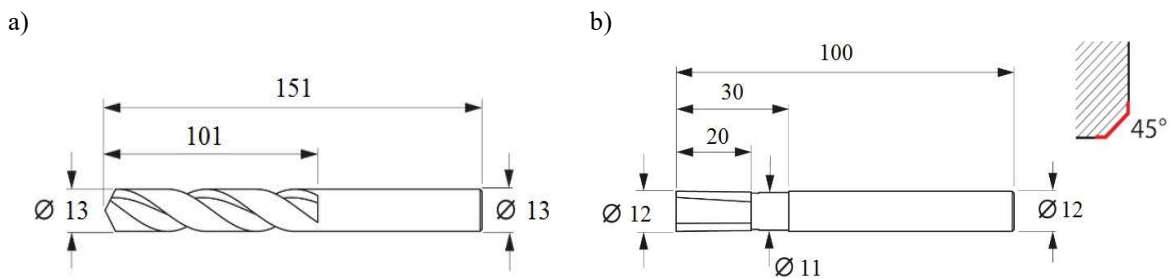

Fig. 3. The tools used in the experiment: a) HSS twist drill, b) PCD milling cutter (Hoffman Group Catalogue)

For the drilling process, a cutting speed in the range of $v_c = 80 – 320$ m/min was initially assumed (Table 2 pre-testing). However, due to the un-acceptable quality of the holes (flow of the metal material in the drill entry zone – Fig. 4), the values of the v_c parameter were reduced after the process was carried out assuming these values (Table 2 – main test).

Table 2. Values of the v_c parameter depending on the type of the process

| No. | Drilling | | Milling |
	Pre-testing	Main test	
1	$v_c = 80$ m/min	$v_c = 15$ m/min	$v_c = 350$ m/min
2	$v_c = 160$ m/min	$v_c = 30$ m/min	$v_c = 425$ m/min
3	$v_c = 320$ m/min	$v_c = 60$ m/min	$v_c = 500$ m/min

Fig. 4. Sample after drilling in the Al/CFRP strategy (pre-testing)

The cutting speed values used were selected based on the recommendations of the manufacturer of the tools used. The milling and drilling processes were carried out using a constant feed rate of $f_z = 0.09$ mm/blade and an axial depth of cut for milling $a_p = 12.9$ mm and for drilling $a_p = 6.5$ mm.

The third factor whose influence on the holes quality was investigated was the sample orientation during the cutting process. Two possibilities were considered:

- Al/CFRP strategy – the Al sheet on the top of the stack of the sandwich structure.
- CFRP/Al strategy – the CFRP sheet on the top of the stack of the sandwich structure.

The dimensional accuracy of the holes was defined by the arithmetic mean of the hole diameter D obtained after machining and the roundness factor F_R. This factor was expressed as:

$$F_R = \left| 1 - \frac{D}{D_N} \right| \qquad (1)$$

where:
F_R – roundness factor,
D – arithmetic mean of the hole diameter [mm],
D_N – nominal hole diameter [mm].

Both parameters were compared with the adopted target values. The value of the hole diameter D was

compared to the nominal hole diameter D_N (D_N = 13 mm), while the F_R factor was compared to 0. In both cases, values closer to the adopted ones indicated better dimensional hole accuracy. The hole diameters were measured using a Zeiss Accura II CMM (Oberkochen, Baden-Württemberg, Germany). Each of the obtained hole diameter values was the arithmetic mean of the three hole measurements.

During machining structures with very different properties, it may not be sufficient to compare the cutting effects solely by means of dimensional accuracy. It is also necessary to determine the condition of the hole edges. The shape accuracy of the holes was assessed visually with a Keyence VHX-500 digital microscope (Japan, Osaka) using a magnification of 500 times.

3. Results and discussion

Figs. 5 – 8 show the effect of the cutting speed and machining strategy on the hole quality in the tool entry and exit zone after the helical milling.

In the case of the milling process with the Al/CFRP strategy, all the actual hole diameters obtained were lower than the nominal diameter (D_N = 13 mm). The closest actual diameter value (D = 12.922 mm, F_R = 0.006) to the nominal diameter was obtained in the tool entry zone using the parameter v_c = 500 m/min. The hole with the lowest dimensional accuracy (D = 12.587 mm, F_R = 0.035) for this milling strategy was also obtained in the tool entry zone, but at the cutting speed of v_c = 350 m/min (Fig. 5 and Fig. 6).
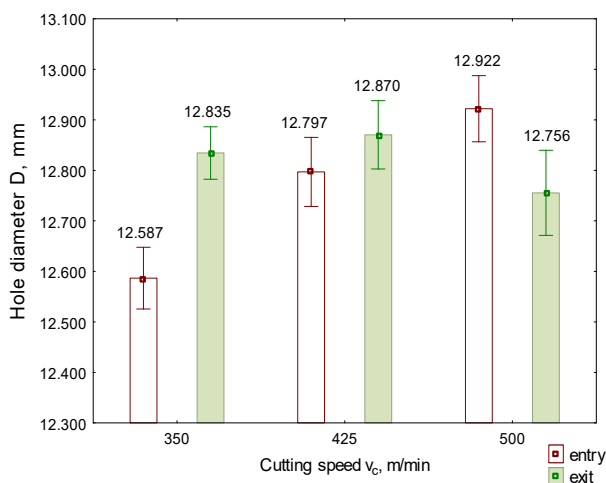

Fig. 5. Hole diameters for the Al/CFRP strategy after milling

It was observed that after the milling process using the Al/CFRP strategy, an increase in the v_c parameter resulted in an increase in the dimensional accuracy of the holes in the tool entry zone (lower F_R values). In the milling cuter exit zone, a similar trend was

observed for the first v_c parameters, but for the highest cutting speed (v_c = 500 m/min), a hole with a diameter least close to the nominal diameter was obtained in the tool exit zone. For the analysed milling strategy, holes with higher dimensional accuracy were obtained in the tool exit zone (composite material) in most of the cases considered. This was probably due to the stiffening effect of the metal layer above the composite material.
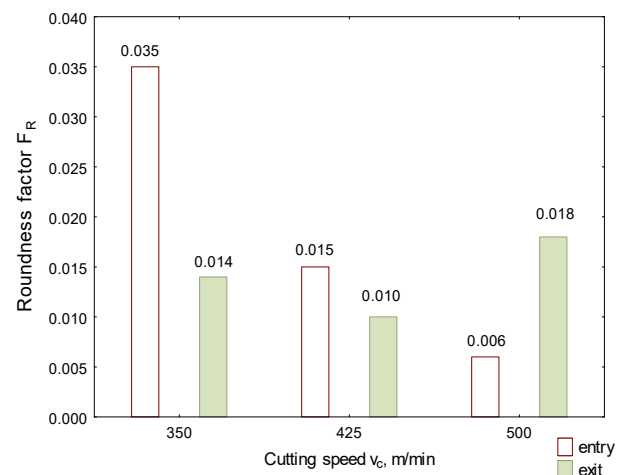
Fig. 6. Roundness factor F_R for the Al/CFRP strategy after milling

Milling with the CFRP/Al strategy produced the highest dimensional accuracy (D = 12.844 mm, F_R = 0.012) in the tool exit zone after using v_c = 500 m/min. Similarly to the Al/CFRP strategy, the lowest dimensional accuracy (D = 13.853 mm, F_R = 0.066) was obtained in the tool entry zone for a cutting speed of v_c = 350 m/min (Fig. 7 and Fig. 8). Increasing the cutting speed resulted in a decrease in the hole quality in the tool entry and exit zones.

Fig. 7. Hole diameters for the CFRP/Al strategy after milling

Comparing the results shown in Fig. 8 it can be observed that for all the cutting speeds considered,

lower F_R values were obtained in the cutting tool exit zone (metal layer). This is due to the better machinability of the aluminium alloy compared to the CFRP (Karataş & Gökkaya, 2018).
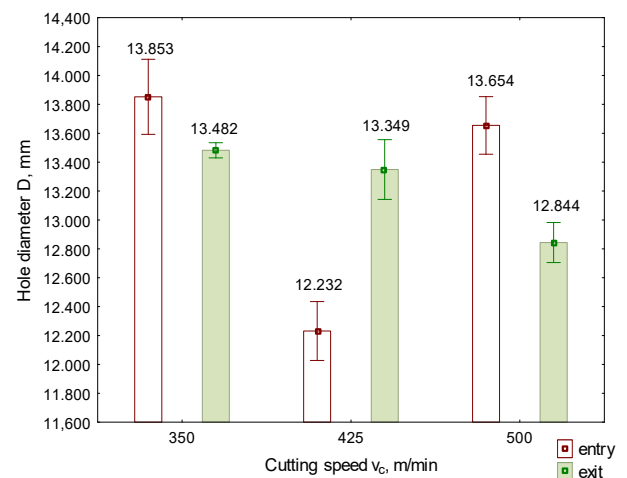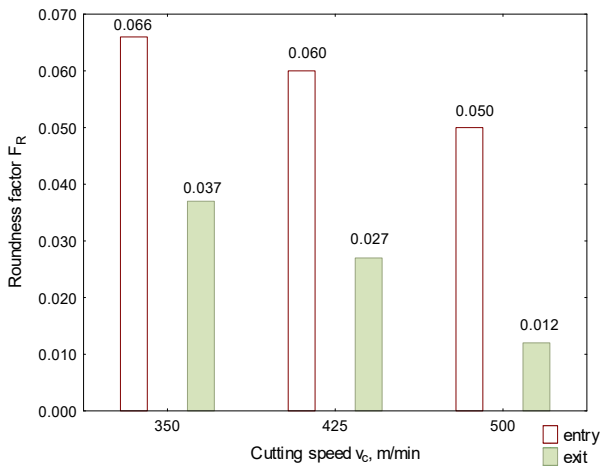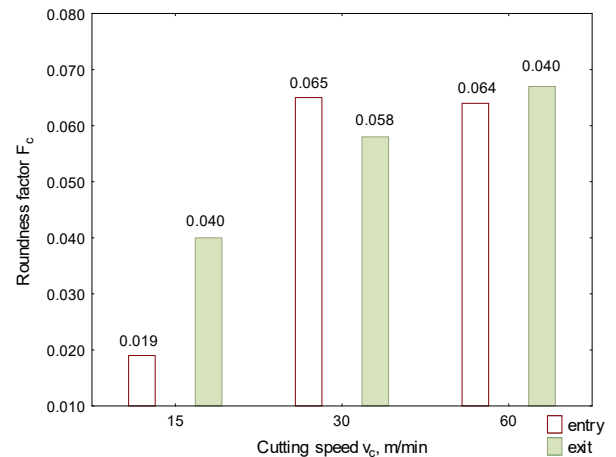

Fig. 8. Roundness factor F_R for the CFRP/Al strategy after milling

After the drilling process using the Al/CFRP strategy, the hole diameter closest to the nominal diameter (D = 13.241 mm, F_R = 0.019) was obtained in the tool entry zone using v_c = 15 m/min (Fig. 9). The hole with the lowest dimensional accuracy for this machining strategy (D = 12.127 mm, F_R = 0.067) was obtained in the tool exit zone after drilling with a cutting speed of v_c = 60 m/min (Fig. 9 and Fig. 10). For all cutting speeds considered in this case, holes with diameters lower than the nominal value were obtained in the drill exit zone. This is due to the presence of numerous defects in the composite layer in the tool exit zone, mainly in the form of undercut, pulled-out carbon fibres, which reduced the measuring area of the CMM.
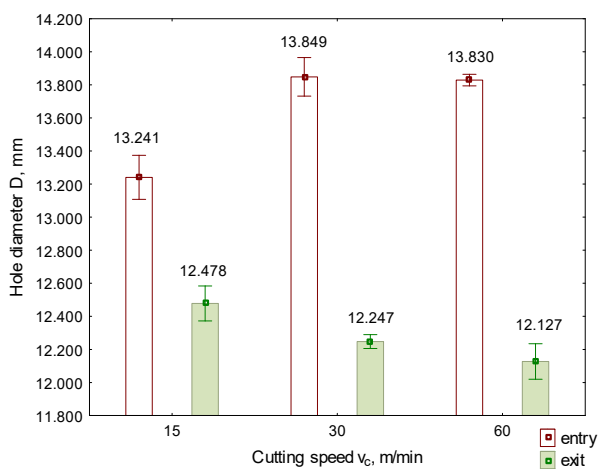
Smaller F_R values were obtained in the tool entry zone for most of the variables considered, indicating higher dimensional accuracy of the holes. The exception was a hole machined at a cutting speed of v_c = 30 m/min, where a lower F_R index value was obtained in the tool exit zone. In most cases, an increase in the v_c parameter resulted in an increase in the F_R value and thus a decrease in the dimensional accuracy of the holes (Fig. 10).

Fig. 10. Roundness factor F_R for the Al/CFRP strategy after drilling

When drilling the holes using the CFRP/Al strategy, the hole with the closest hole diameter (D = 13.160 mm, F_R = 0.012) to the nominal diameter was obtained in the tool entry zone using v_c = 15 m/min (Fig. 11). The hole with the lowest dimensional accuracy for this machining strategy (D = 13.720 mm, F_R = 0.055) was also observed in the drill entry zone when a cutting speed of v_c = 60 m/min was applied (Fig. 11 and Fig. 12). Increasing the v_c parameter resulted in breaking up the holes and reducing their dimensional accuracy (Hoffman Group Catalogue).

Fig. 9. Hole diameters for the Al/CFRP strategy after drilling
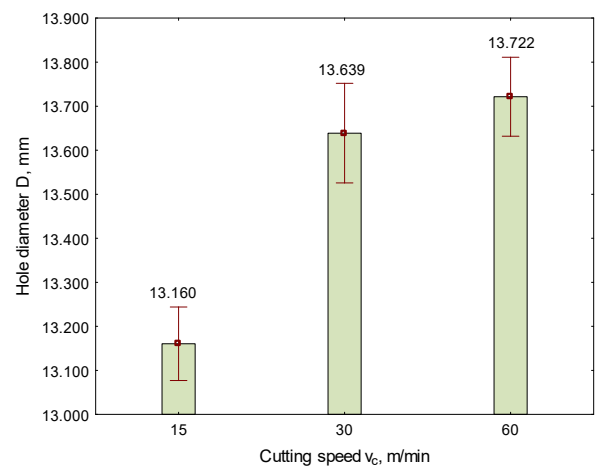
Fig. 11. Hole diameters in the tool entry zone for the CFRP/Al strategy after drilling
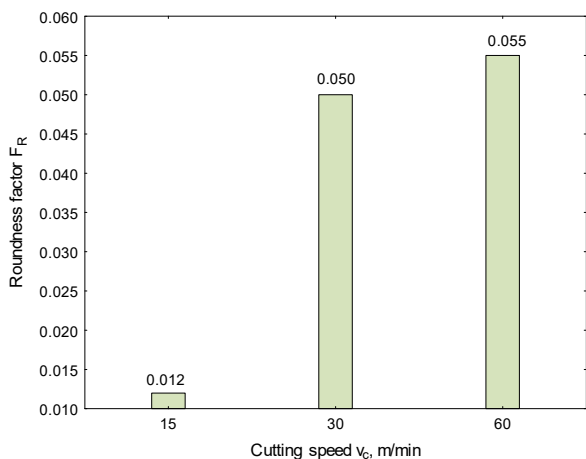
Fig. 12. Roundness factor F_R in the tool entry zone
for the CFRP/Al strategy after drilling

For the CFRP/Al strategy, it was not possible to measure the hole diameter in the tool exit zone – the cutting tool did not punch the bottom of the hole for any of the adopted cutting speeds. The metal layer beneath the composite material underwent plastic deformation in the drill exit zone. The aluminium alloy was pressed deep into the hole, resulting in deformation of the metal and delamination of the entire structure (Fig. 13).
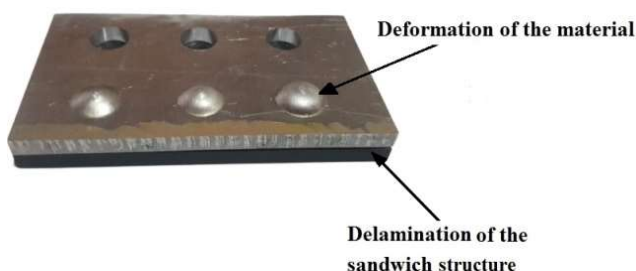

Fig. 13. Exit of the holes after drilling in the CFRP/Al strategy

Analysing the influence of the machining strategy on the machining effects, it can be seen that, for the milling process, the Al/CFRP strategy allowed a higher dimensional accuracy of the holes in the tool entry and exit zones. This is due to the stiffening effect of the metal layer, which increased the stability of the machining. In the case of drilling in the tool entry zone, higher dimensional accuracy was obtained when the CFRP/Al strategy was used. Similar conclusions were reached in (Zitoune et al., 2016; Isbilir and Ghassemieh, 2013). It was observed that the use of the CFRP/Al drilling strategy delays the delamination of the composite material.

In order to determine the influence of the investigated independent variables (cutting speed v_c and strategy of the machining S) on the hole quality in the tool entry and exit zones (hole diameter D) after the milling and drilling processes an analysis of variance (ANOVA) was carried out (Table 3 and Table 4).

Table 3. Two-factor analysis of variance for the milling process

Impact	Entry				
	SS	DF	MS	F	*p*-value
v_c: cutting speed	4.41	2	2.20	271.31	< 0.01
S: strategy	2.05	1	2.05	252.77	< 0.01
v_c x S interaction	5.32	2	2.66	327.82	< 0.01
Error	0.24	30	0.01		
Total	12.02	35			
Impact	Exit				
	SS	DF	MS	F	*p*-value
v_c: cutting speed	0.91	2	0.45	93.30	< 0.01
S: strategy	1.47	1	1.47	302.84	< 0.01
v_c x S interaction	0.49	2	0.25	50.71	< 0.01
Error	0.15	30	0.01		
Total	3.02	35			

For the tool entry and exit zones after milling process all independent variables and their interaction had a significant effect on the dependent variable (Table 3). The $v_c \times S$ interaction had the highest effect ($F_{1,5} = 327.82$; *p*-value < 0.01) on the hole diameter values in the milling cutter entry zone. For the tool exit zone the highest influence on the dependent variable were the strategy of the machining ($F_{1,5} = 302.84$; *p*-value < 0.01), cutting speed ($F_{1,5} = 93.30$; *p*-value < 0.01) and $v_c \times S$ interaction ($F_{1,5} = 50.71$; *p*-value < 0.01), respectively.

Table 4. Analysis of variance for the drilling process

Impact	Entry				
	SS	DF	MS	F	*p*-value
v_c: cutting speed	2.35	2	1.17	115.63	< 0.01
S: strategy	0.15	1	0.15	15.14	< 0.01
v_c x S interaction	0.03	2	0.01	1.34	0.28
Error	0.29	30	0.1		
Total	2.82	35			
Impact	Exit				
	SS	DF	MS	F	*p*-value
v_c: cutting speed	0.38	2	0.19	23.52	< 0.01
Error	0.15	15	0.01		
Total	0.50	17			

The results of the analysis of variance carried out for the holes obtained after the drilling process are shown in Table 4. Based on the results obtained for the tool entry zone, it can be seen that the v_c x S inter-

action ($F_{1,5}$ = 1.34; *p*-value = 0.28) did not affect the dependent variable. The most significant influence on hole quality in this case was the cutting speed ($F_{1,5}$ = 115.63; *p*-value < 0.01). The strategy of the machining affected hole quality less than cutting speed ($F_{1,5}$ = 15.14; *p*-value < 0.01). As no holes were created at the drill exit zone using the CFRP/Al strategy, a one-way ANOVA was performed for the results obtained at the tool exit zone after drilling, where the independent variable was the cutting speed (with the Al/CFRP strategy of the machining held constant). In this case, the cutting speed had a significant effect on the dependent variable ($F_{1,2}$ = 23.52; *p*-value < 0.01).

Fig. 14 and Fig. 15 show selected images of the holes in the tool entry and exit zones after milling process.

For the cutting speeds and machining strategies considered, similar hole edge conditions were obtained in the tool entry and exit zones. However, in the me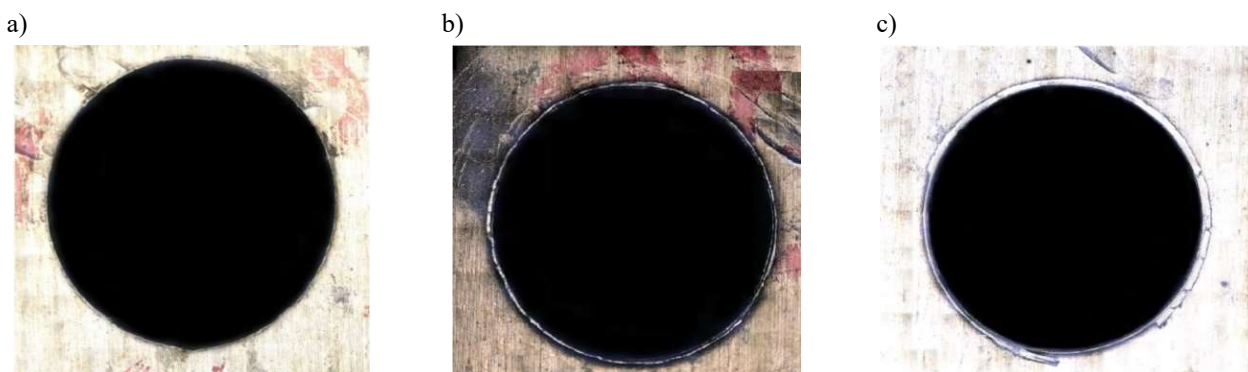tal layer, a more pronounced outline of the holes can be observed than in the composite layer (Fig. 14a and Fig. 15b). In the composite material, single, undercut fibres can be seen, as well as some metal chip inclusions and matrix defects (Fig. 14b and Fig. 15a). However, these defects should not adversely affect future assembly operations.

a)   b)
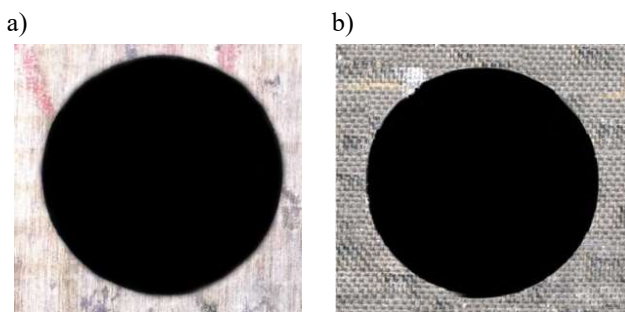
Fig. 14. Holes after milling with the Al/CFRP strategy and the cutting speed v_c = 350 m/min: a) tool entry zone, b) tool exit zone

a)   b)

Fig. 15. Holes after milling with the CFRP/Al strategy and the cutting speed v_c = 350 m/min: a) tool entry zone, b) tool exit zone

For the cutting speeds and machining strategies considered, similar hole edge conditions were obtained in the tool entry and exit zones. However, in the metal layer, a more pronounced outline of the holes can be observed than in the composite layer (Fig. 14a and Fig. 15b). In the composite material, single, undercut fibres can be seen, as well as some metal chip inclusions and matrix defects (Fig. 14b and Fig. 15a). However, these defects should not adversely affect future assembly operations.
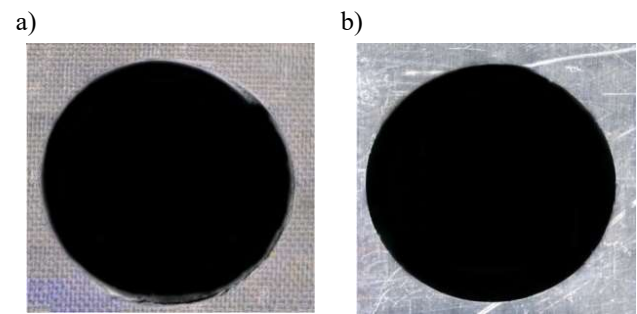
Fig. 16 and Fig. 17 show a comparison of the holes in the tool entry and exit zone after the drilling process using the Al/CFRP strategy. In the drill entry zone (metal layer), when the lowest value of the parameter v_c is used (v_c = 15 m/min), a similar hole condition can be observed as after the milling process. However, as the cutting speed increases, the material plasticises and settles on the edges of the holes (Fig. 16b and Fig. 16c). Increasing the cutting speed causes an increase in cutting temperature, resulting in a chemical reaction between the drill material and the aluminium alloy being machined. This causes build-up at the edge of the hole (Zitoune et al., 2016).

a)   b)   c)

Fig. 16. Tool entry zone after drilling with the Al/CFRP strategy and cutting speeds: a) v_c = 15 m/min, b) v_c = 30 m/min, c) v_c = 60 m/min

In the drill exit zone (composite layer), a decrease in hole diameter can be observed with an increase in

the v_c parameter (Fig. 17). Numerous defects can be seen on the surface of the CFRP: pulled and under-

cut fibres, matrix chipping and delamination. The occurrence of these defects intensifies as the v_c parameter increases (Angelone et al., 2019). The condition of the machined holes would make it very difficult or impossible to make the joint. The resulting holes require additional finishing operations. Moreover, delamination of the entire sandwich structure was also observed at the layer boundary.

The images (Fig. 16 and Fig. 17) show that for such strongly anisotropic structures as the Al/CFRP stacks, the dimensional and shape accuracy of the holes should not be considered separately. Fig. 17 does not present the same hole quality as the results in Fig. 9 and Fig. 10.

a)   b)   c)
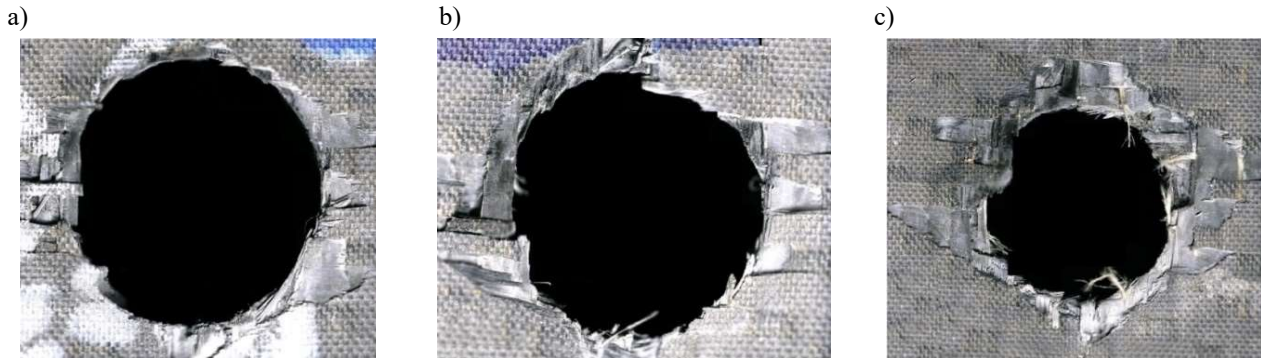
Fig. 17. Tool exit zone after drilling with the Al/CFRP strategy and cutting speeds: a) v_c = 15 m/min, b) v_c = 30 m/min, c) v_c = 60 m/min

This shows that determining the quality of holes machined in this type of structure also requires consideration of the condition of the hole edges and damage to the composite material in the cutting tool entry and exit zone.

4. Conclusions

The following conclusions were drawn from the research:

1. The highest dimensional accuracy of the hole (the hole with the diameter closest to the nominal diameter and the lowest F_R value) was obtained after milling process in the tool entry zone using the Al/CFRP strategy and the cutting speed of v_c = 500 m/min.
2. The lowest dimensional accuracy of the hole was obtained in the drill exit zone using the Al/CFRP strategy and the cutting speed of v_c = 60 m/min.
3. Considering the selection of cutting conditions for the machining of holes in sandwich structures, one cannot be guided solely by the criterion of dimensional accuracy. The condition of the hole edges after machining (shape accuracy) must also be considered.
4. In most cases, the milling process has made it possible to obtain higher dimensional accuracy of the holes than the drilling process.
5. Each use of the drill, irrespective of the machining strategy or the value of the v_c parameter, resulted in delamination of the sandwich structure.
6. Increasing the cutting speed during the milling process produced holes with higher dimensional accuracy, while the reverse was true for the drilling process.
7. For both tools tested, a higher dimensional accuracy of the holes was obtained for the metal layer.
8. The use of high v_c values (v_c = 80 – 320 m/min) during drilling with the Al/CFRP strategy caused deformation of the aluminium alloy in the tool entry zone and led to delamination of the entire structure.
9. The use of the CFRP/Al strategy and the drill, regardless of the v_c parameter value adopted, resulted in deformation of the hole in the tool exit zone (no punched hole) and delamination of the entire structure.
10. The Al/CFRP strategy was more suitable for the milling process and the CFRP/Al strategy for the drilling process.
11. On the basis of the analysis of variance carried out, it can be concluded that, depending on the tool entry and exit zones and its type (milling cutter, drill bit), the independent variables studied have a different impact on the quality of the holes.
12. In the milling cutter entry zone, the v_c x S interaction had the highest influence on the hole diameter, while in the exit zone the machining strategy had the highest effect. For the drilling process the highest influence on the dependent variable for both zones had the cutting speed.

References

1. Ahn, J.H., Kim, G., & Min, B.-K. (2023). Exit delamination at the material interface in drilling of CFRP/metal stack. *Journal of Manufacturing Processes, 85,* 227–235. https://doi.org/10.1016/j.jmapro.2022.11.058.

2. An, Q., Dang, J., Li, J., Wang, Ch., & Chen, M. (2020). Investigation on the cutting responses of CFRP/Ti stacks: With special emphasis on the effects of drilling sequences. *Composite Structures, 253,* 112794. https://doi.org/10.1016/j.compstruct.2020.112794.

3. Angelone, R., Caggiano, A., Improta, I., Nele, L., & Teti R. (2019). Characterization of hole quality and temperature in drilling of Al/CFRP stacks under different process condition. *Procedia CIRP, 79,* 319–324. https://doi.org/10.1016/j.procir.2019.02.074.

4. Bunting, J., & Bunting, J. (2020). Advances in Drilling with PCD (Polycrystalline Diamond). *SAE International Journal of Advances and Current Practices in Mobility, 2,* 1209–1214. https://doi.org/10.4271/2020-01-0035.

5. Caggiano, A. (2018). Machining of Fibre Reinforced Plastic Composite. Materials. *Materials, 11,* 442. https://doi.org/10.3390/ma11030442.

6. Ciecieląg, K. (2023). Machinability Measurements in Milling and Recurrence Analysis of Thin-Walled Elements Made of Polymer Composites. *Materials, 16,* 4825. https://doi.org/10.3390/ma16134825.

7. Ciecieląg, K., & Zaleski, K. (2022). Milling of Three Types of Thin-Walled Elements Made of Polymer Composite and Titanium and Aluminum Alloys Used in the Aviation Industry. *Materials, 15,* 5949. https://doi.org/10.3390/ma15175949.

8. Doluk, E., & Rudawska, A. (2022). Effect of Machining Settings and Tool Geometry on Surface Quality After Machining of Al/CFRP Sandwich Structures. *Advances in Science and Technology Research Journal, 16,* 22–33. https://doi.org/10.12913/22998624/147787.

9. Doluk, E., Rudawska, A., & Miturska-Barańska, I. (2022). Investigation of the Surface Roughness and Surface Uniformity of a Hybrid Sandwich Structure after Machining. *Materials, 15,* 7299. https://doi.org/10.3390/ma15207299.

10. Fleischer, J., Teti, R., Lanza, G., Mativenga, P., Möhring, H.C., & Caggiano A. (2018). Composite materials parts manufacturing. *CIRP Annals, 67,* 603–626. https://doi.org/10.1016/j.cirp.2018.05.005.

11. Gola, A. (2021). Design and Management of Manufacturing Systems. *Applied Sciences, 15,* 2216. https://doi.org/10.3390/app11052216.

12. Hegde, S., Shenoy, B.S, & Chethan, K.N. (2019). Review on carbon fiber reinforced polymer (CFRP) and their mechanical performance. *Materials Today*: *Proceedings, 19,* 658–662. https://doi.org/10.1016/j.matpr.2019.07.749

13. Hoffman Group. Machining and Clamping. Catalogue 52, 2021/2022.

14. Isbilir, O, & Ghassemieh, E. (2013). Comparative study of tool life and hole quality in drilling of CFRP/Titanium stack using coated carbide drill. *Machining Science Technology, 17,* 380–409. https://doi.org/10.1080/10910344.2013.806098.

15. Karataş, A.M., & Gökkaya, H. (2018). A review on machinability of carbon fiber reinforced polymer (CFRP) and glass fiber reinforced polymer (GFRP) composite materials. *Defence Technology*; *14,* 318–326. https://doi.org/10.1016/j.dt.2018.02.001.

16. Kuczmaszewski, J., Zaleski, K., Matuszak, J., & Mądry J. (2019). Testing Geometric Precision and Surface Roughness of Titanium Alloy Thin-Walled Elements Processed with Milling. *Advances in Manufacturing II*, 95–106. https://doi.org/10.1007/978-3-030-18682-1_8.

17. Kuoa, C.L., & Sooa, S.L. (2014). The effect of cutting speed and feed rate on hole surface integrity in single-shot drilling of metallic-composite stacks. *Procedia CIRP; 13,* 405–10. https://doi.org/10.1016/j.procir.2014.04.069.

18. Labidi, A. (2020). Boeing 787 Dreamliner Represents Composites Revolution. *Aviation Knowledge – Aerodynamics-Meteorology, 3,* 1–2.

19. Lepretre, E., Chataigner, S., Dieng, L., & Gaillet, L. (2018). Fatigue strengthening of cracked steel plates with CFRP laminates in the case of old steel material. *Construction and Building Materials*, *174,* 421–432. https://doi.org/10.1016/j.conbuildmat.2018.04.063.

20. Matuszak, J.; Zaleski, K., Ciecieląg, K.; & Skoczylas A. (2022). Analysis of the Effectiveness of Removing Surface Defects by Brushing. *Materials, 15,* 7833. https://doi.org/10.3390/ma15217833.

21. Polish Committee for Standardization. (2017). Aluminium and aluminium alloys – Wrought products – Temper designations. (EN 515:2017).

22. Poutord, A., Rossi, F., Poulachon, G., Saoubi, R.M., & Abrivard, G. (2013). Local approach of wear in drilling Ti6Al4V/CFRP for stack modeling. *Procedia CIRP, 8,* 316–321. https://doi.org/10.1016/j.procir.2013.06.109.

23. Shyha, I.S., Soo, S.L., Aspinwall, D.K., Bradley, S., Perry, R., Harden, P., & Dawson, S. (2011). Hole quality assessment following drilling of metallic-composite stacks. *International Journal of Machine Tools and Manufacture, 51,* 569–578. https://doi.org/10.1016/j.ijmachtools.2011.04.007.

24. Torres Marques, A., Durão, L.M., Magalhães, A.G., Silva, J.F., & Tavares, J.M. (2009). Delamination analysis of carbon fibre reinforced laminates: Evaluation of a special step drill. *Composites Science and Technology, 69,* 2376–2382. https://doi.org/10.1016/j.compscitech.2009.01.025.

25. Wang, B., Wang, Y., Zhao, H., Sun, L., Wang, M., & Kong X. (2020). Effect of a Ti alloy layer on CFRP hole quality during helical milling of CFRP/Ti laminate. *Composite Structure, 252,* 112670. https://doi.org/10.1016/j.compstruct.2020.112670.

26. Zitoune, R., Krishnaraj, V., & Collombet, F. (2010). Study of drilling of composite material and aluminium stack. *Composite Structures, 92,* 1246–1255. https://doi.org/10.1016/j.compstruct.2009.10.010.

27. Zitoune, R., Krishnaraj, V., Collombet F., & Le Roux, S. (2016). Experimental and numerical analysis on drilling of carbon fibre reinforced plastic and aluminium stacks. *Composite Structure, 146,* 148–158. https://doi.org/10.1016/j.compstruct.2016.02.084.

Original Research

AUTOMATED SYSTEM OF INTER-OPERATIONAL TRANSPORT WITH A PNEUMATIC DRIVE

ZAUTOMATYZOWANY SYSTEM TRANSPORTU MIĘDZYOPERACYJNEGO Z NAPĘDEM PNEUMATYCZNYM

Jacek DOMIŃCZUK[1] (iD), Małgorzata GAŁAT[2]

[1] Department of Information Technology and Robotics in Production, Lublin University of Technology, Nadbystrzycka 36 street, Lublin, Poland
[2] CER, Energetyków 17 street, Lublin, Poland

* Corresponding author: j.dominczuk@pollub.pl,

Abstract

This paper presents a design solution for a system used for the inter-operational transport of tanks. Thanks to its innovative design, this solution allows to carry out the processing and assembly of components on the tank without the need to change its orientation. The application of the solution allows for the reduction of line dimensions and its full automation. Thanks to the use of commercially available modular components for the construction of the system, the time and cost of its implementation has been significantly reduced. Pneumatic drives were used in the solution to reduce costs and optimise design. By using appropriately selected and configured actuators and controls, the expected efficiency and reliability of the system was achieved.

Keywords: automation, transport, assembly.

Streszczenie

W artykule przedstawiono rozwiązanie konstrukcyjne systemu służącego do międzyoperacyjnego transportu zbiorników. Rozwiązanie to dzięki swojej innowacyjnej konstrukcji pozwala na realizację procesu obróbki I montażu komponentów na zbiorniku bez potrzeby zmiany jego orientacji. Zastosowanie rozwiązania pozwala na ograniczenie wymiarów linii oraz pełną jej automatyzację. Dzięki wykorzystaniu do budowy systemu dostępnych na rynku komponentów modułowych znacząco ograniczono czas oraz koszty jego wykonania.

Słowa kluczowe: automatyzacja, transport, montaż.

1. Introduction

Automation of a technological process is possible once the activities occurring in the process have been mechanised. Mechanisation involves replacing physical work of a human being with the machine work. To achieve this, it is necessary to use appropriate mechanical devices that will perform the work under human supervision. We can distinguish here four basic groups of driving elements: mechanical, pneumatic, electrical and hydraulic. Once the process has been mechanised, it is possible to automate it so that the machines can carry out the planned process without human involvement or with limited human involvement (Domińczuk, Kost, & Łebkowski, Automatyzacja i robotyzacja procesów produkcyjnych, 2022). It is possible thanks to the use of control systems including microprocessor-based programmable logic controllers (PLCs) (Kluz, 2012).

Companies manufacturing a variety of products tend to increase automation of basic, auxiliary as well as service processes. It also applies to assembly processes, although undoubtedly the advancement of the implementation of automated systems in assembly

does not yet match the intensity of similar processes in other manufacturing techniques. This is due to a number of reasons with more important ones as follow (Łunarski, 2011):

- increasing complexity of the construction and operation of various electromechanical products, the possible automatic assembly of which would require special assembly equipment, expensive and often unreliable,
- limited serial nature of product manufacturing, which makes it not cost-effective to implement automatic technological devices for assembly,
- diversity of manufactured products into series of typically dimensioned, modular, functional, etc., which requires ensuring considerable flexibility of automatic assembly equipment,
- frequent cases of insufficient refinement of technological design due to the requirements of automatic assembly,
- lack of mass production of typical modules for the implementation of automatic assembly, allowing for easy configuration of automatic assembly devices due to the diversity of assembly needs,
- the need to manufacture specialised assembly units dedicated to a specific application (Salonitis, 2014).

Despite the above mentioned factors limiting the use of automated systems in machine assembly, the systems are gradually becoming more widespread, influencing the repeatability of the process and ensuring that it can be supervised automatically.

The most common reasons for assembly automation include:

- the need to increase productivity and to make optimal use of the technological possibilities of the mechanised and semi-automated manufacturing techniques present on the production line,
- the need to ensure process feasibility within a defined period of time (Domińczuk, Analiza możliwości budowy wysokowydajnych elastycznych linii pakowania w oparciu o konstrukcje modułowe, 2018),
- the need to offer competitive technical solutions limiting the probability of producing defective products,
- the need to reduce human involvement in monotonous, repetitive tasks often connected with high physical effort.

Such situations create opportunities for companies specialising in the design and manufacture of semi-automatic and automatic assembly machines and,

indirectly, also for suppliers of components for such machines.

According to the author of the publication, (Łunarski, 2011) in order to take advantage of such opportunities, which increase in periods of economic prosperity and decrease in periods of crisis, it is necessary to:

- have an experienced, creative and innovative designers capable of solving complex problems quickly,
- have appropriate information systems to support the work of designers and the activities of planners implementing these projects (supplying, prioritising and scheduling tasks, utilising existing production capacities, resources, etc.),
- have appropriate technical infrastructure to enable projects to be carried out quickly and with a high standard of quality, and have links with suppliers, collaborators and subcontractors to facilitate execution of works.

The need for creativity results primarily from the fact that assembly automation should not always imitate manual procedures and operations. In such situations, there is a need to solve problems in an innovative way that guarantees high productivity, stable quality, safety of works and reliable operation of the automated assembly system.

Meeting these requirements often creates the necessity to develop basic, applied and developmental research (Kozioł, Samborski, & Zbrowski, Design of an innovative window-to-balcony building module, 2021) (Kozioł, Samborski, Siczek, & Zbrowski, 2018). The aim of these efforts is to develop and offer a variety of solutions, methods, tools, instrumentation and other elements necessary for efficient and reliable process automation.

2. Design requirements

The project task involved building a station for the automated process of machining and assembly of fuel tanks. The requirement was to base the tank at each station in a repeatable manner using dedicated surfaces and characteristic points. The design of the tank required completion of technological processes on all surfaces of the 1190 mm x 520 mm x 230 mm cube surrounding it (Fig. 1.). In order to ensure proper efficiency of process execution, the inter-operational transport time had to be within 5 s. The requirement for the process was to be run fully automatically both in the phase of supplying the container to the machining and assembly line and in the phase of product flow between the stations. The operator's task was to pick up the ready tank from the line and to deliver it to the feeding systems of components, which,

due to their nature, cannot be fed by vibratory dispensing systems. According to requirements, if a process error was detected, the product separation (good/bad) was to take place automatically. Due to the existing transport solutions ergonomic conditions in the company, it was required that the transport height

of the tank along the line was 1200 mm. It was assumed that the tank would not change its orientation during transport and that the transport would take place in a position consistent with the position of delivery of the tank to the line (Fig. 2).
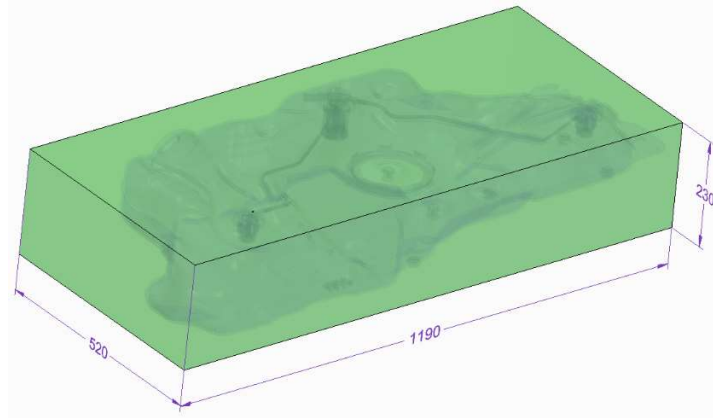

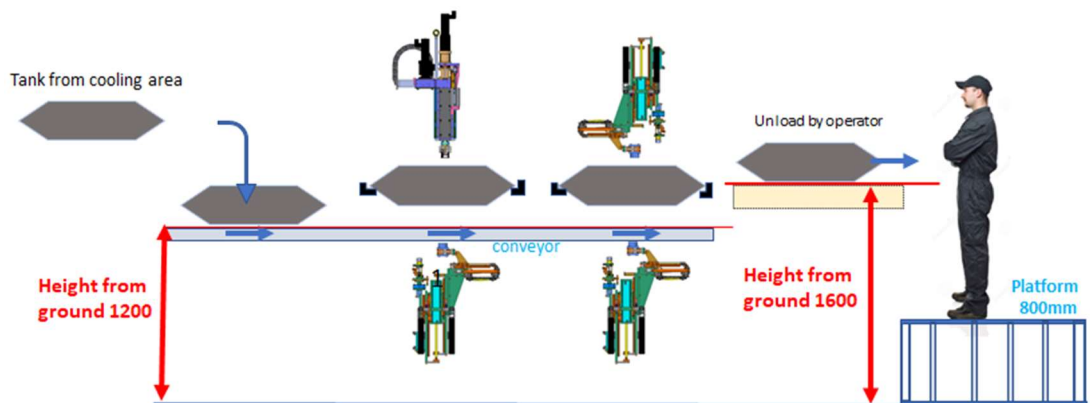**Fig. 1.** View of the cube surrounding the tank

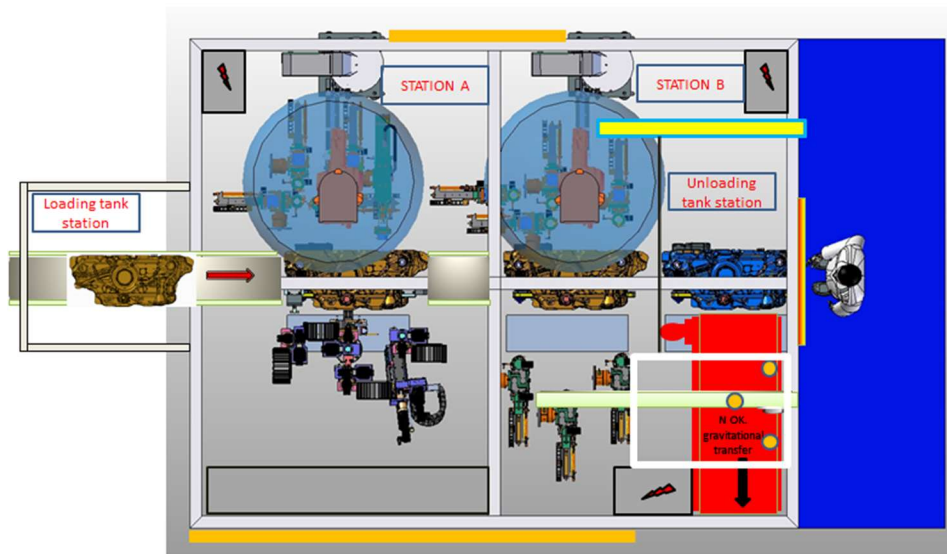**Fig. 2.** Concept of tank transport through the production line

Fig. 3. Concept of tank transport through the production line – plan view

According to the developed concept, the machining and assembly line will consist of two automated machining stations. There will be a loading station in front of station A. The unloading station will be located directly behind station B. It will enable the separation of tanks into those correctly made and the faulty ones. The tanks classified as faulty ones will be removed from the line automatically with the use of the station dedicated for this purpose. Correct tanks will be directed to the unloading station, where they will be collected by the operator and placed in storage racks.

According to the concept adopted for the tank processing, its movement will be carried out using a feeder and the tank will move sequentially from the loading station through station A, station B to the unloading station. Due to the difference in height between the transport and unloading heights (Fig. 2.), it will be required to lift the tank by 400 mm. As it can be seen in the diagram (Fig. 2., Fig. 3.) the transport system must be designed in a way to enable each side

of the tank to be processed according to specific technological requirements.

3. Technical solutions

The main problem in designing the line was determining the method of transporting the tank between the stations. The problem stems from the lack of free surface area of the tank that could provide a base surface for transport. As a result of the analyses carried out, the following transport system solution was proposed (Fig. 4.). It assumes moving the tank between stations in a sequential system after all technological operations at the machining and assembly stations have been performed. The task of the transport system would be to move the tank on slides along the track laid between the stations (from left to right, Fig. 4.). The tank would be initially based during movement. After moving to the work station, it would be based by being lifted to a defined position required for performing technological operations.
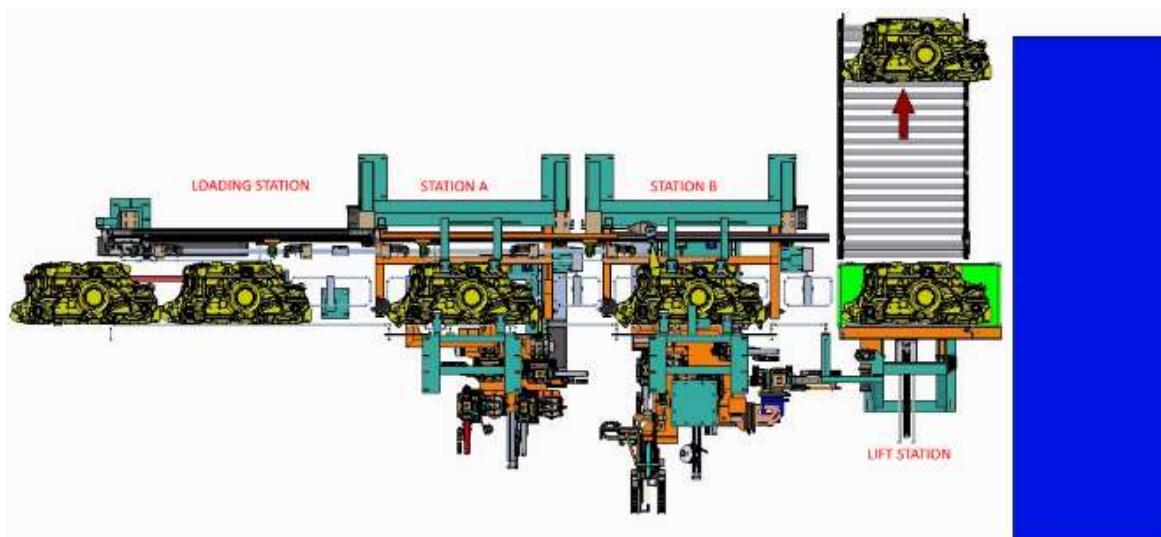

Fig. 4. Concept of transport system

This solution assumes that the drive elements of the transport system will be placed along one side of the tank. By using the tank lift system during basing, all tank surfaces will be exposed. Due to the necessity of removing the guiding elements used for tank transport from the bottom surface of the tank, the guiding system was integrated with the transfer of the work units, resulting in its removal from the work zone when the units occupy the working position (Fig. 5.).

The principle of operation of the feeder is illustrated in Fig. 6 and Fig. 7. The tank is transported to the loading station by the belt feeder (1) and its position is determined with the use of a stopper (2) (Fig. 6). The main feeder structure is based on an

aluminium profile (3) to which a rail guide (4) is attached. On the guide, there are trolleys (5) with bearing units (6) attached. A sleeve guide (7) is fitted to the bearing units. This guide forms the base for the tank orientation and, thanks to its ability to move along the station line, it ensures that the tank is transported. This assembly is driven by a pistonless cylinder (8), which, thanks to its equipment, makes it possible to set precisely the drive stroke. The container is gripped during transport by movable arms (9), which are rotated by the cylinder (10). The tank between the arms is blocked in place with the use of clamping cylinders (11) (Fig. 7.). Once the displacement is complete, the arms are released and rotated into

position and then moved to the parking position. Thanks to clamping units (12), the distance between the gripping units can be freely configured. This

distance is determined by the mutual positioning of station B relative to station A (Fig. 8.).
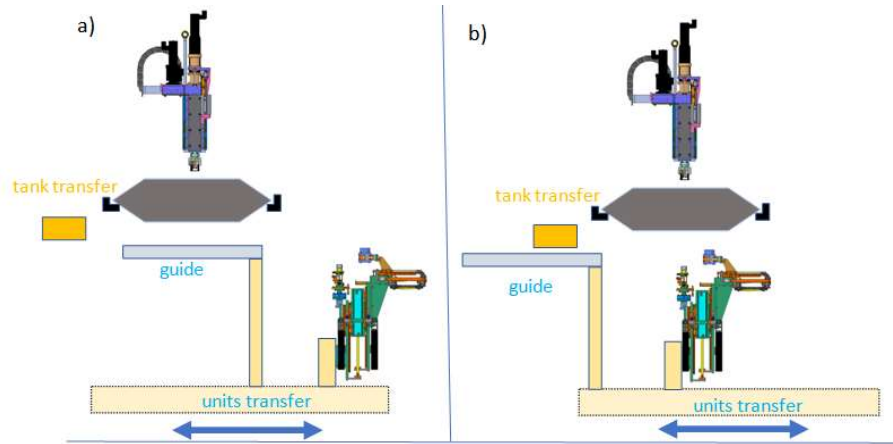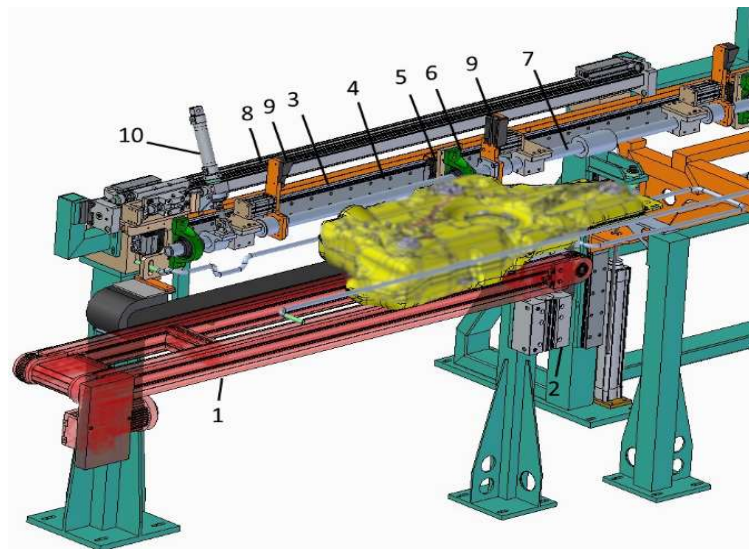

Fig. 5. Concept of the tank guiding system

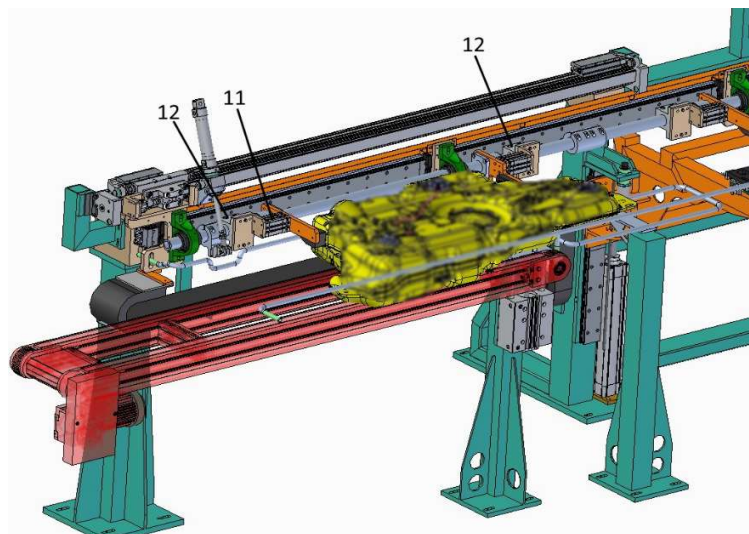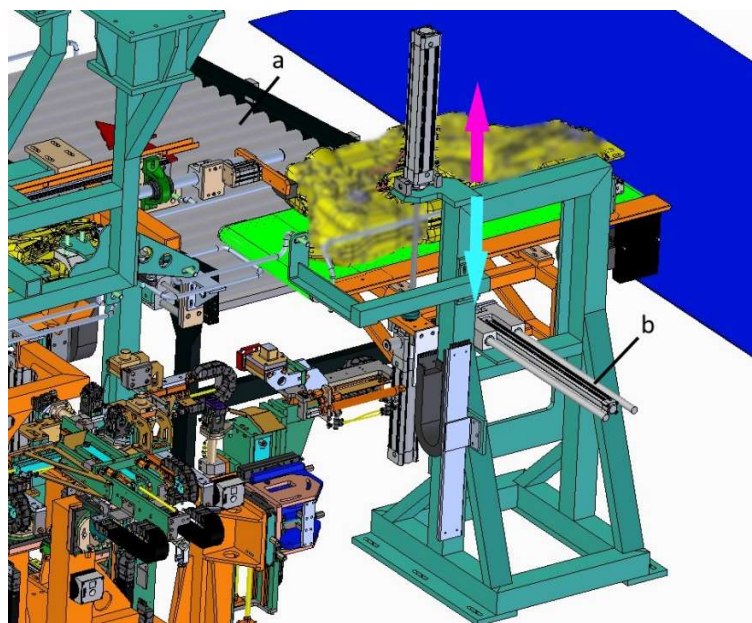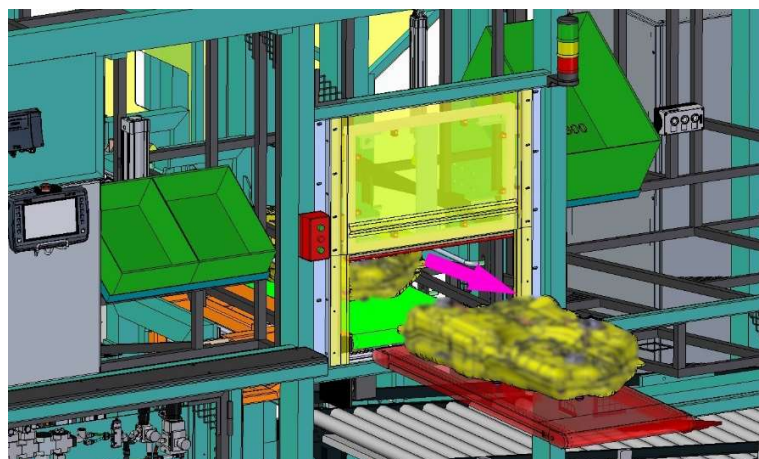**Fig. 6.** Construction of the inter-operational feeder

Fig. 7. Construction of the inter-operational feeder

Fig. 8. Position of the feeder during tank loading

Fig. 9. Position of the feeder during tank loading

Fig. 10. Zone of collection of the tank by the operator

The unloading system is designed in the form of a lift equipped with a belt feeder. Loading of the tank onto the lift is carried out in the central position using a single ejector arm (Fig. 9.). The lift, thanks to the coupling of two pneumatic cylinders, can occupy three positions. The lower position allows tanks with NOK status to be unloaded onto the gravity feeder (a) using a transverse ejector (b). The upper position is used to safely transport the tank to the collection area by the operator (Fig. 10.).

4. Summary

The design solution presented in this paper, an automated inter-operational transport system with a pneumatic drive, allowed to perform the technological process without the need to change the tank orientation, which brought the following benefits:

- ensured the possibility of using an identical basing system at each station, which has a positive impact on the final quality of the product,
- reduced the cost of manufacturing basing systems due to their unification,
- provided the possibility to carry out the process on two work stations,
- ensured optimum use of production space,
- reduced costs of manufacturing the machine due to the relatively low manufacturing costs of the transport system built from modular systems.

The implemented innovative design solution of the transport system based on pneumatic drives is an example of the possibility to use simple and low-cost drives to perform important tasks in automated production lines operating within the framework of Industry 4.0 (Stadnicka, et al., 2022) (Kolberg & Zuhlke, 2015) (Brzozowska & Gola, 2021). The presented solution is the result of the search for optimal process execution conditions, which is one of the basic activities while designing robotic production systems. The presented system has a modular design, which allows it to be easily adapted to other industrial applications. It can be scaled and controlled using programmable flow control systems. By using this type of solution, it is possible to adapt its operating parameters to the requirements of the application at control program level. All these factors make the system concept versatile and universally applicable to a wide range of operating parameter variants.

References

1. Brzozowska, J., & Gola, A. (2021). Computer aided assembly planning using MS Excel software – a case study. *Applied Computer Science*(17(2)), pp. 70-89. doi:https://doi.org/10.35784/acs-2021-14.

2. Domińczuk, J. (2018). Analiza możliwości budowy wysokowydajnych elastycznych linii pakowania w oparciu o konstrukcje modułowe. *Technologia i Automatyzacja Montażu*(2), pp. 11-15. doi:https://doi.org/10.1515/tam-2018-0017.

3. Domińczuk, J., Kost, G., & Łebkowski, P. (2022). *Automatyzacja i robotyzacja procesów produkcyjnych.* Warszawa: Polskie Wydawnictwo Ekonomiczne.

4. Kluz, R. (2012). Projektowanie modułowego stanowiska montażowego. *Technologia i Automatyzacja Montażu*(1), strony 9-13.

5. Kolberg, D., & Zuhlke, D. (2015). Lean Automation enabled by Industry 4.0 Technologies. *IFAC-Papers OnLine*(3), pp. 1870-1875. doi:https://doi.org/10.1016/j.ifacol.2015.06.359.

6. Kozioł, S., Samborski, T., & Zbrowski, A. (2021). Design of an innovative window-to-balcony building module. *Technologia i Automatyzacja Montażu*(3), pp. 10-14. doi:https://doi.org/10.1515/tam-2021-0022.

7. Kozioł, S., Samborski, T., Siczek, M., & Zbrowski, A. (2018). System for testing resistance for static exposure to dust. *Technologia i Automatyzacja Montażu*(2), pp. 11-15. doi:https://doi.org/10.1515/tam-2018-0017.

8. Łunarski, J. (2011). Wprowadzenie. In J. Sęp, & F. Stachowicz (Ed.), *Technika i technologia montażu maszyn* (Vol. 83, pp. 5-6). Rzeszów: Oficyna Wydawnicza Politechniki Rzeszowskiej.

9. Salonitis, K. (2014). Modular design for increasing assembly automation. *CIRP Annals, 63*(1), pp. 189-192. doi:https://doi.org/10.1016/j.cirp.2014.03.100.

10. Stadnicka, D., Sęp, J., Amadio, R., Mazzei, D., Tyrovolas, M., Stylios, C., Navarro, J. (2022). Industrial Needs in the Fields of Artificial Intelligence, Internet of Things and Edge Computing. *Sensors*. doi:https://doi.org/10.3390/s22134501.

Technologia i Automatyzacja Montażu

Original Research

THE INFLUENCE OF ADHESIVE MATERIAL PROPERTIES ON THE IMPACT STRENGTH OF ADHESIVE BLOCK JOINTS

WPŁYW WŁAŚCIWOŚCI MATERIAŁU KLEJONEGO NA UDARNOŚĆ POŁĄCZEŃ KLEJOWYCH BLOKOWYCH

Andrzej KOMOREK[1]* (ID), **Jan GODZIMIRSKI[2], Szymon IMIŁOWSKI[1]**

[1] Lotnicza Akademia Wojskowa, Dywizjonu 303, nr 35, 08-530 Dęblin, Poland
[2] Wojskowa Akademia Techniczna, ul. S. Kaliskiego 2, 00-908 Warszawa, Poland

* Corresponding author: a.komorek@law.mil.pl, tel. 261 518 863

Abstract

Adhesive joints are becoming increasingly popular in the construction of aircraft and other means of transport. Today, bonding is mainly used in the construction of helicopter fuselages, wings or lifting rotors. The increased popularity of bonding is forcing designers to seek new and improve research methods as well as enhancing the existing test methods which specify the static, fatigue or impact strength of joints. A variety of tests are used to determine the strength of structures, although new ones are constantly being sought so as to be applied more quickly and without specialised equipment. Current testing standards are also being modified in order to speed up and simplify the testing process, resulting in safer structures that use adhesive joints.

The aim of the research presented in this paper was to test whether there is a relationship between the mechanical properties of adhesive materials and the impact strength of adhesive block joints with a cylindrical top element.

Construction steel S235JR, commercially marked wear-resistant steel Raex 400 and 2017A aluminium alloy were used for the manufacture of the samples. From each material, 10 samples were prepared with upper elements of different diameters, namely: 17.8 mm, 12.6 mm and 8.9 mm. A pendulum hammer was used to determine the strength of the adhesive joint against dynamic load application. For the sake of the research, the authors used a modified PN-EN ISO 9653 with a mounted hammer equal to the maximum energy of 15 J.

Lower failure energy was characteristic of samples made from material with a lower value of Young's modulus (aluminum alloy) and from steel with a lower yield strength. The joint failure energy grew with increasing the joint area, which was approximately parabolic.

Keywords: bond, adhesive joint, impact strength, block sample

Streszczenie

Połączenia klejowe są coraz bardziej popularne w konstrukcji statków powietrznych oraz innych środków transportu. Dziś klejenie stosuje się głównie przy budowie kadłubów, skrzydeł lub wirników nośnych śmigłowców. Zwiększenie popularności klejenia zmusza konstruktorów do poszukiwania nowych oraz udoskonalania istniejących metod badawczych określających wytrzymałość połączeń statyczną, zmęczeniową czy udarową. Stosuje się różnorodne badania by określić wytrzymałość konstrukcji, lecz wciąż poszukiwane są nowe, które można stosować szybciej oraz bez specjalistycznego wyposażenia. Także obecne normy badawcze są modyfikowane by przyśpieszyć oraz uprościć proces badawczy co skutkuje zwiększeniem bezpieczeństwa konstrukcji w których wykorzystano połączenia klejowe.

Celem przedstawionych w artykule badań było sprawdzenie czy istnieje zależność pomiędzy właściwościami mechanicznymi materiałów klejonych i wytrzymałością udarową połączeń klejowych blokowych z górnym elementem o kształcie cylindrycznym.

Do wykonania próbek wykorzystano stal konstrukcyjną S235JR, stal trudnościeralną o oznaczeniu handlowym Raex 400, oraz stop aluminium 2017A. Z każdego materiału przygotowano po 10 próbek z górnymi elementami o różnej średnicy, mianowicie: 17,8 mm, 12,6 mm oraz 8,9 mm. W celu określenia wytrzymałości połączenia klejowego na dynamiczne

przyłożenie obciążenia wykorzystano młot wahadłowy. Do badania wykorzystano zmodyfikowaną normę PN-EN ISO 9653 z zamontowanym młotem o maksymalnej energii wynoszącej 15 J.

Niższa energia niszczenia cechowała próbki wykonane z materiału o mniejszej wartości modułu Younga (stopu aluminium) oraz ze stali o mniejszej granicy plastyczności. Energia niszczenia połączeń rosła wraz ze wzrostem powierzchni spoin – w przybliżeniu parabolicznie.

Słowa kluczowe: klej, połączenie klejowe, udarność, próbka blokowa

1. Introduction

Joints made with bond are just as stable and durable as their counterparts made by riveting or welding (Adams et al. 1997). They are used in the production of, for example, lightweight and very strong sandwich composites, which are used, among other things, in the construction of aircraft flight controls such as ailerons, flaps and rudders. Also, wing or fuselage plating is now made using adhesive joints (Higgins, 2000).

The large-scale use of adhesive joints necessitates testing their strength, and while static property tests are well known and widely used (Naito et al., 2012; Grant et al., 2009; Ramalho et al., 2020), certain types of tests are not widespread for various reasons (Casas-Rodriguez, et al., 2007; Goglio & Rosetto, 2008). One type of such tests is the impact test of adhesive block joints performed with a pendulum hammer (Sato 2005) This test provides information about the strength of a joint (or rather an adhesive bond) against a dynamic application of load to joint elements.

The energy of the pendulum is used to destroy a sample while the testing machine software calculates the value of the joint destruction energy, taking into account the part of the kinetic energy used to reject the sample element. The manner in which the upper element is bonded to the block allows the large face of the upper element of the sample to be struck easily (Fig. 1). If the top piece is bonded properly, the hammer strikes parallel to the bonded surface and the load distribution is even across the entire impacted surface of the top piece. However, such an impact is very difficult to achieve in practice. The bonded plate is usually minimally shifted from the lower element of the sample, resulting in misalignment with the pendulum, leading to incorrect results (Adams 2005; Komorek 2018).

The use of a cylindrical top block sample in adhesive bonding impact tests is a way to make them less complicated and independent of incorrectly bonded sample pieces. In a standard test, as mentioned earlier, the main problem is to very accurately bond the upper element to the block (Godzimirski, et al. 2019; Komorek, et al. 2020; Adams & Harris 1996). The use of a cylindrical upper sample element may solve the presented problem, however the phenomenon, which is likely to occur in this type of testing, is plastic

deformation of the impacted element. In a standard sample, the hammer strikes the rectangular side of the sample, i.e. the energy is transferred onto a large area and the element does not deform plastically. With a cylindrical element, the energy is transferred linearly, which can lead to plastic deformation of this sample element (Adams 2005; Komorek 2018).
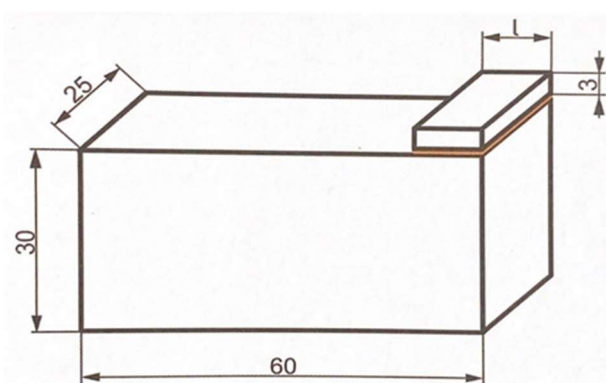
Fig. 1. Diagram of the examined object, undergoing impact testing of adhesive bonds in accordance with ISO 9653:1998

The aim of the examination was to check whether the cylindrical upper parts of the samples, to which the load is applied, deform plastically. The elements were made from different materials. Each type of material served to prepare elements of three different diameters. Each material was characterized with yield strength.

It is assumed that some of the elements will deform plastically during the examination. This deformation consumes some energy which is not subtracted from the indicated failure energy. In this way, the impact strength of the joint is overestimated. In the research, the authors want to prove that decreasing the diameter of the impacted piece and increasing the yield strength should result in the absence of plastic deformation of the impacted element, If the authors' expectations are confirmed, the use of samples with smaller upper elements will significantly increase the reliability of the obtained results, which will increase the usefulness of this research method.

2. Research methodology

In order to carry out research aimed at checking the authors' assumptions, it was decided to adopt the following research scheme: - preparation of the lower

elements of the samples (using the water jet cutting method), preparation of the upper elements of the samples with three different diameters and from three different materials (laser cutting method), - preparation of the surface of the glued elements (abrasive blasting and degreasing), making glue joints, removing glue flashes, impact testing of all prepared joints, visual observation of plastic deformations of sample elements.

Cylindrical shapes were used as the upper elements of the samples to test the impact strength of block joints. The diameters were as follows: 17.8 mm, 12.6 mm and 8.9 mm. They were all 3 mm thick (Fig. 2), and they were made of three different materials - S235JR and wear-resistant steel Raex 400 as well as 2017A aluminium alloy.

Fig. 2. Upper elements of block samples with diameters of 17.8 mm and 12.6 mm

The diameters of the upper elements were selected in such a way that the area of the smallest fittings constituted 1/2 surface area of the average piece and 1/4 surface area of the largest piece (the surface area of this piece was equal to 250 mm^2). The material properties of the sample elements are given in Table 1.

Table 1. Material properties of bonded pieces

	Yield stress $R_{p0,2}$, (MPa)	Tensile strength, (MPa)
Raex 400	1,000	1,250
S235JR	235	410
2017A	240-260	350-390

Each of the upper parts of the samples was blasted in a sandblasting chamber. Dried quartz sand (Airpress, Poland) (quartz content above 97%) with a grain size of 0.1-0.5 mm was used as the abrasive medium. This treatment was intended to mattify and create a uniform surface for gluing. After cleaning by abrasive blasting, the sample elements were immersed in 99% isopropyl alcohol (Archem, Poland) for 5 minutes and then washed with a brush to remove dirt and degrease from the adherends' surfaces. After washing, the sample elements were placed in a laboratory drying chamber at a temperature of 40°C for 2 minutes to evaporate the isopropyl alcohol.

The lower elements to which the cylindrical elements were bonded were cuboidal in shape, measuring 60x25x30 mm. They were made of steel and aluminium alloy, depending on the exploited upper sample element. The bottom elements were prepared for gluing using the same method as the upper elements.

Loctite Hysol EA9464 adhesive was used as the adhesive material. Loctite Hysol EA 9464 is manufactured by Henkel Corporation, USA. Loctite Hysol 9464 formula ensures short setting and hardening times. Parts can be moved after curing for 3-4 hours at 22 0C. Maximum strength properties are achieved after curing for 3 days at room temperature. The shear strength (adhesive hardened for 7 days at 22°C) of connections between shot-blasted structural steel elements is 22 MPa, and of connections between aluminum elements, ground with sandpaper (P400A grain) - 18.2 MPa. The peel strength when bonding elements made of structural steel is 10.5 N/mm, and when bonding etched aluminum elements it is 7 N/mm (Technical sheet of Loctite 2003).

The samples were bonded in batches of 10 under identical conditions. EA 9464 adhesive is a two-component adhesive, and the ingredients are contained in a double cartridge. A special gun for this type of cartridge is used to squeeze the glue ingredients from the cartridges. The gun allows you to simultaneously squeeze out equal amounts of both ingredients from both cartridges, so that they can be mixed together in a 1:1 ratio. The glue was squeezed onto a clean sheet of paper through a special mixing nozzle attached to the cartridge. Then the thin layer of adhesive mixture was applied with a spatula to the joining elements. The authors assembled the samples by placing the upper element in the middle of the lower element, at its very edge. When assembling the sample elements, auxiliary marks on the lower element and a magnifying glass were used to determine the correct positioning of the elements. (Fig. 3).

Fig. 3. Test sample

After an assembly, the samples were subjected to a load that produced a joint thickness of approximately 0.10 mm in each piece. The joints were hardened at room temperature for 7 days, applying constant pressure on the glued batches of samples (10 pieces) during the hardening period using a 10 kg weight.

The aim of the test was to check the strength of the adhesive bond against impact loads applied to the upper part of the sample. The test stand used for the tests was the "Julietta" pendulum hammer for testing lap and block joints (Fig. 4).

Fig. 4. "Julietta" device for testing impact strength of adhesive joints

The samples were placed in a special test machine handle (Fig. 5) prior to testing in order to stabilise them and ensure that the load was applied perpendicularly to the sample face. The examination was conducted in accordance with PN-EN ISO 9653 with a mounted hammer whose maximum energy was equal to 15 J and whose velocity was equal to 2,96 m/s.

Fig. 5. Sample mounted in the handle of the testing device
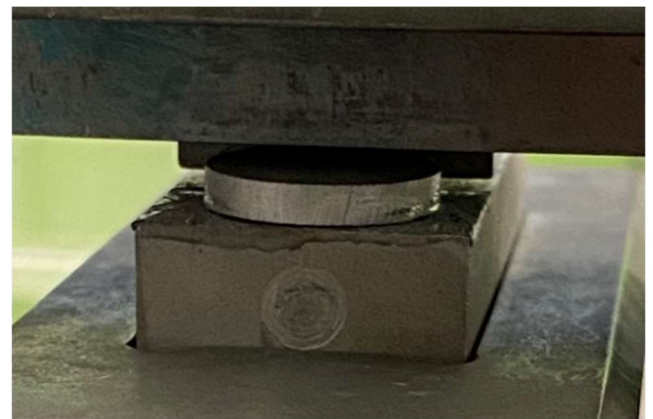

Fig. 6. Hammer prior to sample impact


Fig. 7. View of sample during a hammer is striking

3. Research findings and their analysis

First, the authors examined the samples in which the upper element was made of PA6 aluminium alloy and whose diameter was 17.8 mm, which corresponds to the surface area of a standard adhesive bonding impact test sample in accordance with the norm PN-EN ISO 9653 equal to 250 mm^2. Most of the damage was cohesive in its nature, however some samples were damaged in an adhesive or mixed manner (Fig. 8).

Fig. 8. Method of failure of samples whose upper elements were made of 2017A alloy with a diameter of 17.8 mm

Next, samples with a diameter of 12.6 mm and a surface area of 125 mm^2 were examined. The last samples made from 2017A material had diameters of upper elements equal to 8.9 mm, which corresponded to a surface area of 62.5 mm^2. In the last group, slightly larger areas of adhesive damage were observed than in the two previous studies, involving PA6 material (Fig. 9).
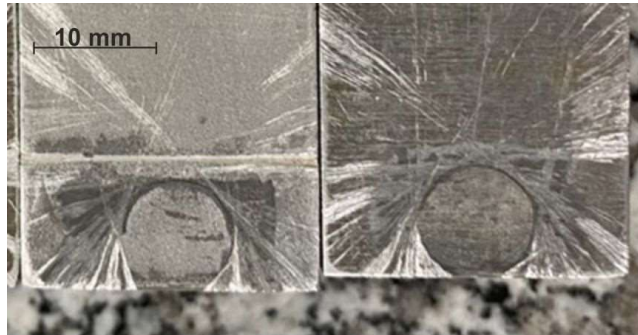
Fig. 9. Manner of destruction of the 2017A sample
with a diameter equal to 8.9 mm

Most of the damage was cohesive in its nature with a small proportion of adhesive damage in each batch.

As expected, larger surface areas of adhesive joints corresponded to higher destruction energies (Fig. 10).
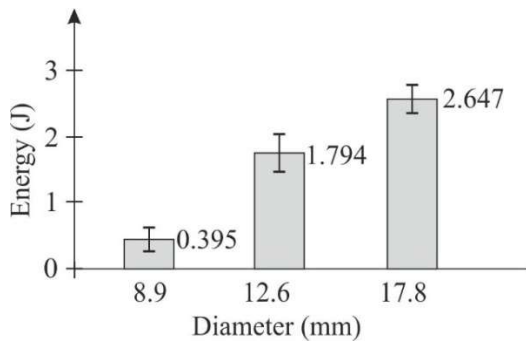

Fig. 10. Average destruction energy of all examined
2017A samples

In subsequent tests, samples made of Raex 400 material with a diameter of 17.8 mm were tested. The destruction observed in this batch was cohesive in its nature with little adhesion damage (Fig. 11).
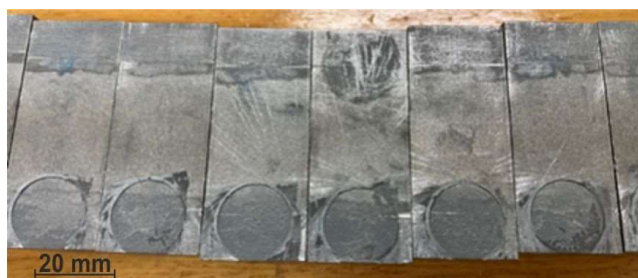
Fig. 11. Destruction of Raex 400 samples

In the next step, the authors examined ten samples of the same material with a diameter of 12.6 mm. Similarly to the samples which are 17.8 mm in diameter, mainly cohesive damage was observed in this batch (Fig. 12).
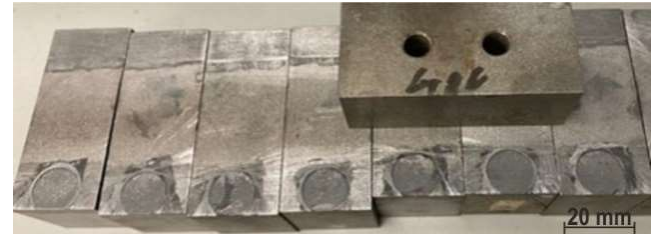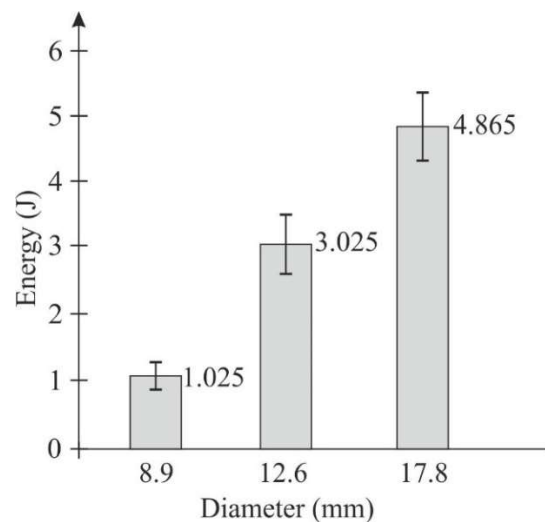

Fig. 12. Cohesive destruction of Raex 400 material samples
with a diameter of 12.6 mm

In a batch made up of 8.9-mm-diameter samples, adhesive damage with a small amount of mixed damage was mainly observed (Fig. 13).

Fig. 13. Adhesive destruction of samples made up of Raex 400
material, 8.9 mm in diameter

**Fig. 14.** Average destruction energy of all examined
Raex 400 samples

The relationship between the energy of destruction and the surface area of the adhesive joint of elements made of Raex400 steel (Fig. 14) was similar to that in the joint of elements made of 2017A.

In the first two batches, it is possible to observe mostly cohesive damage with a small share of adhesive damage. In the last test batches, 8.9 mm in

diameter, it was possible to observe mainly adhesive damage.

Finally, a series of samples was tested with the upper elements made up of S235JR steel. Firstly, the authors examined samples with a diameter of 17.8 mm. In this case, mainly cohesive damage was observed. Adhesive damage was identified on a small area of three samples (Fig. 15).
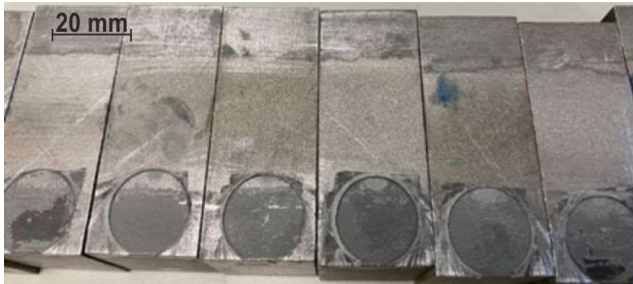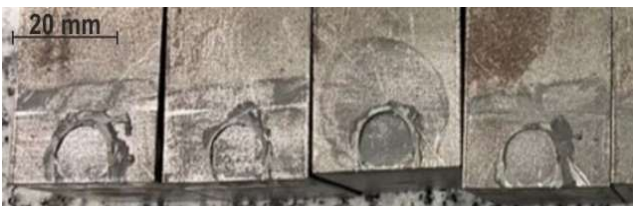

Fig. 15. Adhesive destruction of samples made up of S235JR material, 17.8 mm in diameter

The S325JR steel specimens with a 12.6 mm upper element also demonstrated mostly cohesive damage. Mixed damage appeared on several samples (Fig. 16).
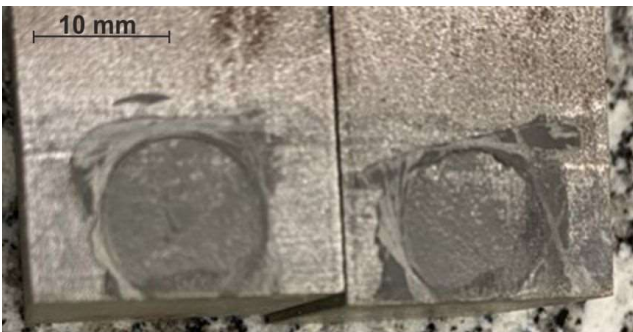

Fig. 16. Cohesive and mixed destruction on samples made up of S235JR material, 12.6 mm in diameter

In the case of S235JR steel samples with the top element of 8.9 mm in diameter, the damage to the samples was mostly cohesive in nature with small areas of adhesion damage and one sample adhesively damaged (Fig. 17).

Fig. 17. Adhesive destruction of samples made up of S235JR material, 8.9 mm in diameter
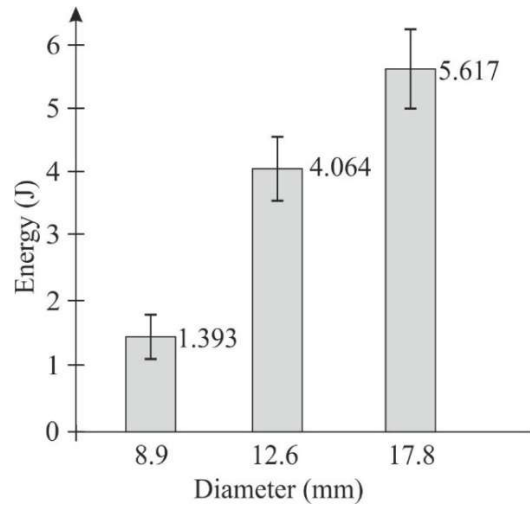
Fig. 18. Average destruction energy of all examined S235JR samples

In the samples, 8.9 mm in diameter, it was mainly possible to observe adhesion damage, while the remaining batches showed cohesive damage.

The destruction energy of the examined joints increased disproportionately along with increasing the joint area, which was approximately parabolic (Fig. 18).

Impact strength of samples made of different materials

The impact strength was defined as the quotient of the energy of joint destruction to its surface area.

The results of the conducted examination for samples, 17.8 mm in diameter, have been presented in Fig. 19.
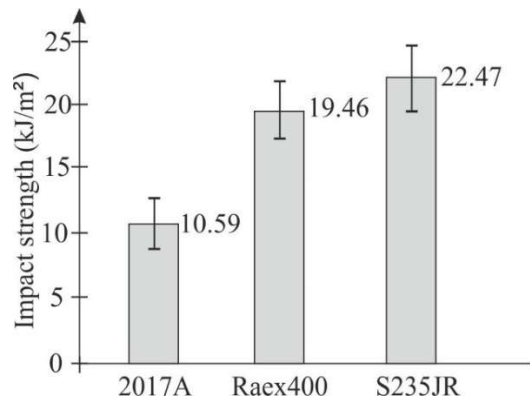
Fig. 19. Average impact strength of samples which are 17.8 mm in diameter

Samples made from S235JR steel had the highest impact strength (Fig. 19). Their impact strength was 112% higher than that of the aluminium alloy samples and 15% higher than that of the test series made from Raex 400 steel.

The average values of impact strength of the samples, 12.6 mm in diameter, of all the materials have been presented in Fig. 20.

Fig. 20. Average impact strength of samples which were 12.6 mm in diameter

While analysing the results of samples whose upper element equalled 12.6 mm in diameter, a significant difference can be seen between samp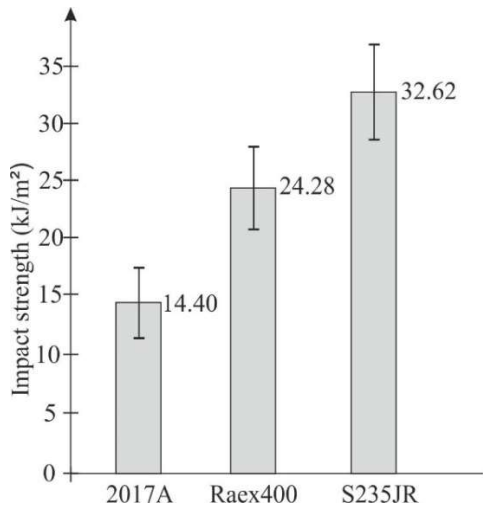les made of steel. The impact strength of the S235JR steel samples is 35% higher than that of the Raex 400 steel samples. The impact strength of aluminium alloy samples is 56 % lower than the impact strength in samples made from S235JR steel.
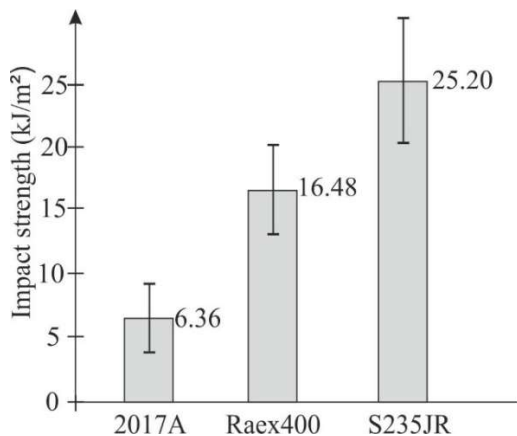

Fig. 21. Average impact strength of samples which are 8.9 mm in diameter

Fig. 21 shows the average impact strength of the samples whose upper elements are equal to 8.9 mm in diameter. Similarly to samples which are 12.6 mm in diameter, there is a clear difference in impact strength between the steel samples. S235JR steel samples have an impact strength which is 35% higher than that of Raex 400 and 75% higher than that of 2017A alloy. Aluminium alloy samples have a significantly lower impact strength than steel samples.

Plastic deformation

After a visual inspection of all the damaged samples, plastic deformation was found on two materials with the lowest yield strength, namely S235JR steel and 2017A aluminium alloy, respectively.

The deformation of S235JR steel components was observed with samples of 17.8 mm (Fig. 22) and 12.6 mm (Fig. 23) in diameter. At 8.9 mm in diameter, no distortion was observed.
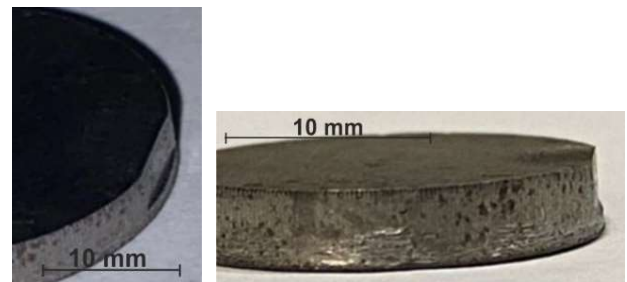
Fig. 22. Plastic deformation of a sample element, 17.8 mm in diameter, made of S235JR steel

Fig. 23. Plastic deformation of a sample element, 12.6 mm in diameter, made of S235JR steel

The deformation of the 2017A aluminium alloy samples was also observed in pieces whose diameter equalled 17.8 mm (Fig. 24) and 12.6 mm (Fig. 25). No plastic deformation was observed with the smallest diameter.

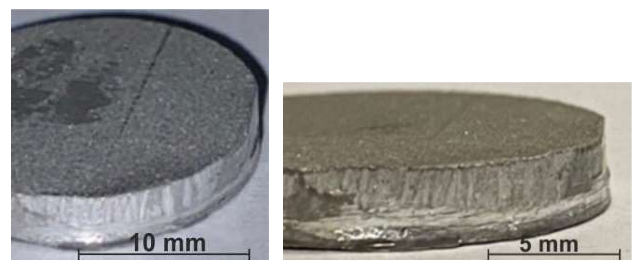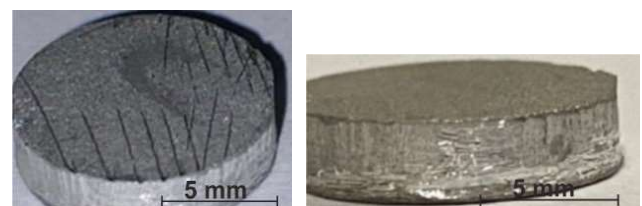**Fig. 24**. Plastic deformation of a piece, 17.8 mm in diameter, made of 2017A alloy

Fig. 25. Plastic deformation of a sample piece whose diameter equalled 12.6 mm, made of 2017A alloy

No plastic deformation was found in samples made from Raex 400 steel with any diameter (Fig. 26).

Fig. 26. Non-plastically deformed sample pieces, 17.8 mm in diameter, made up of Raex 400 steel

4. Conclusions

Based on the obtained results, the following conclusions were drawn:

1. by making the upper cylindrical parts of the block samples from a high yield strength material, plastic deformation of these parts can be avoided, thereby increasing the reliability of the impact test results obtained by this method;
2. plastic deformation of the upper parts of the samples made of low yield strength materials only occurred at diameters of 17.8 mm and 12.6 mm. No deformation was observed in the upper 8.9 mm diameter elements;
3. the upper parts of the samples made of Raex 400, which had the highest yield strength of the tested materials, did not deform at any of the diameters of the upper parts;
4. the joints failure energy increased with increasing the joint area, which was approximately parabolic. This shows that the stresses in the loaded joints are not distributed uniformly and the destruction of the joint starts at the point of contact between the dropping tool and the cylindrical element;
5. the lowest failure energy of aluminium alloy samples is due to the low value of the Young's modulus of this material. The same load force corresponds to almost three-fold elastic deformation of the aluminium alloy element than of the steel element. Greater deformation of the bonded component corresponds to greater deformation of the joint and its faster destruction;
6. higher destruction energy of S235JR steel samples compared to Raex 400 steel is due to low yield strength of S235JR steel. The plastic deformation of the loaded components made of this steel requires providing energy, which adds up to the fracture energy of the joint.

References

1. Adams, R. D., Comyn, J., Wake, W. C. (1997). Structural Adhesive Joint in Engineering. Springer Science & Business Media, London.
2. Higgins, A. (2000) *Adhesive bonding of aircraft structures*. International Journal of Adhesion and Adhesives, 20, 367–376, doi:10.1016/S0143-7496(00)00006-3.
3. Naito, K., Onta, M., Kogo, Y. (2012*) The effect of adhesive thickness on tensile and shear strength of polyimide adhesive*. Journal of Adhesion and Adhesives, 36, 77–85, doi:10.1016/j.ijadhadh.2012.03.007.
4. Grant, L.D.R., Adams, R.D., da Silva, L.F.M. (2009) *Experimental and numerical analysis of single-lap joints for the automotive industry*. J Journal of Adhesion and Adhesives, 29, 405–413, doi:10.1016/j.ijadhadh.2008.09.001.
5. Ramalho, L.D.C., Campilho, R.D.S.G., Belinha, J., da Silva, L.F.M. (2020) *Static strength prediction of adhesive joints: A review*, International Journal of Adhesion and Adhesives, 96, 102451.
6. Casas-Rodriguez, J.P., Ashcroft, I.A., Silberschmidt, V.V. (2007) *Damage evolution in adhesive joints to impact fatigue*, Journal of sound and Vibration, 308, 467-478.
7. Goglio, L., Rosetto, M., (2008) *Impact rupture of structural adhesive joints under different stress combinations,* International Journal of Impact Engineering, 35, 635–643.
8. Sato, C. Impact behavior of adhesively bonded joints. In: Adhesive Bonding: Science, Technology and Applications, edited by Adams, R D. WPL, Cambridge 2005, pp. 164-188.
9. Adams, R.D. Adhesive bonding. Woodhead Publishing Limited, Cambridge 2005.
10. Komorek, A. Studium udarności połączeń klejowych blokowych. Wydawnictwo Naukowe Instytutu Technologii Eksploatacji, Dęblin 2018.
11. Godzimirski, J, Komorek, A, Komorek, Z. (2019) *An Energy Analysis of Impact Strength Tests Using Pendulum Hammers*, Advances in Science and Technology Research Journal vol. 13 (4).
12. Komorek, A., Godzimirski, J., Rośkowicz, M. (2020) *Analysis of a New Shape of Test Specimen for Block Shear Impact Test*. Materials, 13, 1693.
13. Adams, R.D., Harris, J.A. (1996) *A critical assessment of the block impact test for measuring the impact strength of adhesive bonds.* International Journal of Adhesion and Adhesives 16: 61-71.
14. Technical sheet of Loctite Hysol EA 9464, Henkel Corporation, USA, 2003.

A SIMULATION MODEL FOR SMALL AIRCRAFT FUEL SYSTEM DESIGN

MODEL SYMULACYJNY PROJEKTOWANIA UKŁADU PALIWOWEGO MAŁYCH SAMOLOTÓW

Leonardo MAZZITELLI[1] , **Paulo WATANABE**[2], **José C. TEIXEIRA**[1] **José MACHADO**[1]

[1] MEtRICs Research Center, University of Minho, 4800-058, Guimarães, Portugal
[2] Propulsion Systems Department, CEiiA, 7005-841, Évora, Portugal

* Corresponding author: a87049@alunos.uminho.pt, tel. +351 930580341

Abstract

An aircraft fuel system is responsible for storing, managing and properly delivering fuel to the engines. Fuel systems models are used to simulate various configurations and analyse how the system responds to different flight conditions and failure scenarios. In this paper, a generic aircraft fuel system model architecture is proposed and modelled using MATLAB and Simulink's Simscape add-on to analyse the pressure and flow rate variations in different locations of the system. The model capabilities are explored with meaningful simulations and analyses focused on the feed and transfer functions, such as the sensitivity analysis of the scavenge jet pump, showing that the position where the jet pump is assembled in the wing can highly impact its performance. Additionally, the wing dihedral is modelled and simulated to prove that a positive dihedral angle benefits the fuel transfer and helps minimize unusable fuel quantities. The results also demonstrate how computational tools such as Simscape Fluids can be integrated with MATLAB and used on the system's modelling, providing a reference for small aircraft fuel system design and an approach for analysing complicated non-linear systems.

Keywords: Aircraft Fuel System, System modelling, Simscape

Streszczenie

Układ paliwowy samolotu odpowiada za przechowywanie, zarządzanie i prawidłowe dostarczanie paliwa do silników. Modele układów paliwowych służą do symulacji różnych konfiguracji i analizy reakcji systemu na różne warunki lotu i scenariusze awarii. W tym artykule zaproponowano ogólną architekturę modelu układu paliwowego samolotu, którą zamodelowano przy użyciu programu MATLAB i dodatku Simulink Simscape w celu analizy zmian ciśnienia i natężenia przepływu w różnych lokalizacjach układu. Możliwości modelu bada się za pomocą znaczących symulacji i analiz skupiających się na funkcjach zasilania i przenoszenia, takich jak analiza czułości przepłukiwania pompy strumieniowej, pokazująca, że położenie pompy strumieniowej zamontowanej w skrzydle może mieć duży wpływ na jej działanie. Dodatkowo modeluje się i symuluje dwuścienny skrzydło, aby wykazać, że dodatni kąt dwuścienny korzystnie wpływa na transfer paliwa i pomaga zminimalizować nieużyteczne ilości paliwa. Wyniki pokazują również, w jaki sposób narzędzia obliczeniowe, takie jak Simscape Fluids, można zintegrować z MATLAB-em i wykorzystać w modelowaniu systemu, zapewniając odniesienie do projektowania układów paliwowych małych samolotów i podejście do analizy skomplikowanych układów nieliniowych

Słowa kluczowe: Układ paliwowy statku powietrznego, modelowanie systemu, Simscape

1. Introduction

An aircraft fuel system is a critical and complex system which is responsible for several functions that ensure the aircraft's reliability, safety, and high performance. Although the fuel system might seem simple, it is a complex connection of fluid mechanical components which interact with each other, making it difficult for one to study it relying on fundamental laws of physics. Moreover, physical prototypes are not the best solution to analyse these systems since they

are expensive to build and test. Therefore, for clever engineering design, manufacturing and assembly processes, these systems must be modelled and simulated to support the development process, especially in the early design phase.

While the aircraft fuel system encompasses various functions, including storage, engine feed, transfer, refuelling/defueling, and jettison, this paper concentrates on the storage and transfer functions. The transfer function is of great importance for modern fuel systems since it provides a means of actively controlling the centre of gravity (CG) position, reducing the amount of bending moment felt by the wings and ensuring that the main tanks never run out of fuel. One important aspect of many fuel transfer systems is that the collector tank is kept full during all flight phases, so the feed pumps never run out of fuel, even in negative g conditions. The transfer function also allows fuel to be transferred by gravity to inner tanks by the flapper valves, also called baffle check valves, and they are responsible for letting the fuel flow in between tanks when the fuel is being consumed or replenished in the aircraft tanks.

Fuel system models have been extensively studied and applied to various problems. Many fuel system models are developed to be used as an auxiliary tool for aircraft systems design. (do Nascimento Pinheiro & Góes, 2017) describe a study that develops a simulation model to study the system's performance during pressure refuelling and single-engine operation, emphasising the importance of the system's sub-functions integration. (Li et al., 2023) studied the inerting system performance, the variation of the oxygen concentration and airflow into the tank during a complete flight envelope, proposing a method for fire prevention and explosion suppression. (Jimenez et al., 2007) developed a simulation environment in MATLAB-Simulink to study the logic of fuel management under different failure circumstances. The simulation environment provides a platform for developing an onboard fuel system management program with predefined actions for each studied failure mode. (Ellström & Gavel, 2013; Hutchison et al., 2014; Tu et al., 2022) developed methods to predict and assess pressure surges in aircraft fuel systems, discussing critical design and safety considerations. (Yue et al., 2010) analysed the heat management in a fighter aircraft fuel system through 1D thermal fluid simulations. (Feng et al., 2022) study the system's failure modes from a component-level perspective and correlate with fluid mechanical behaviour, bringing insights into the system's health management and maintenance strategies. (Liu et al., 2022) studies the ventilation system performance during the pressure refuelling process, suggesting design solutions.

(Tiwari & Harrison, 2019) proposes a method for solving flow equations for complex 3D tank geometry using a 1D flow solution.

Most of the studies assume a predefined parametrisation of the model components, so the geometrical and spatial configuration of the system components is considered fixed and, therefore, is not analysed. The aircraft fuel system is highly influenced by the wing geometry and the location of its components, and after a careful analysis of the works published in this domain, it is possible to identify some gaps, namely the absence of the wing dihedral effect on fuel transfer and the jet pump's optimisation, considering its position within the system.

This paper is intended to propose a simulation model of a fuel system that is used to assess aircraft design parameters such as the wing dihedral angle and the jet pump's location and geometry and how these variables affect the fuel system functions, namely the fuel transfer and storage. This research aims to prove the influence of the assessed parameters and expose a process of modelling a non-linear system which can later be adapted to various engineering systems. In order to achieve these goals, this document is organised as follows: Chapter 2 proposes a model for the studied system and describes the implementation of the jet pump and wing dihedral angle in the model. Chapter 3 presents some of the simulation results generated post-simulations for a typical flight envelope, highlighting the benefits of each parameter in the overall system's performance by analysing the flow rate and pressure and fuel tank level variation over time. Chapter 4 draws conclusions on the modelling approach taken, the results obtained and how this can benefit the fuel system design process.

2. System Modeling

System modelling is often required when dealing with complex systems with high non-linearity. Examples of non-linear systems that are studied through modelling and simulation are road traffic management systems (Valente et al., 2022), manufacturing processes and assembly stations (Brzozowska et al., 2023), air traffic control systems (Glover & Lygeros, 2004), wireless networks for automated factories (Ming et al., 2021), and many other engineering systems. All of these systems can be classified as non-linear, as even small changes in the input parameters can result in significant changes in the output. The fuel system on an aircraft includes a complex network of pipes, valves, elbows, joints, pumps, and other flow devices. All of these components work together in a highly interdependent

manner, resulting in intricate interactions that make the system complex and non-linear.

The model for this study was built based on the architecture presented in Fig. 1. The Simscape tool available in the Simulink environment was used to build the model which appears in Figure 2. Simscape provides a library of pre-modelled fluid system components, such as pumps, valves, lines, etc. The approach for the model development initially considered a basic feed system and gradually added more complexity while continuously checking if the simulation produced the expected values of flow rate and pressure at the engine inlet, according to the engine chosen for the aircraft. Regarding the system's parametrisation, most of the values were left at their default value, not affecting much of the final result. Components like the centrifugal and pipe pumps had their parametrisation based on datasheets from aeroplane fuel system's components suppliers.
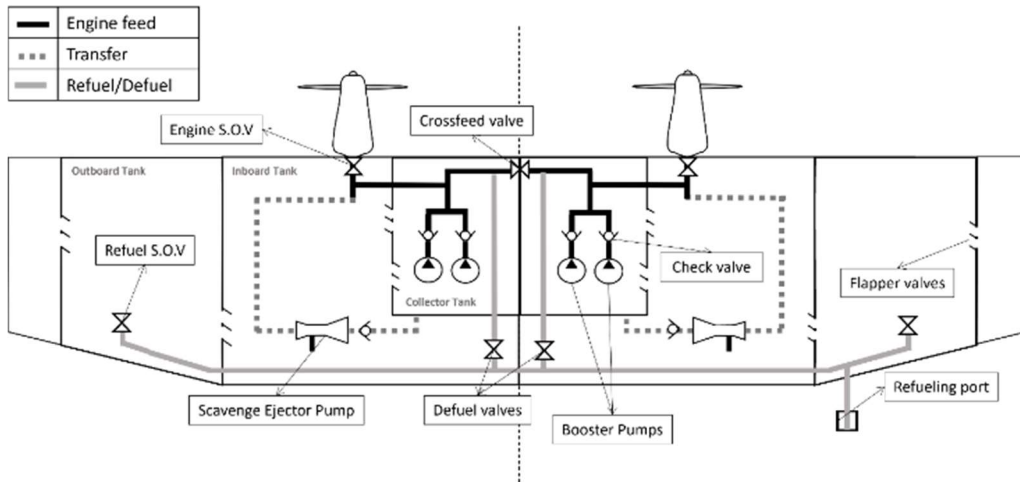

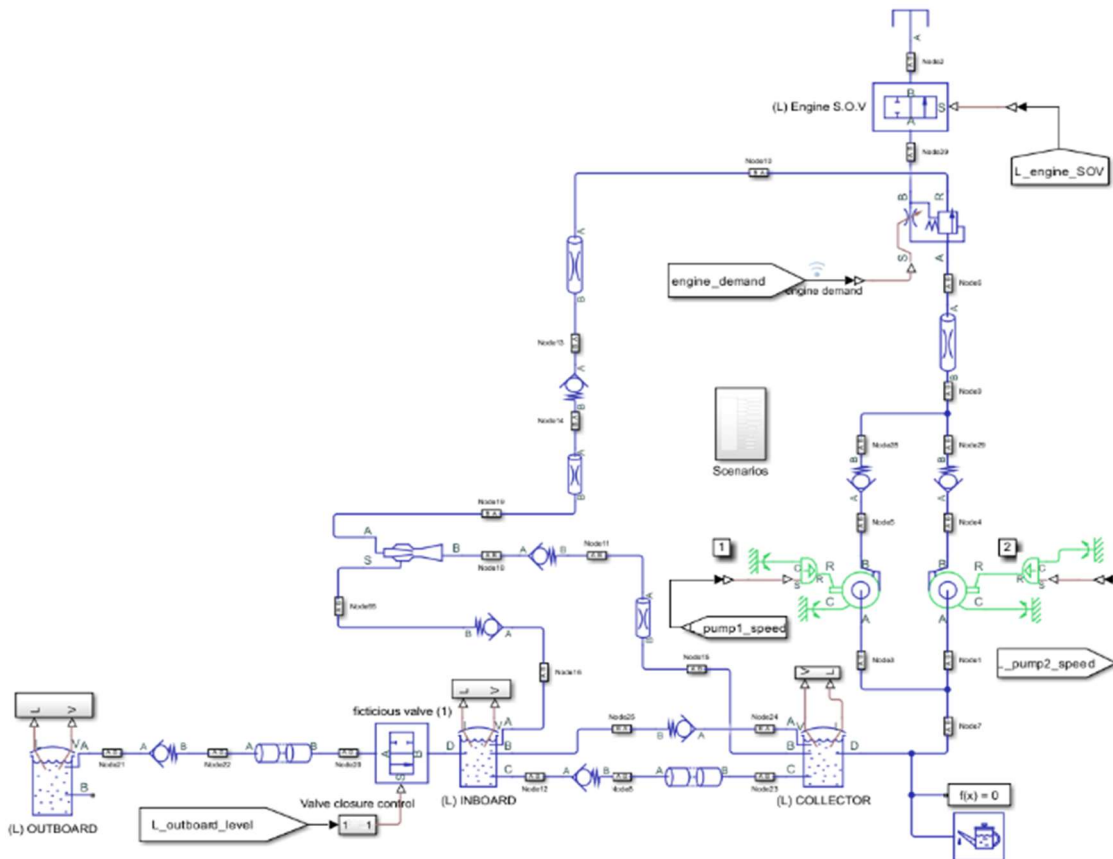Fig. 1. Fuel system reference architecture.

Fig. 2. Fuel system model in Simulink Simscape environment

The proposed architecture also aimed to eliminate some of the complexities of unnecessary functions for this study, such as jettison, refuel/defuel and venting. Given the simplified system functionality, this initial architecture considered some premises based on small civil aircraft types, such as the absence of centre tanks, Auxiliary power unit (APU) and centrifugal transfer pumps. In contrast, the system should include an outboard, inboard, and collector tank in each wing, having a scavenge jet pump at the inboard tank powered by the additional flow coming from the feed lines, transferring fuel from the inboard tank to the collector tank. The presented studies analyse mainly the fuel flow rate and pressure variations, so the components for the modelling were extracted from the Isothermal Liquid library from Simscape, neglecting the temperature variations. Since both sides of the system include the same components, the system can be considered symmetrical for normal engine feed operation, so only the left side was used to perform the simulations, as illustrated in the model from Fig. 2., resulting in reduced computational effort.

The figure shows the model of the previously presented architecture; however, the crossfeed valve component is not modelled since the system is only simulated during normal twin-engine operation. The storage part of the system consists of an outboard, inboard, and collector tanks, each one with the same height and flapper valve location. The feed function consists of a feed pipe, two booster pumps positioned in parallel for redundancy purposes, check valves, a pressure-compensated flow control valve, and an engine shutoff valve. The transfer function is also included by adding the check valves and pipe components between tanks, allowing for gravity transfer and a jet pump drawing fuel from the inboard tank and transferring it to the collector tank in every phase of the flight.

2.1. Dihedral angle

The dihedral angle is the upward angle of the wing measured from the lateral axis, shown in Fig.. It is an important parameter for the aircraft's stability since it helps bring it to its original position after rolling moment perturbations. stability since it helps bring the aircraft to its Also, in some cases, it helps give the engines a better ground clearance. In the context of a fuel system, the dihedral angle can increase the pressure difference between tanks, increasing the flow rate towards the wing root and minimising unusable fuel quantities for the same flapper valve heights.

In Simscape Fluids, the modelling of the dihedral angle Γ is not straightforward since there is no way to introduce an angle of inclination for the defined tank geometry. In this case, the modelling approach

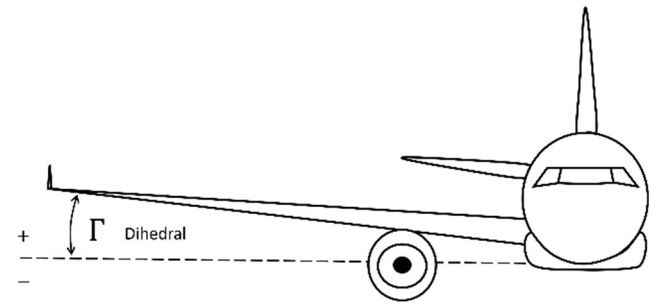considered the neighbouring tanks' centre distance L_{tank} and height difference e, as shown in Fig. 4.

Fig. 3. Dihedral angle schematic
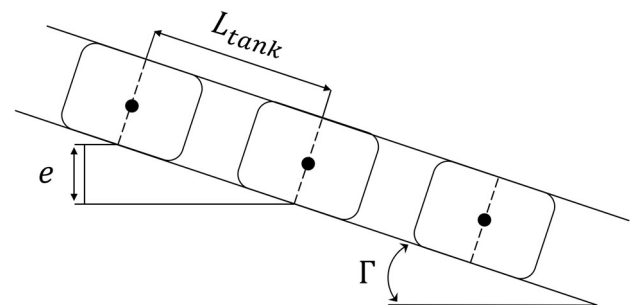
Fig. 4. Pipe elevation proposed model

To model this effect in Simscape, an elevated pipe connection was used, as demonstrated in the schematic from Fig. 5.
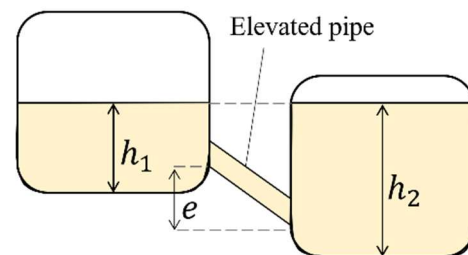
Fig. 5. Elevated pipe model approach

From Fig. 4., the equation for the pipe elevation can be expressed as:

$$e = -\sin(\Gamma) \times L_{tank} \tag{1}$$

The minus sign appears because the elevation is negative from port A to B, assumed to be the normal direction of the flow. Equation 1 was included in a MATLAB script used for the system's initialisation function, so the pipes' elevation is computed at the beginning of each simulation.

The transfer system also accounts for gravity transfer, which is done through the flapper valves. These valves represent connections between the tanks that allow flow only in the wing root direction to avoid

excessive centre of gravity (CG) variation. The flapper valves are modelled as check valves with a very low cracking pressure differential, thus allowing fuel to flow only inboards with low fuel level differences between the tanks.

2.2. Jet Pump Considerations

A jet pump, often called an ejector or eductor pump, is an extremely reliable device because it has no moving parts. This pump operates according to the venturi's effect, where the momentum of a motive fluid will be transferred to a secondary fluid, often called the induced flow, thus generating an additional flow rate at the discharge port. The jet pump's motive flow can come from several sources; in this case, the booster pumps provide more fuel than what the engines need, so part of it is bypassed and reused as the motive source. The inclusion of the jet pump in the model was mainly to ensure that while fuel is being drawn from the collector tank, it can be replenished by the inboard tank during engine feed, ensuring a constant volume during all flight phases, as required for negative g operation and to avoid booster pump's fuel starvation.

In the model, the feed line has a 3-way pressure-compensated flow control valve, which controls the flow directed to the engine and bypasses the additional flow to the motive line of the jet pump, still keeping the pressure at the required range for optimal engine operation. The motive flow will go through the nozzle area of the jet pump and create a vacuum pressure that induces fuel from the inboard tank to mix with the motive fuel flow. An important parameter that characterises the performance of the jet pump is the flow ratio, represented by:

$$M = \frac{Q_i}{Q_m} \tag{2}$$

Where Q_i and Q_m are the induced and motive flow rates, respectively. The sum of the motive and induced flow will result in the discharge flow rate Q_d, shown in Fig. 6. The presented system has the necessary components to simulate the engine feed process, which triggers the fuel transfer process. The booster pump angular velocity is assumed to be constant during the engine feed process, while the engine feed flow rate can be controlled by the flow control valve's spool position upstream of the engine interface.

3. Model Simulation and Analyses

3.1. Jet pump performance evaluation

The scavenge jet pump keeps the collector tank always full by replacing the fuel taken to feed its respective engines. This is extremely important to minimise the unusable fuel quantities and prevent

pumps from running out of fuel when in negative g conditions (when the fuel tends to move up in the tank). By isolating the collector tank, the flow requirement for keeping it always full can be expressed as follows:

$$Q_{in} \geq Q_{out} \tag{3}$$

Where Q_{in} and Q_{out} are the flow in and out of the collector cell, illustrated in Fig. 6. Considering that part of the fuel sent to the feed lines is bypassed to serve as the motive flow of the scavenge jet pump, equation 3 can be re-written as a function of the induced and feed flow rates:

$$Q_i \geq Q_{feed} \tag{4}$$

Where Q_{feed} is the fuel used to power the engines. This means that the induced flow rate from the inboard tank must be at least equal to the current engine flow rate demand. When transferring more fuel than needed, the excess flow can return to the inboard tank by a return line at the top of the collector tank.
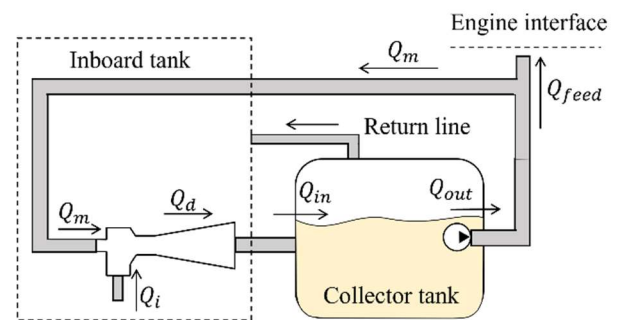
Fig. 6. Jet pump and collector tank flow balance

As mentioned before, the flow ratio is an important quantity to evaluate the jet pump's performance, as it is proportional to the jet pump's efficiency:

$$\eta = N \times M \tag{5}$$

Where N is the jet pump's pressure ratio, not discussed in the present analysis. On the other hand, the flow ratio M will be critical to ensure that the motive flow rate coming from the feed lines will produce enough induced flow to maintain the collector tank full. A sensitivity analysis was conducted to understand how the flow ratio is impacted by system variables and some of its geometric parameters. In Fig. 7., the length of the motive, suction, and discharge pipes, represented respectively by L_1, L_2, and L_3 were chosen as potentially correlated variables since they affect the pressure drop due to friction, and consequently, the pressure values at the jet pump's ports.

Fig. 7. Jet pump study variables
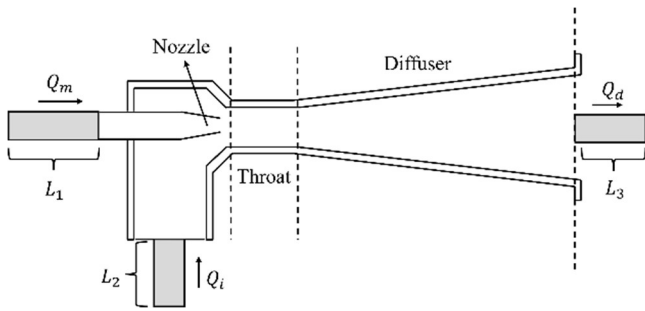
The sensitivity study considered the seven variables previously mentioned. The approach taken was to generate 50 sets of random values for each variable, uniformly distributed within a specified range. The selected variables and their respective ranges are shown in Table 1, where the variables $ratio_1$ and $ratio_2$ are the nozzle-to-throat and diffuser inlet-to-outlet area ratios, respectively.

Table 1. Parameter range specification for random value generation

Parameter	Min	Max	Type of Distribution
Nozzle area (m^2)	1e-5	1e-4	
$ratio_1$	0.1	0.4	
$ratio_2$	0.1	0.4	
L_1 (m)			Uniform
L_2 (m)	0.01	2	
L_3 (m)			
Eng. demand (L/min)	0.8	5.3	

The first study considered 50 simulations with randomised values for each variable. Then, the flow ratio was calculated in each simulation and plotted against each variable. A line obtained from the data linear regression was overlayed to visualise the correlation between variables. The plots in Fig. 8. show that the flow ratio ranges from almost zero to around 0.8, indicating a high variability.

From the plots, the only correlation evidence was found in the nozzle area plot, where the linear fit indicates a strong negative correlation between the flow ratio and the jet pump's nozzle area. In fact, a smaller nozzle area can be beneficial to increasing the flow ratio, though it is expected to increase the pressure at the nozzle entry, thus reducing the amount of flow coming from the feed line.

Although the remaining six parameters did not show any clear correlation with the flow ratio, it probably happened because the flow ratio's strong impact has hidden the influence of other parameters, so a second study was performed. The second case excluded the nozzle area from the analysis by fixing its value at the best option from the previously specified range, 10^{-5} m^2. For the second study, 50 new sets of values were generated for each variable, and after the simulations, the nozzle-to-throat ratio has shown itself to be more relevant than in the previous simulation. Fig. 9. shows the plots from the second sensitivity study, and the flow ratio fluctuated between approximately 0.9 and 2.4, still showing a high variability.
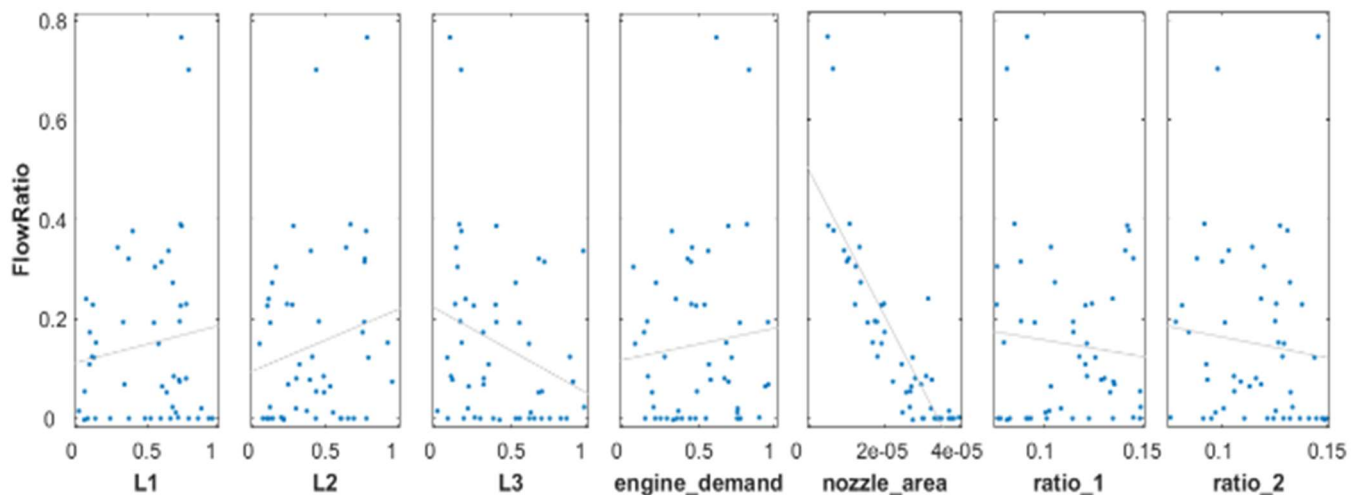

Fig. 8. Sensitivity analysis of the flow ratio considering all 7 study variables
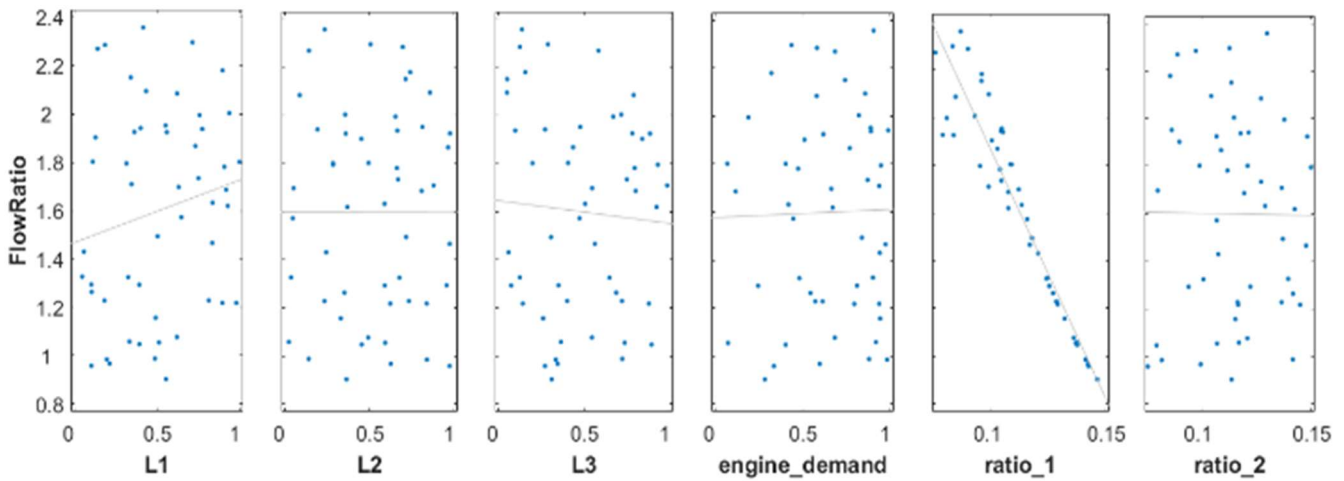
Fig. 9. Sensitivity analysis with 6 variables, neglecting
the nozzle area influence

So far, the most influential parameters were the geometric variables of the jet pump's component. Although the other variables do not show any evident correlation with the system's output, the high variability of the flow ratio motivated a third study, excluding the variability of $ratio_1$. The nozzle-to-throat ratio was set to its best value from the specified range, 0.1 for the next study, and the results appear in Fig. 10. The plots show that the flow ratio ranges approximately from 1.9 to 3.1, but most of the values appear between 1.9 and 2.5. The higher values of the flow ratio resulted from the lowest values of L_1, L_2, and L_3, which agrees with the hypothesis that the pressure drop in the lines affects the amount of flow drawn from the inboard tank. Although this hypothesis may sound obvious, the lengths of the lines have different impacts on the system's output. Unlike in the previous studies, this analysis shows evidence of two correlated variables: the discharge line length L_3 and suction line length L_2. The motive line length L_1 did not show any influence over the flow ratio results, demonstrating that the pressure drop at each section of the system will have different impacts, and in this case, placing the jet pump closer to the collector tank's inlet is the best option.
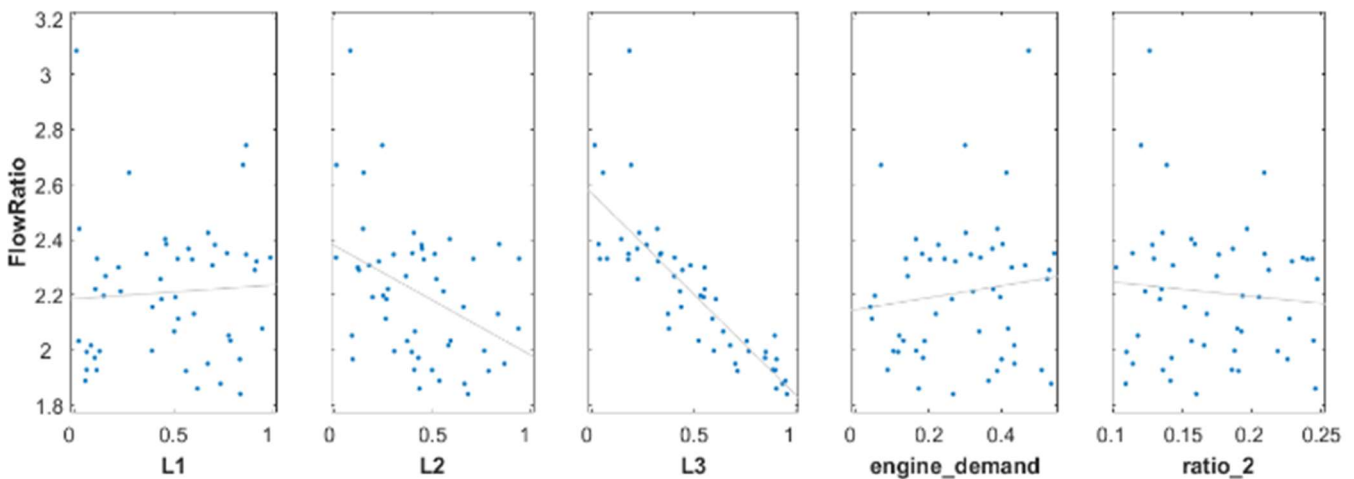
Fig. 10. Sensibility analysis with the 5 remaining variables

As per the previous analyses, it became evident that a careful study of the placement of the jet pump can greatly benefit in achieving an optimised jet pump performance, namely a higher flow ratio. In this scenario, where the flow ratio must be high enough to maintain the collector tank at its maximum capacity, the strategy for optimising its performance should involve placing it as close as possible to the collector tank, minimising the pressure drop in the lines and keeping the nozzle area at a lower value. The study

also indicates that the engine demand does not significantly influence the flow ratio. Therefore, the flow ratio during flight is expected to remain constant regardless of the fuel consumption rate.

3.2. Dihedral angle effect on fuel transfer

The fuel transfer function is highly integrated into the storage and feed function and is an essential part of the fuel management task. Besides the scavenge jet pump, gravity can also transfer fuel through the flapper valves, used during engine feed and refuelling/defueling operations. In this study, the effect of the dihedral angle is analysed during the engine feed process.

During engine feed, the fuel is drawn from the collector tank and pressurised to the feed lines, while the excess fuel is redirected to the motive port of the jet pump, thus allowing the fuel to be replenished in the collector tank. Over time, the inboard tank level will decrease, creating a height difference between the outboard and inboard tanks. In this situation, the flapper valves allow fuel to be transferred from the outboard tank to the inboard tank when there is enough head difference to overcome the valve's cracking pressure. In the proposed configuration, the objective is to empty the outboard tank first, considering the absence of a scavenge jet pump within the outboard tank. To understand the impact of the dihedral angle on the fuel transfer, the engine feed process was simulated by inputting a simplified engine consumption signal based on a typical mission profile, as shown in Fig. 11. The first analysis considered zero dihedral, so the fuel transfer happened only because of the head difference created by the fuel consumption itself. Fig. 12. shows that the collector tank is kept full during all phases of the flight, as expected. In addition, as the inboard tank fuel level decreases, the head difference between the outboard and inboard tanks increases until the flapper valve opens, allowing fuel at the outboard tank to migrate toward the wing root.
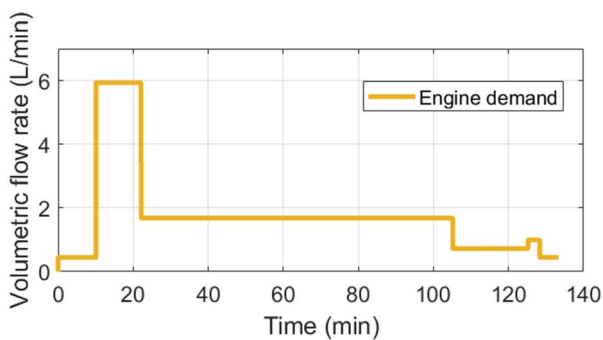

Fig. 11. Engine demand for a simplified typical flight envelope
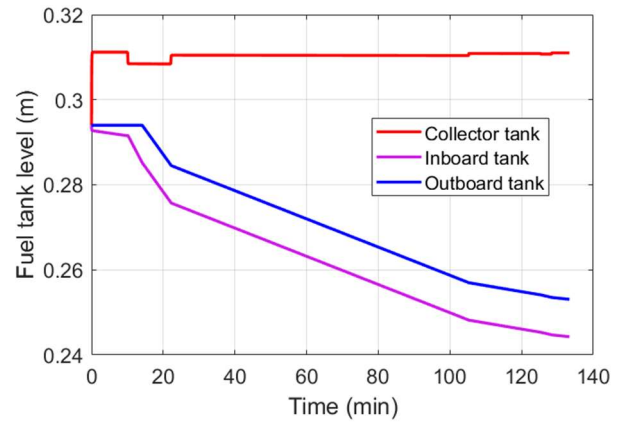

Fig. 12. Fuel tank levels for zero dihedral configuration

However, the inboard tank level is always below the outboard tank, suggesting that in the long run, the inboard tank will empty first, leading to a high amount of unusable fuel at the outboard tank, which will no longer be transferable to the collector tank.

A second simulation was performed, with the same configuration but adding 2 degrees of dihedral to the wings. Fig. 13. demonstrates that adding a dihedral increases the head difference between outboard and inboard tanks, thus making the outboard empty first. From the plot, it can be seen that, initially, the tanks have the same level as in the previous simulation, but in a short time interval, the levels reach another equilibrium position, and this is because now there is a pipe elevation between the tanks. In addition, the collector tank level has a higher value because the dihedral also influences the available fuel pressure at the jet pump's suction inlet, resulting in an increased transfer flow into the collector tank.

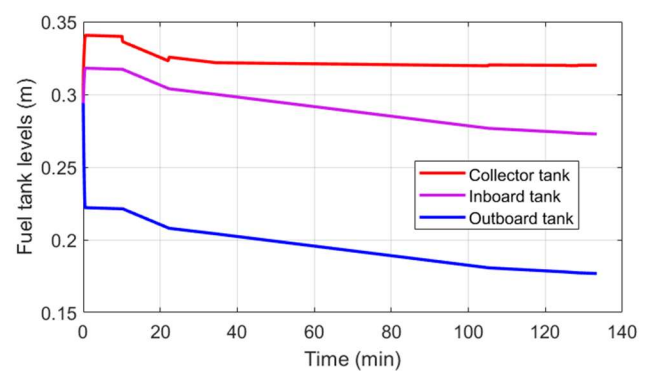**Fig. 13.** Fuel tank level for 2 degrees of wing dihedral

The previous simulations show that, although the dihedral angle is often mentioned in the aerodynamics and stability context, this variable can influence the amount of unusable fuel in the outboard tank, especially in architectures where not all tanks have a scavenge ejector pump. For the zero dihedral configuration, an additional jet pump may be needed.

4. Conclusions and future works

This paper proposed a reference architecture and simulation model of a typical small aeroplane fuel system to aid the fuel system design during the product development process, especially during the preliminary design phase. With the proposed architecture, a modelling approach for fuel system was adopted and the dihedral angle effect on the model was discussed. Within Simulink, simulations related to the fuel transfer function were performed, where the jet pump performance and dihedral angle effects on the system were analysed. The obtained results from the simulations have shown that the nozzle area, suction and discharge line lengths are strongly correlated with the resulting jet pump's flow ratio. These results demonstrate that the jet pump is influenced by the distance it is placed from the discharge and suction ports. With this, it can be concluded that the jet pump should be placed as close as possible to the collector tank for optimising its efficiency. Additionally, a second study was conducted, where the dihedral angle proved to be significant for fuel transfer, directly affecting the order in which the fuel tanks empty, thus the number of jet pumps required in the fuel system architecture.

The fuel system model presented in this paper was explored in terms of simulation to highlight its capabilities inside the Simulink environment and show how complex and non-linear systems can be modelled using the physical library from Simscape. The obtained results are consistent with the ones available in the literature, and, therefore, the presented methods and simulation results can provide a reference for smaller aircraft fuel system design. Moreover, the sensitivity analysis of the jet pump demonstrated a statistical method for studying complex systems and/or components, and it must serve as a reference for other works which deal with engineering systems.

This work demonstrated one of the possible approaches when modelling and simulating an aircraft fuel system. It would be interesting, for future works, to improve the accuracy of the developed model, since the present version has been developed purely based on previous works which used the physical modelling software. Additionally, the model considered some simplifications, such as neglecting temperature variations, heat transfer effects, and the gas phase inside the fuel tanks, creating some constraints regarding the range of possible analysis. Future work can also be dedicated to integrating the existing system model with the control and automation system, where the valves and pumps can be controlled automatically to respond to new scenarios conditions.

References

1. Brzozowska, J., Gola, A., & Kulisz, M. (2023). Problems of forecasting the length of the assembly cycle of complex products realized in the MTO (make-to-order) model. *Technologia i Automatyzacja Montażu*, *121*(3), 13–20. https://doi.org/10.7862/tiam.2023.3.2.

2. do Nascimento Pinheiro, N. R., & Góes, L. C. S. (2017). Modeling and simulation of a single engine aircraft fuel system. *Proceedings of 15: Th Scandinavian International Conference on Fluid Power, June 7-9, 2017, Link{\"o}ping, Sweden*, 45–50.

3. Ellström, H., & Gavel, H. (2013). Simulation of Cavitation and Pressure Surge: An Engineering Approach. *Journal of Aircraft*, *50*(4), 1038–1045. https://doi.org/10.2514/1.C031886.

4. Feng, D., Jiang, C., Lu, M., Li, S., & Ye, C. (2022). Simulation of One Aircraft Fuel Supply System Based on AMESim. *2022 14th International Conference on Measuring Technology and Mechatronics Automation (ICMTMA)*, 812–818. https://doi.org/10.1109/ICMTMA54903.2022.00166.

5. Glover, W., & Lygeros, J. (2004). A Stochastic Hybrid Model for Air Traffic Control Simulation. *International Workshop on Hybrid Systems: Computation and Control*, 372–386. https://doi.org/10.1007/978-3-540-24743-2_25.

6. Hutchison, M., Lenoble, G., Badiali, U., Sommerer, Y., Verseux, O., & Desmet, E. (2014). Jet Engine Fuel System Integration in Aircraft Environment - Methodology for Pressure Surge Simulation through Model-Based System Engineering. *SAE International Journal of Aerospace*, *7*(1), 2014-01–2135. https://doi.org/10.4271/2014-01-2135.

7. Jimenez, J.F., Giron-Sierra, J.M., Insaurralde, C., & Seminario, M. (2007). A simulation of aircraft fuel management system. *Simulation Modelling Practice and Theory*, *15*(5), 544–564. https://doi.org/10.1016/j.simpat.2007.01.007.

8. Li, C., Yang, H., Liu, S., Feng, S., Xu, L., & Wang, Z. (2023). Performance Analysis and Optimization of Fuel Tank Ground-Based Washing Inerting on Unmanned Aerial Vehicles. *Aerospace*, *10*(3), 244. https://doi.org/10.3390/aerospace10030244.

9. Liu, M., Wang, Z., & Ren, J. (2022). Study on impact pressure and ventilation capability of aircraft pressure refueling system. *CSAA/IET International Conference on Aircraft Utility Systems (AUS 2022)*, 745–750. https://doi.org/10.1049/icp.2022.1653.

10. Ming, W. H., Hawari, M. Z. K., & Apandi, N. I. (2021). Mathematical modeling on application of wireless networks for industrial automation-factory automation. *Journal of Physics: Conference Series*, *1988*(1), 012024. https://doi.org/10.1088/1742-6596/1988/1/012024.

11. Tiwari, A., & Harrison, J. (2019). Simulation of Aircraft Fuel System with Complex 3D Tank Geometry Using a 1D Flow Solution. *AIAA Propulsion and Energy 2019 Forum*. https://doi.org/10.2514/6.2019-4360.

12. Tu, Y., Chen, X., Yin, L., Zheng, Q., & Zeng, Y. (2022). Numerical Study on Pipeline Pressure Surge of the Large Aircraft Fuel System. *Shock and Vibration*, *2022*, 1–13. https://doi.org/10.1155/2022/7529857.

13. Valente, E., Avram, C., Astilean, A., & Machado, J. (2022). A systematic approach for microscopic models based on cellular automata for road traffic. *Technologia i Automatyzacja Montażu*, 14–27. https://doi.org/10.7862/tiam.2022.1.2.

14. Yue, Z., Guiping, L., Yi, T., & Mao, X. (2010). Conceptual Design and Dynamic Simulation of Thermal Management for Fighter Aircraft Fuel System. *AIAA Modeling and Simulation Technologies Conference*. https://doi.org/10.2514/6.2010-8087.

Original Research

MECHANICAL MIXING AND DEAERATION STATION FOR ADHESIVE COMPOSITIONS

STANOWISKO DO MECHANICZNEGO MIESZANIA I ODPOWIETRZANIA KOMPOZYCJI KLEJOWYCH

Izabela MITURSKA-BARAŃSKA[1],*

[1] Lublin University of Technology, Faculty of Mechanical Engineering, Department of Computerization and Production Robotization, Nadbystrzycka 36, 20-618 Lublin, Poland

* Corresponding author: i.miturska@pollub.pl

Abstract

This paper presents the design of a specialised mixing and deaeration station for adhesive compositions. The aim of the work was to present a device for simultaneous mixing and gas bubble removal, as well as to verify the correctness of the practical application of the station by conducting experimental tests. In the experimental research, the subject of the study was an adhesive composition of the Epidian 5 epoxy resin with the PAC curing agent, which was prepared using four mixing methods carried out with the use of the station for simultaneous mixing and deaeration. The first mixing variant (V1) consisted of mixing the adhesive composition with a paddle mixer at 1170 rpm for 3 minutes, while in the second variant (V2) mixing was carried out with a dispersing disc mixer at 1170 rpm for 3 minutes. The third variant (V3) of mixing was carried out as variant 2, except that the adhesive composition was subjected to deaeration during mixing, while variant 4 (V4) additionally used deaeration of the composition after the mixing process for 2 minutes. The tested adhesive composition was physically modified by adding particles of calcium carbonate $CaCO_3$ to verify the correct mixing of the composition components. The prepared samples were subjected to tensile and compressive strength tests. The structure of the prepared samples was also analysed using scanning electron microscopy (SEM). The tests carried out showed that the stand for simultaneous mixing and deaeration of adhesive compositions meets the expectations set for it. Mixing variant 4, in which mixing was realised using a dispersing disc mixer, proved to be the most favourable mixing method. Mixing was carried out at a speed of 1170 rpm for 3 minutes. In addition, during the mixing process, a deaeration process of the mixed composition was carried out, as well as deaeration was realised after the mixing process in a time of 2 minutes. Changing the mixing parameters contributed to an increase in both the tensile strength and compressive strength of the tested compositions. SEM analysis of the observed samples showed that changing the mixing parameters reduced the amount of air bubbles in the adhesive structure and, in the case of modified compositions, resulted in a better distribution of the filler in the structure of the mixed compositions.

Keywords: mixing, adhesive process, adhesive composition, SEM

Streszczenie

W niniejszej pracy przedstawiono projekt specjalizowanego stanowiska do mieszania i odpowietrzania kompozycji klejowych. Celem pracy była prezentacja urządzenia do jednoczesnego mieszania i usuwania pęcherzy gazowych, a także sprawdzenie prawidłowości praktycznego zastosowania stanowiska przez przeprowadzenie badań doświadczalnych. W badaniach doświadczalnych przedmiotem badań była kompozycja klejowa żywicy epoksydowej Epidian 5 z utwardzaczem PAC, którą przygotowano z zastosowaniem 4 sposobów mieszania realizowanych z użyciem stanowiska do jednoczesnego mieszania i odpowietrzania. Pierwszy wariant mieszania (V1) polegał na mieszaniu kompozycji klejowej mieszadłem łopatkowym z prędkością 1170 obr/min w czasie 3 minut, w drugim wariancie (V2) mieszanie realizowano z zastosowaniem mieszadła tarczowego dyspergującego z prędkością 1170 obr/min w czasie 3 minut. Trzeci wariant (V3) mieszania był realizowany tak jak wariant 2, z tym że kompozycję klejową poddano odpowietrzaniu w trakcie mieszania, natomiast w wariancie 4 (V4) zastosowano dodatkowo odpowietrzanie kompozycji po procesie mieszania w czasie 2 minut. Badaną

kompozycję klejową poddano fizycznej modyfikacji poprzez dodanie cząsteczek węglanu wapnia CaCO$_3$ celem weryfikacji poprawności zmieszania składników kompozycji. Wykonane próbki poddano badaniom wytrzymałości na rozciąganie i ściskanie. Analizowano również strukturę wykonanych próbek z zastosowaniem skaningowej mikroskopii elektronowej. Przeprowadzone badania wykazały, że stanowisko do jednoczesnego mieszania i odpowietrzania kompozycji klejowych spełnia stawiane mu oczekiwania. Najkorzystniejszym sposobem mieszania okazał się 4 wariant mieszania, w którym mieszanie zrealizowano z użyciem mieszadła tarczowego dyspergującego. Mieszanie realizowano z prędkością 1170 obr/min w czasie 3 minut. Dodatkowo w trakcie mieszania przeprowadzano process odpowietrzania mieszanej kompozycji, jak również odpowietrzanie realizowano po procesie mieszania w czasie 2 minut. Zmiana parametrów mieszania przyczyniła się do wzrostu wytrzymałości zarówno na rozciąganie, jak i wytrzymałości na ściskanie badanych kompozycji. Analiza SEM obserwowanych próbek wykazała, że zmiana parametrów mieszania pozwala zmniejszyć ilość pęcherzy powietrza w strukturze kleju, a w przypadku kompozycji modyfikowanych spowodowała lepsze rozprowadzenie napełniacza w strukturze mieszanych kompozycji.

Słowa kluczowe: mieszanie, proces klejenia, kompozycja klejowa, SEM

1. Introduction

Bonding technology is a fundamental part of many areas of industry and everyday life. Its importance stems from its ability to combine a variety of materials into durable joints, which contributes to production efficiency, product durability and innovation. The bonding process is a complex technological process that involves several steps. Among the main stages of the bonding process are: preparation of the surfaces of the parts to be joined, selection of the appropriate adhesive, preparation of the adhesive and the method of application, setting and assembling of the parts to be joined, curing of the adhesive joint, inspection of the joints and finishing operations. Various instruments and equipment are often used to carry out both the main bonding steps and the numerous intermediate operations. These are often dedicated special or specialised tools for specific applications.

An extremely important step in the bonding process is the adhesive preparation process, as it affects the quality and performance of the bonding. The correct preparation of the adhesive composition is the key to achieving a durable and reliable joint. The adhesive composition preparation procedure has a direct impact on the degree of dispersion of the composition components in the matrix, as well as on the degree of aeration of the resulting composition. The strength and performance properties of the final material depend on these parameters, so the proper mixing of the adhesive components is critical to the joining process (Godzimirski, 1997; Miturska-Barańska, 2022).

The preparation of an adhesive depends mainly on its form (Cognard, 2006). Structural adhesives in solid or liquid form are usually two or more component compositions, the components of which need to be mixed into homogeneous substances in order to fully perform their functions. In the case of two-component adhesives, care must be taken to ensure that all of its components are properly combined to form a homogeneous adhesive mixture (Axentowicz & Karpiński, 1994; Ebnesajjad, 2008). It is also important to ensure that there are no air bubbles in the adhesive composition, as this is undesirable and can cause non-adhesive bonding of the materials to be bonded, as well as affecting the strength of the adhesive joint (Katnam et al., 2011; Michels et al., 2016). In addition to the basic component, auxiliary substances such as solvents, activators or catalysts for the crosslinking process, curing agents and other additional components are sometimes required. Sometimes, the components of multi-component adhesive compositions include modifying additives, called fillers or modifiers. Primary filler particles in non-agglomerated form are extremely rare under real-world conditions. The occurrence of agglomerates of particles in the matrix can cause defects that result in a reduction in the properties of the modified adhesive, so it is important to select a suitable method of mixing the adhesive composition that will enable the required dispersion of particles to be achieved and their proper wetting by the matrix material (Chikhi et al., 2002; Miturska et al., 2020, 2021). Both manual and mechanical methods are used in the mixing operation, using appropriate tools and equipment. For different types of production, the process can be automated, using appropriate devices, tools or equipment (Rudawska, 2016).

The mixing process for multi-component adhesives is usually carried out using special equipment and stations designed for this purpose. Currently, many design variations of mixers are known. The variety is much greater than for other equipment used in bonding technology (Habenicht, 2009; Kamieński, 2004; Miturska-Barańska, 2022; Rudawska, 2019).

In this paper, the design of a specialised mixing and deaeration station for adhesive compositions is presented. The aim of the study was to present a device for simultaneous mixing and removal of gas bubbles and to verify the correctness of the practical application of the stand by conducting experimental tests. In the experiments, the subject of the study was an adhesive composition of Epidian 5 epoxy resin with

a PAC curing agent, which was prepared using four mixing methods carried out with the use of a stand for simultaneous mixing and deaeration. In addition, the composition was physically modified by adding particles of calcium carbonate $CaCO_3$ to verify the correct mixing of the composition components.

2. Concept and construction of a mixing and deaeration station for adhesive compositions

The paper presents the construction of a mixing and simultaneous deaeration station for multi-component adhesive compositions, in which the most important part is the working part of the station, hereinafter also referred to as the device. A pre-requisite for the correct functioning of the station is that the construction and technological requirements affecting the construction and correctness of the adhesive mixing process are met.

2.1. Technological and operational assumptions

The designed device should fulfil specific functions and enable the reproducibility of the adhesive mixing process and, consequently, the reproducibility of the strength properties of the adhesive compositions associated with their manufacturing process. Among the technological and application assumptions adopted, the following can be distinguished:

- the possibility of mixing two or more adhesive components, e.g. resin, modifier and curing agent,
- ensuring that the adhesive mixing process is carried out repeatably,
- that the adhesive composition can be mixed and deaerated at the same time,
- making it possible to adjust the size of the mixing tank,
- that the mixing tank can be quickly cleaned or replaced,
- adaptability to any bench-top drilling machine acting as a mixer drive,
- ease and speed of operation.

The assumptions outlined above have enabled the design of a station that, when used appropriately, will improve the mixing process of adhesive compositions.

2.2. Design assumptions

Figure 1 shows a general schematic of the construction of the described station.

The detailed structure with the main components included in the working part of the adhesive mixing and deaeration device is presented in Figure 2.
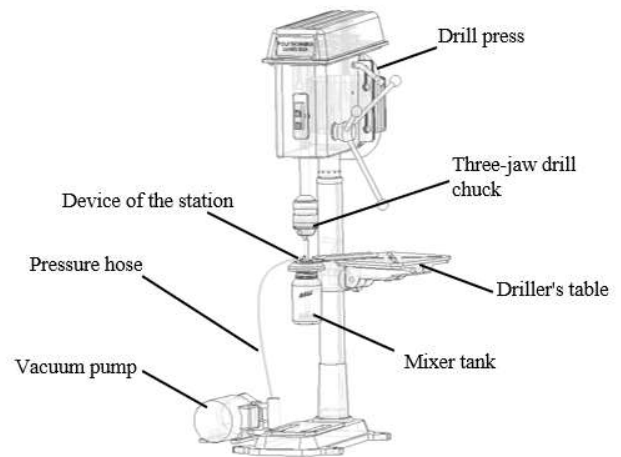

Fig. 1. Schematic overview of mixing and deaeration station for adhesive compositions
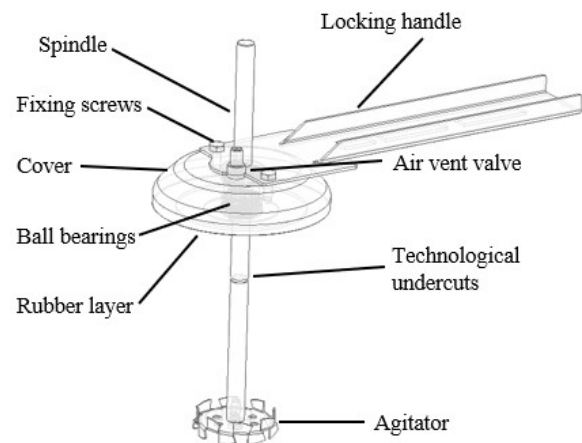

Fig. 2. Construction of a mixing and deaeration device for adhesive compositions

The mixing device consists of a cover in which a spindle is centrally mounted in three identical ball bearings with seals placed parallel to each other. The cover is semi-circular in shape and a vent valve is also fitted into it. A rubber layer is bonded onto the lower surface of the cover to ensure tightness between the cover and the mixed substance tank. The original design concept included the idea of making a thread in the lower part of the lid, the purpose of which would be to fix the mixing tank. However, this solution did not meet the assumption of tightness between the lid and the tank, so that the deaeration process did not proceed correctly. A locking handle, made from a section of sheet metal, is attached to the top of the cover. Rectangular holes are made in the locating handle to allow the handle to be fixed to the drill table. Technological undercuts are made on the spindle to allow the length of the agitator to be locked in place with a circlip. An agitator of any shape is screwed onto the lower part of the spindle. The design of the unit makes it compatible with any type of drill press

equipped with a three-jaw self-clamping chuck, so it is characterised by its ability to be quickly mounted and dismounted. The design of the device also allows the agitator to be changed depending on the properties of the adhesive composition to be mixed.

Among the design considerations of the adhesive mixing and deaeration device, it was assumed that the adhesive mixing tank is made of glass, so that it is not exposed to the negative pressure created when deaeration the composition as are commonly available tanks made of plastic. The cover was made of aluminium alloy, while the other components were made of stainless steel, making it possible to wash all components with cleaning agents.

2.3. Operation of the device for simultaneous mixing and deaeration of the adhesive composition

The operation of the adhesive composition mixing and deaeration device is based on fastening the locating handle to the drill table using a screw. The spindle, on the other hand, is fixed in a self-clamping drill chuck. The design of the device allows the spindle to rotate at the speed set in the drill settings. A air vent valve fitted in the cover allows the mixed substances to be deaerated, also during the mixing process by connecting to the vacuum pump via a pressure hose. The technological undercuts on the spindle make it possible to adjust the working length of the spindle and the agitator mounted on it by means of a locking ring, depending on the size of the tank in which the mixing process is carried out. The size of the tank, on the other hand, depends on the amount of substance to be mixed. The vessel must be supported during mixing, as it is only held by the vacuum applied.

3. Experimental studies

In order to verify the correctness and validity of the presented station for simultaneous mixing and deaeration of adhesive compositions, experimental tests were carried out. Within the scope of these tests, adhesive compositions were prepared using 4 mixing variants differing in terms of the parameters used, which were then subjected to strength tests

3.1. Materials used in the study

Epidian 5 epoxy resin and PAC curing agent were used to make the adhesive compositions. In addition, modified adhesive compositions were also produced, to which 5% $CaCO_3$ calcium carbonate was added, in order to check the distribution of the modifier particles in the adhesive structure when using different mixing variants.

The matrix function in the tested adhesive compositions was performed by the Epidian 5 epoxy

resin. This is a pure form of epoxy resin, which is a product of the reaction of bisphenol A with epichlorohydrin. It has excellent adhesion to most plastics, chemical resistance, as well as resistance to aggressive environmental factors and good electrical properties (*BN- 89 6376-02*; *Information catalogue of Ciech S.A.*, Czub & Penczek, 2002; Yoon et al., 2011). Epidian 5 epoxy resin and compositions based on it are used in the manufacture of fibreglass laminates, bonding metals, ceramics and thermosetting plastics. Adhesives prepared on the basis of this resin are also used in building structures as anti-corrosion and electro-insulating coatings.

The curing agent used in the study was polyamide PAC curing agent. PAC curing agent is a mixture of fatty acids, C18-unsaturated, dimers, polymeric reaction products with triethylenetetramine. It is used to cure liquid epoxy resins. This curing agent increases the elasticity and impact strength of the composition and is therefore used for joints subject to deformation. The PAC curing agent belongs to the group of slow-reacting hardeners and, as an indication, its use time can be taken at room temperature - 180 minutes. This is followed by an initial hardening in a further 6-8 hours to achieve an approx. 80-90% hardening after 72 hours. Complete curing is achieved after 7-14 days.

The basic physical and chemical properties of the adhesive components used are summarised in Table 1.

Table 1. Physical and chemical properties of the adhesive compositions components used in the study (Bereska et al., 2014; *BN-89 6376-02*; *Information catalogue of Ciech S.A.*; Czub & Penczek, 2002; Królikowski & Rosłaniec, 2004)

Properties	Epidian 5 epoxy resin	PAC curing agent
Epoxy number (resin) / Amine number (curing agent)	0.48 – 0.52 mol/100 g	290 – 360 mg KOH/g
Viscosity at 25ºC	20 000 – 30 000 mPa·s	10 000 – 25 000 mPa·s
Density at 20°C	1.16 g/cm³	1.10 – 1.20 g/cm³

The filler used in the study was $CaCO_3$ calcium carbonate. The calcium carbonate used in the study was produced by Zakłady Przemysłu Wapienniczego Trzuskawica S.A. in Siatkówka and has a molecular weight of 100.09 g/mol with particle size ≤ 5 μm (at least 99%). The typical concentration of $CaCO_3$ is 98.23%, while the concentration range is between 92-99%. Calcium carbonate is widespread in nature, being a basic component of many minerals (e.g. calcite and aragonite), as well as some rocks (dolomite, chalk and coral). The use of chalk as a modifying additive in appropriate proportions, which according to the literature (He i in., 2011; Jin & Park, 2008; Kacperski, 2004; Park, Su-Jin, 2009; Zebarjad & Sajjadi, 2008)

are in the range of 2-8 parts by weight, alters certain physical properties. The use of calcium carbonate $CaCO_3$ in adhesive compositions allows, among other things: to increase bending strength (Kacperski, 2004; Miturska i in., 2020), to increase impact strength (Miturska et al., 2021; Miturska & Rudawska, 2020) and to improve the thermal stability of the composition (Park, Su-Jin, 2009; Zebarjad & Sajjadi, 2008).

In the tests, the adhesive compositions were mixed in the appropriate weight ratios. For 100 parts by weight of resin, 80 parts by weight of curing agent were introduced. In the case of modified compositions, the epoxy resin and modifier were mixed in the first step at a ratio of 5 parts by weight per 100 parts by weight of resin, followed by the addition of the curing agent.

Weighing of the components of the adhesive compositions was done using a KERN CKE 3600-2 laboratory balance with a measurement accuracy of ±0.01 g.

3.2. Variants for mixing adhesive compositions

The mixing method of adhesive compositions significantly affects the strength properties of the compositions produced. In the course of achieving the stated aims of the study, four mixing methods were used (Table 2).

Table 2. Parameters of the mixing variants

Mixing variant	Description of the mixing process
V1	Mixing with paddle agitator: - speed 1170 rpm, - time: 3 min.
V2	Mixing with dispersing disc agitator: - speed 1170 rpm, - time: 3 min.
V3	Mixing with dispersing disc agitator: - speed 1170 rpm, - time: 3 min. Deaeration of the composition during mixing.
V4	Mixing with dispersing disc agitator: - speed 1170 rpm, - time: 3 min. Deaeration of the composition during mixing. Deaeration of the composition after the mixing process: - time: 2 min.

Mixing of the composition was carried out using two types of agitator, differing in geometry. The first was a paddle mixer, the geometry of which is shown in Figure 3. The second type of agitator, was a dispersing disc agitator with holes and trapezoidal teeth, which geometry is presented in Figure 4.

The mixers were made according to the standards in force in this area (*BN-72/2222-06*; *BN-75/2225-06*;

BN-75/2225-07; Miturska-Barańska, 2022), so that the dimensions of the mixers were appropriate in relation to the tank in which the adhesive compositions were mixed.
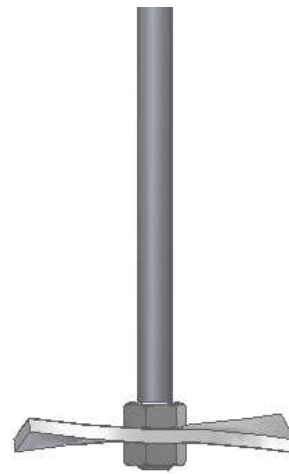
**Fig. 3.** Blade agitator used in the study   **Fig. 4.** Dispersing disc agitator used in the tests

Deaeration of the compositions during mixing was made possible by a valve fitted into the cover of the composition mixing and deaeration device. Venting was carried out using a CPS model VP6D two-stage vacuum pump.

Mixing was carried out by adapting an OPTIMUM B20 drill press. Mixing was carried out in a glass jar, thus avoiding the reaction that could occur if the composition was mixed in a tank made of polymer plastic. In addition, the glass jar facilitates thorough mixing and the deaeration process during mixing of the compositions.

After the adhesive compositions were prepared using appropriate moulds, samples of standardised dimensions were cast (Broniewski et al., 2000; *ISO 604*; *PN-EN ISO 527-1*). The geometry of the samples used during the tests is shown in Figures 5 and 6. For each composition and each mixing variant, 5 samples were prepared for testing.
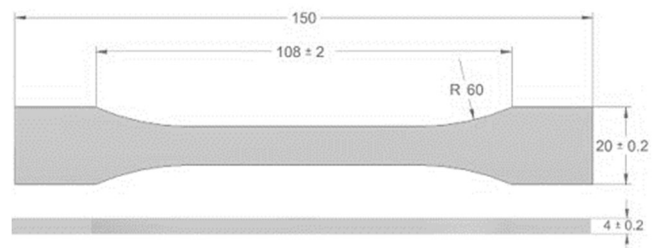
Fig. 5. Shape and dimensions of adhesive compositions sample for tensile strength testing
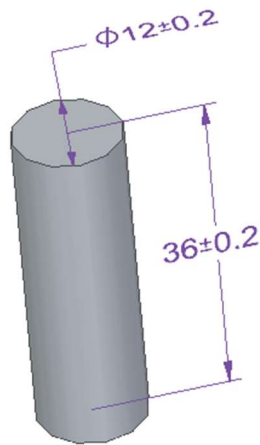
Fig. 6. Shape and dimensions of the cylindrical sample of adhesive compositions for the compressive strength tests

Samples of the epoxy adhesive compositions were prepared at a temperature of 23°C ± 2°C at an air humidity of 23% ± 3%, followed by a one-step cold curing process for a period of 7 days under unchanged conditions.

3.3. Results of strength tests

After the curing time, the samples were subjected to strength tests. Tensile and compressive strengths were tested. The tests were carried out on a Zwick/ Roell Z150 testing machine. In the tensile strength test, the crosshead travel speed during the test was 5 mm/min. For the compressive strength test, the crosshead speed used during the test was 10 mm/min. The results obtained are shown in the figure below (Fig. 7, Fig. 8).
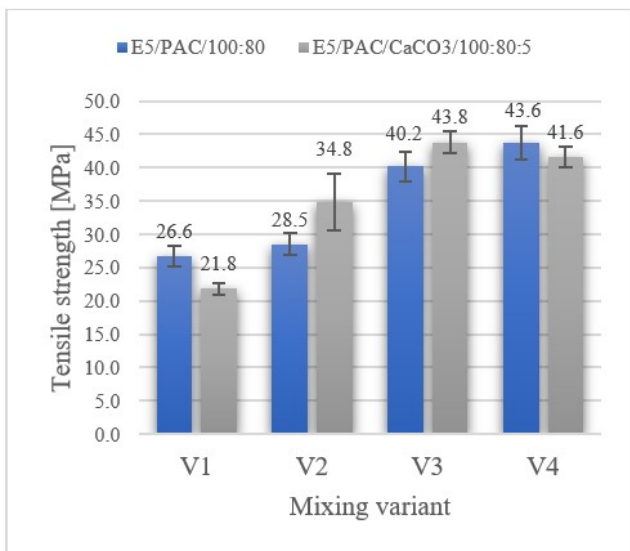

Fig. 7. Tensile strength of adhesive compositions
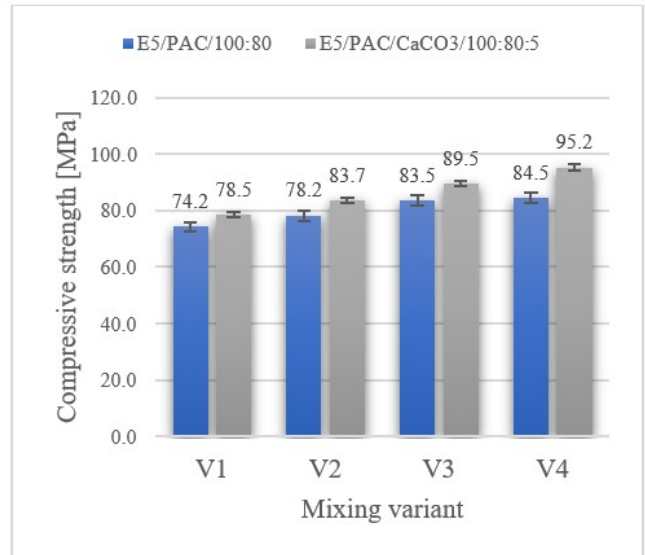

Fig. 8. Compressive strength of adhesive compositions

Due to the similar values in several groups of results obtained, a statistical analysis was carried out at a further stage of the analysis of the test results obtained. The assumption of normality of distribution for tensile strength was tested. The results of this test are summarised in Table 3.

Table 3. Normality test results for tensile strength

Adhesive composition	Mixing variant	W²	p²
E5/PAC/100:80	V1	0.9827	0.9484
E5/PAC/100:80	V2	0.9827	0.9484
E5/PAC/100:80	V3	0.9827	0.9484
E5/PAC/100:80	V4	0.9827	0.9484
E5/PAC/CaCO$_3$/100:80:5	V1	0.9340	0.6241
E5/PAC/CaCO$_3$/100:80:5	V2	0.7050	0.0108
E5/PAC/CaCO$_3$/100:80:5	V3	0.9340	0.6241
E5/PAC/CaCO$_3$/100:80:5	V4	0.9340	0.6241

[1] Statistical value W Shapiro-Wilk test
[2] Level p for the Shapiro Wilk test

From the results obtained, it can be seen that for the Shapiro-Wilk W-test, the p-value is not greater in all groups than the accepted significance level of α = 0.05 and therefore it must be assumed that the distribution does not follow a normal distribution. Therefore, non-parametric statistics parameters were used to further analyse both tensile strength and compressive strength. A post-hoc test was then per-formed to determine significant differences between the different groups of samples tested. The results of this test are presented in Tables 4-7.

Table 4. Results of post-hoc test of significant differences in average tensile strength depending on mixing variant - E5/PAC/100:80 adhesive composition

No.	Mixing variant	Tukey's HSD test; Approximate probabilities for post hoc tests Error: MS between-group = 4.1733, df = 16.00			
		{1} 26.645	{2} 28.465	{3} 40.161	{4} 43.637
1	V1		0.5122	0.0002	0.0002
2	V2	0.5122		0.0002	0.0002
3	V3	0.0002	0.0002		0.0692
4	V4	0.0002	0.0002	0.0692	

Table 5. Results of post-hoc test of significant differences in average tensile strength depending on mixing variant - E5/PAC/CaCO$_3$/100:80:5 adhesive composition

No.	Mixing variant	Tukey's HSD test; Approximate probabilities for post hoc tests Error: MS between-group = 6.0127, df = 16.00			
		{1} 21.823	{2} 34.764	{3} 43.803	{4} 41.620
1	V1		0.0002	0.0002	0.0002
2	V2	0.0002		0.0003	0.0023
3	V3	0.0002	0.0003		0.5131
4	V4	0.0002	0.0023	0.5131	

Table 6. Results of post-hoc test of significant differences in average compressive strength depending on mixing variant - E5/PAC/100:80 adhesive composition

No.	Mixing variant	Tukey's HSD test; Approximate probabilities for post hoc tests Error: MS between-group = 3.5631, df = 16.00			
		{1} 74.237	{2} 78.189	{3} 83.516	{4} 84.547
1	V1		0.0208	0.0002	0.0002
2	V2	0.0208		0.0021	0.0005
3	V3	0.0002	0.0021		0.8233
4	V4	0.0002	0.0005	0.8233	

Table 7. Results of post-hoc test of significant differences in average compressive strength depending on mixing variant - E5/PAC/CaCO$_3$/100:80:5 adhesive composition

No.	Mixing variant	Tukey's HSD test; Approximate probabilities for post hoc tests Error: MS between-group = 1.1453, df = 16.00			
		{1} 78.505	{2} 83.670	{3} 89.523	{4} 95.205
1	V1		0.0002	0.0002	0.0002
2	V2	0.0002		0.0002	0.0002
3	V3	0.0002	0.0002		0.0002
4	V4	0.0002	0.0002	0.0002	

Values marked in red indicate that there are significant differences between the analysed groups at a significance level of $p < 0.05$. Analysing the results obtained, it can be observed that, in the case of tensile strength, mixing variants 3 and 4 were significantly different from mixing variants 1 and 2 for both the basic and modified compositions. A similar distribution of results can be observed for the compressive samples. This indicates that changing the mixing conditions significantly affects the properties of the adhesive compositions.

## 3.4. SEM tests of adhesive compositions

The structure of the analysed adhesive compositions in the cured state was also studied by scanning electron microscopy (SEM) in order to assess the effect of the mixing method on the structure of the resulting composition. Figures 9-14 show SEM micrographs of the compositions studied.
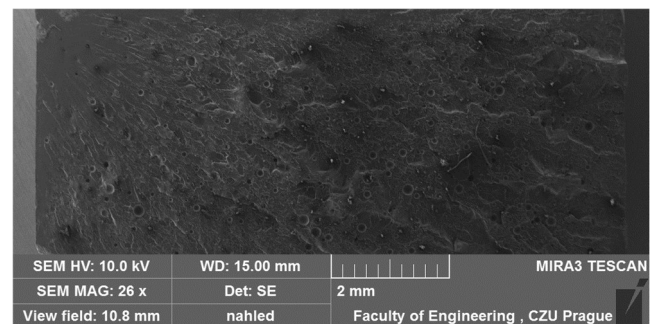
Fig. 9. SEM micrograph of unmodified E5/PAC/100:80 adhesive composition, 1st mixing variant
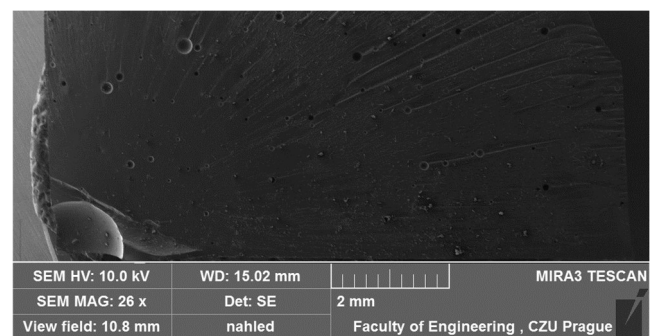
Fig. 10. SEM micrograph of unmodified E5/PAC/100:80 adhesive composition, 4th mixing variant
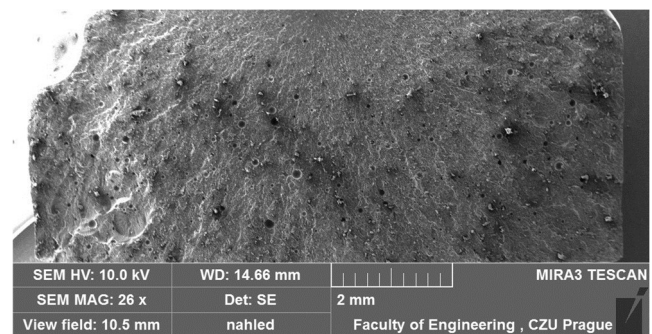
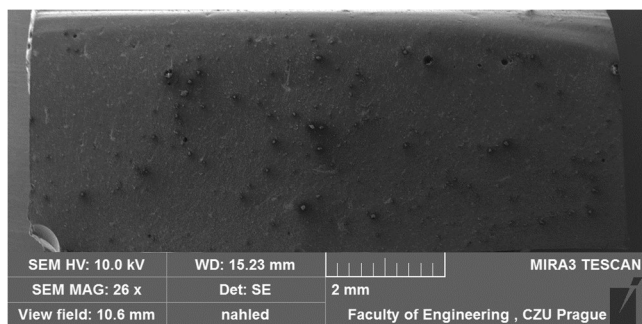**Fig. 11.** SEM micrograph of E5/PAC/CaCO$_3$/100:80:5 adhesive composition, 1st mixing variant

Fig. 12. SEM micrograph of E5/PAC/CaCO$_3$/100:80:5 adhesive composition, 4th mixing variant

Fig. 13. SEM micrograph of E5/PAC/CaCO$_3$/100:80:5 adhesive composition, 1st mixing variant

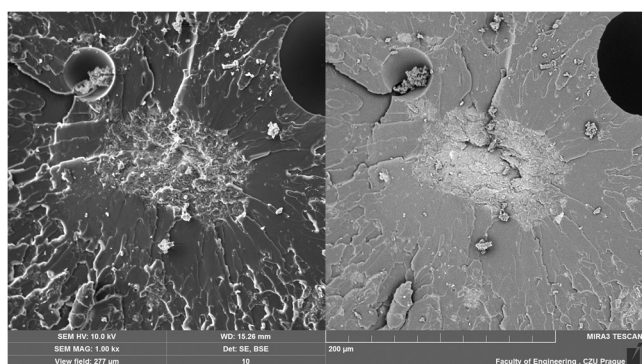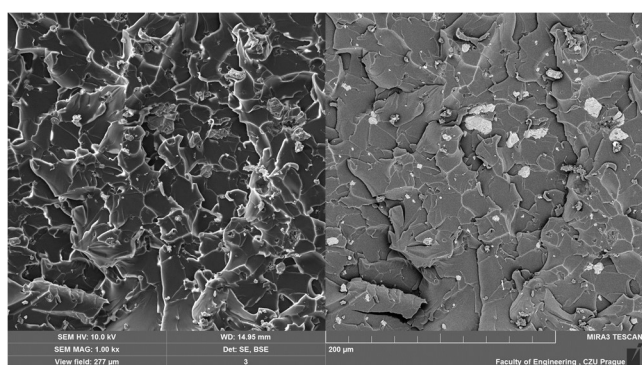**Fig. 14.** SEM micrograph of E5/PAC/CaCO$_3$/100:80:5 adhesive composition, 4th mixing variant

The presented SEM microphotographs of the tested adhesive compositions show that the process of deaeration of the composition allows the amount of gas bubbles present in the structure of the composition to be significantly reduced. Based on the photographs shown in Figure 10, it can be seen that the unmodified E5/PAC/100:80 adhesive composition mixed with the mixing variant 4 is characterised by a homogeneous, solid structure. Few gas bubbles are visible on the surface. In the case of the reference composition, the breakthrough is soft and malleable.

Analysing the SEM micrographs of E5/PAC/CaCO$_3$/100:80:5 modified composition prepared using mixing variant 4, good wettability at the filler-matrix interface can be observed, which is due to the interaction of the filler with the matrix (Fig. 14). It can also be observed that there are fewer filler agglomerates, i.e. better distribution in the structure of the mixed composition compared to the modified composition prepared using mixing variant 1 shown in Figure 13.

4. Summary and conclusions

This paper presents the design of a specialised station for mixing and venting adhesive compositions.

The research carried out shows that the station for simultaneous mixing and deaeration of adhesive compositions meets the expectations set for it. The application of mixing methods using the capabilities of the designed stand (4th mixing variant), contributed to:

- An increase in tensile strength by 39% for the unmodified composition compared to compositions prepared using the basic mixing method (mixing variant 1).
- An increase in tensile strength by 47.6% for the composition modified with 5% CaCO$_3$ calcium carbonate compared to compositions prepared using the basic mixing method (mixing variant 1).
- An increase in compressive strength by 12.2% for the unmodified composition compared to the compositions prepared using the basic mixing method (mixing variant 1).
- An increase in compressive strength by 17.5% for the composition modified with 5% CaCO$_3$ calcium carbonate compared to compositions prepared using the basic mixing method (mixing variant 1).
- A reduction in the amount of gas bubbles in the structure of the cured adhesive compositions, which can be observed by comparing the SEM micrographs shown in Figures 9 and 10, in the case of unmodified compositions - E5/PAC/100:80, and in Figures 11 and 12 in the case of compositions modified with calcium carbonate - E5/PAC/CaCO$_3$/100:80:5.
- A better distribution of the filler in the structure of the mixed compositions, as can be observed by comparing the SEM micrographs in Figures 13 and 14.

However, there are still a few gas bubbles in the adhesive structure. Perhaps extending the deaeration time would allow air bubbles to be completely removed from the adhesive, which could then have a positive effect on improving the strength properties of the adhesive joints and improving the quality of the adhesive joints.

The station designed and described in the paper has several advantages. These include:

- simple and functional design,
- ease and simplicity of operation,
- easy mixer replacement,
- the possibility of using mixers with different geometries,
- compatibility with various models of drill press acting as agitator drive,
- mixing speeds can be varied to match the capacity of the drive unit,
- possibility to mix two-component adhesives, as well as adhesives consisting of several components,
- small overall dimensions,
- construction in stainless steel and aluminium alloys eliminates the possibility of component corrosion,
- simple construction allows quick cleaning of the device,
- easy replacement of the mixer tank,
- possibility to adjust the length of the mixer to tanks with smaller and larger capacities, and thus the possibility to mix the appropriate amount of adhesive composition at one time.

The stand for simultaneous mixing and deaeration of adhesive compositions also has some limitations, although they are few compared to its advantages. Chief among these limitations is the inability to heat the adhesive or adhesive composition components during mixing.

In conclusion, the designed station fully meets the expectations set for it, and the simple design allows the station to be adapted both in laboratory, workshop and production spaces.

References

1. Axentowicz, M., & Karpiński, J. (1994). One- and two-component adhesives manufactured by Ciba-Geigy offered as Araldit 2000 and Araldit 4000. Assembly Techniques and Technologies, 2, 43–46.

2. Bereska, B., Iłowska, J., Czaja, K., & Bereska, A. (2014). Curing agents for epoxy resins. Chemical Industry, 93(4), 443–448.

3. BN-89 6376-02 – Industry standard. Epoxy resins Epidian 1, 2, 3, 4, 5, 6. (b.d.).

4. BN-72/2222-06 – Two-blade mixers (in Polish). (b.d.).

5. BN-75/2225-06 – Open steel rotor stirrers d=200÷800 mm (in Polish).

6. BN-75/2225-07 – Closed Steel Rotor Mixers (in Polish).

7. Broniewski, T., Kapko, J., Płaczek, W., & Thomalla, J. (2000). Test methods and evaluation of the properties of plastics (2nd revised edition). Scientific and Technical Publishers.

8. Chikhi, N., Fellahi, S., & Bakar, M. (2002). Modification of epoxy resin using reactive liquid (ATBN) rubber. European Polymer Journal, 38(2), 251–264.

9. Cognard, P. (Red.). (2006). Handbook of adhesives and sealants (1st ed). Elsevier.

10. Czub, P., & Penczek, P. (2002). Chemistry and technology of epoxy resins. Scientific and Technical Publishers.

11. Ebnesajjad, S. (2008). Adhesives technology handbook (2nd ed). William Andrew Pub.

12. Godzimirski, J. (1997). Structural adhesive joints of metal components in mechanical engineering. Rzeszów University of Technology Publishing House.

13. Habenicht, G. (2009). Applied adhesive bonding: A practical guide for flawless results. Wiley-VCH.

14. He, H., Li, K., Wang, J., Sun, G., Li, Y., & Wang, J. (2011). Study on thermal and mechanical properties of nano-calcium carbonate/epoxy composites. Materials & Design, 32(8–9), 4521–4527.

15. Information catalogue of Ciech S.A. - https://ciechgroup.com/produkty/chemia-organiczna/zywice/zywice-epoksydowe/ [access: 20.02.2018].

16. ISO 604 – Plastics–Determination of properties in compression.

17. Jin, F.-L., & Park, S.-J. (2008). Interfacial toughness properties of trifunctional epoxy resins/calcium carbonate nanocomposites. Materials Science and Engineering: A, 475(1–2), 190–193.

18. Kacperski, M. (2004). Preliminary study on the effect of modifier type on the properties of epoxy/bentonite nanocomposites. Composites, 9, 28–32.

19. Kamieński, J. (2004). Mixing of multiphase systems. Scientific and Technical Publishers.

20. Katnam, K.B., Stevenson, J.P.J., Stanley, W.F., Buggy, M., & Young, T.M. (2011). Tensile strength of two-part epoxy paste adhesives: Influence of mixing technique and micro-void formation. International Journal of Adhesion and Adhesives, 31(7), 666–673.

21. Królikowski, W., & Rosłaniec, Z. (2004). Polymer nanocomposites. Composites, 9(4), 3–16.

22. Michels, J., Sena Cruz, J., Christen, R., Czaderski, C., & Motavalli, M. (2016). Mechanical performance of cold-curing epoxy adhesives after different mixing and curing procedures. Composites Part B: Engineering, 98, 434–443.

23. Miturska-Barańska, I., & Rudawska, A. (2021). Possibility of increasing the strength of adhesive joints of aluminium alloy sheets in terms of epoxy adhesive modification: Experimental studies. Lublin University of Technology Publishing House.

24. Miturska, I., Rudawska, A., Müller, M., & Hromasová, M. (2021). The Influence of Mixing Methods of Epoxy Composition Ingredients on Selected Mechanical Properties of Modified Epoxy Construction Materials. Materials, 14(2), 411.

25. Miturska, I., Rudawska, A., Müller, M., & Valášek, P. (2020). The Influence of Modification with Natural Fillers on the Mechanical Properties of Epoxy Adhesive Compositions after Storage Time. Materials, 13(2), 291.

26. Miturska-Barańska, I. (2022). Mixing of multicomponent adhesive compositions. Lublin University of Technology Publishing House.

27. Park, Su-Jin. (2009). Thermal Stability of Trifunctional Epoxy Resins Modified with Nanosized Calcium Carbonate. Bulletin of the Korean Chemical Society, 30(2), 334–338.

28. PN-EN ISO 527-1 – Plastics–Determination of mechanical properties in static tension (in Polish).

29. Rudawska, A. (2019). Adhesive mixing and applying device. Technologia i Automatyzacja Montażu, 3, 42–45.

30. Rudawska, A. (2016). Instrumentation in bonding technology. Lublin University of Technology Publishing House.

31. Yoon, I.-N., Lee, Y., Kang, D., Min, J., Won, J., Kim, M., Soo Kang, Y., Kim, S., & Kim, J.-J. (2011). Modification of hydrogenated Bisphenol A epoxy adhesives using nanomaterials. International Journal of Adhesion and Adhesives, 31(2), 119–125.

32. Zebarjad, S.M., & Sajjadi, S.A. (2008). On the strain rate sensitivity of HDPE/CaCO3 nanocomposites. Materials Science and Engineering: A, 475(1–2), 365–367.

Original Research

MODULAR INJECTION MOULD WITH A CONFORMAL COOLING CHANNEL FOR THE PRODUCTION OF HYDRAULIC FILTER HOUSINGS

MODUŁOWA FORMA WTRYSKOWA Z CHŁODZENIEM KONFORMALNYM DO WYTWARZANIA TYPOSZEREGU OBUDÓW FILTRÓW HYDRAULICZNYCH

Tomasz SAMBORSKI*[1] , Andrzej ZACHARSKI[2] , Przemysław POSZWA[3] Andrzej ZBROWSKI[4] , Stanisław KOZIOŁ[5]

[1] Łukasiewicz Research Network – Institute for Sustainable Technologies, ul. K. Pułaskiego 6/10, 26-600 Radom, Poland, e-mail: tomasz.samborski@itee.lukasiewicz.gov.pl, t.: 48 3649232.

[2] Łukasiewicz Research Network – Institute for Sustainable Technologies, ul. K. Pułaskiego 6/10, 26-600 Radom, Poland, e-mail: andrzej.zacharski@itee.lukasiewicz.gov.pl, t.: 48 3649359.

[3] PROCAD S.A., ul. Kartuska 215, 80-122 Gdańsk, Poland, e-mail: przemyslaw.poszwa@procad.pl

[4] Łukasiewicz Research Network – Institute for Sustainable Technologies, ul. K. Pułaskiego 6/10, 26-600 Radom, Poland, e-mail: andrzej.zbrowski@itee.lukasiewicz.gov.pl, t.: 48 3649306.

[5] Łukasiewicz Research Network – Institute for Sustainable Technologies, ul. K. Pułaskiego 6/10, 26-600 Radom, Poland, e-mail: stanislaw.koziol@itee.lukasiewicz.gov.pl, t.: 48 3649290.

* Corresponding author: tomasz.samborski@itee.lukasiewicz.gov.pl, t.: 48 3649232

Abstract

The article presents the idea, design, construction, and implementation of a production technology for hydraulic filter housings using a modular injection mould. The annual demand for filters for specialised marine hydraulics systems by HYDROMEGA averages about 1,000 pieces. Two sizes of filters with the same housing connection dimensions are used. Due to the small scale of production, the modular injection mould was designed and manufactured to press two types of a polyamide housing. Changing the shape of a moulded part requires removing or installing modules that change the die and punch dimensions, which reduces the costs of production of a single tool compared to the costs of production of two separate tools. The mould design process was supported by the numerical analyses of operation and processes of plastic injection, cooling, moulded part shrinkage, and mould cavity deaeration. A mould and a series of moulded parts were manufactured and verified positively for dimensions and durability.

Keywords: injection mould, moulded part, modular mould, mould cooling

Streszczenie

W publikacji opisano koncepcję, proces projektowania, budowę i wynik wdrożenia technologii wytwarzania typoszeregu obudów filtrów hydraulicznych z zastosowaniem modułowej formy wtryskowej. Zapotrzebowanie na filtry do specjalistycznych systemów hydrauliki siłowej wykorzystywanych w gospodarce morskiej, budowanych przez firmę HYDROMEGA, wynosi do 1000 szt./rok. Stosowane są filtry w dwóch rozmiarach o takich samych wymiarach przyłączeniowych obudowy do pozostałych elementów instalacji. Ze względu na niewielką skalę produkcji zaprojektowano i wykonano modułową formę wtryskową do prasowania dwóch rodzajów obudowy z poliamidu. Zmiana kształtu wypraski wymaga usunięcia lub zainstalowania modułów zmieniających wymiary matrycy i stempla, co zmniejsza koszt wykonania oprzyrządowania w porównaniu z budową dwóch osobnych przyrządów. Projektowanie formy było wspomagane analizami numerycznymi działania oraz procesów wtrysku tworzywa, chłodzenia, skurczu wypraski i odpowietrzenia gniazda formującego. Wykonano formę i wyprodukowano serię wyprasek, które przeszły kontrolę wymiarową i wytrzymałościową z wynikiem pozytywnym.

Słowa kluczowe: forma wtryskowa, wypraska, forma modułowa, chłodzenie formy

1. Introduction

Plastic injection moulding technology is commonly used to manufacture everyday products, toys, household appliances, medical devices, and machine parts. The combination of excellent material properties of modern plastics and composites (including good mechanical and sliding properties, lower density, good corrosion and chemical resistance) with the development of processing methods means that plastic parts are increasingly replacing expensive and labour-intensive metal parts. Compared to moulded metal parts which require labour-intensive machining, complex moulded parts with high dimensional accuracy and good condition of the surface can be obtained with well-planned part manufacturing processes and properly designed instruments. The decision to apply the injection moulding technology is made based on a financial calculation, in which the design and manufacture of special manufacturing equipment, i.e. an injection mould, constitutes a high cost. This means that the technology is most economically viable particularly in the case of batch and flow production. Another way to make the manufacturing process more cost-effective is to maximise performance by using multiple moulds and shorten the cycle time (i.e. the time of mould filling and moulded part cooling, with the latter accounting for up to 80% of the total cycle time). However, it must be remembered that the cycle time may not be shortened at random, as the mould cooling rate critically impacts on the product's dimensional accuracy stability,

residual stresses (in the plastic and in the components of the mould), and on the product's surface quality and smoothness (Sołtysik & Moczała, 2020; Wang et al., 2023) The design of the cooling circuit and its distance relative to the mould cavity have a great impact on the efficiency of mould cooling and on the course of the heat transfer from the moulded part (Arman & Lazoglu, 2023; Hassan et al., 2010; Muszyński et al., 2016.) Moulds intended for the manufacture of parts of products with complex shapes in which the circulation of the coolant through drilled channels does not ensure even cooling of the moulded part are particularly problematic. The development of 3D printing technology, namely selective laser melting technology (Strzelec, 2020), allows the design and manufacture of mould components with optimised cooling channels adjusted to the shape of the moulding surfaces (Dimla & Miani 2005; Gotlih et al., 2023; Kazmer 2007; Strzelec 2020) On the other hand, computer-aided design tools enable the development of spatial models of products and moulds used for their manufacture, as well as simulation of the processes of mould filling with plastic (Heneczkowski, 2016) and heat flow at each stage of the production cycle. A special modular injection mould for batch production of oil filter housings used in large hydraulics systems was designed and developed at the Łukasiewicz – Institute for Sustainable Technologies. The work involved the development and implementation of a new polyamide filter housing to replace costly housings made of aluminium alloys.
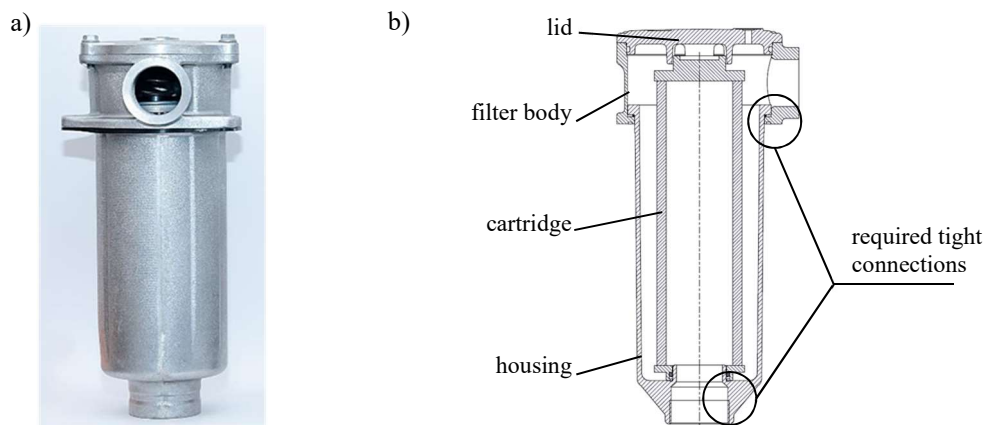
Fig. 1. Oil filter: a) with an aluminium housing; b) with a housing made of pressed polyamide

Figure 1 presents an image of a filter with a housing made of cast aluminium alloy and a technical drawing of a filter with a housing made of pressed plastic. Both filters (Figure 1) have the same structure and contain identical filter cartridges. However, they differ in terms of shape and the material of which the

housing is made. Due to the conditions in which the hydraulics system operates, the housing must meet the following technical requirements: the working pressure of the hydraulic agent – 0.2 MPa; the maximum non-destructive pressure – 1 MPa; and the operating temperature between -25ºC and +80ºC. The

requirements concerning the dimensional accuracy of the moulded part stem from the necessity to ensure connection between the filter housing and the body, and between the body and the cartridge (Figure 1b). The type of the plastic to be used (PA6 polyamide) was agreed and the technical documentation of the finished product was developed in consultation with the industrial client (HYDROMEGA, a Polish company based in Gdynia). The authors assumed that the design of the instrumentation would allow easy modification of the height of the moulded part, and thus enable the production of two sizes of housings (RF100 and RF150), without the need to build two separate injection moulds.

The PA6 polyamide[1] has high tensile strength and stiffness at high temperature, good resistance to hydrocarbons, high humidity absorption, moulding shrinkage of approximately 2%, very good flow properties in a liquid state, and a high solidification rate during injection moulding. The thickness of the moulded part walls of minimum 6 mm, resulting from the strength requirements, and the large weight of about 1,350 g called for an in-depth analysis of thermal

processes occurring at the time of pressing and for a proper design of the mould cooling system [10], and efficiently cooled to achieve favourable production cycle time.

2. Calculations and mould design

In the design of the mould, the capabilities of modelling the structure and simulating thermal and flow processes in a virtual environment (Jaskulski, 2020; Zbrowski et al., 2012; Zbrowski et al. 2012) were used to the greatest extent possible, to eliminate costly and labour-intensive modifications and corrections at the test run stage. The authors used Autodesk INVENTOR Professional to build a 3D model of the injection mould (Figure 2), which is composed of a punch and die with replaceable modules that can be removed from the mould to change the shape of the moulded part. The bigger RF150 filter housing is pressed in the fully configured mould (Figure 2a) and the smaller RF100 filter housing – after the replaceable modules have been removed (Figure 2b).
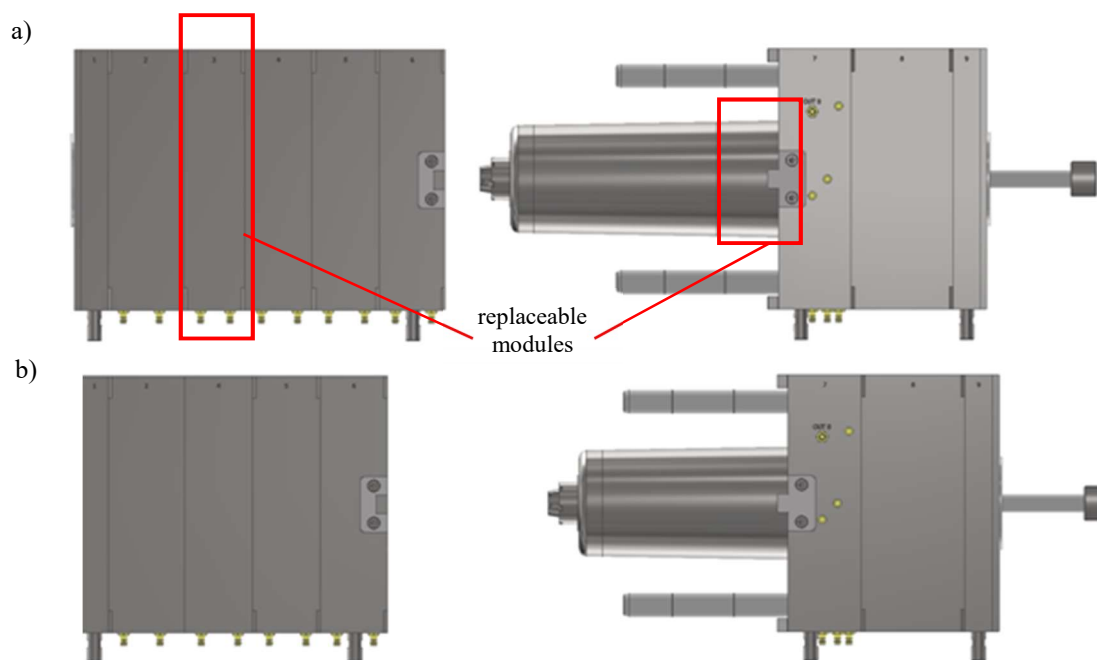
Fig. 2. 3D model of the modular mould: a) configuration used to make RF150 filter housings; b) configuration used to make RF100 filter housings

In the mould, a conformal cooling system with cooling channels evenly distributed near the moulding cavity of the die and outer surface of the punch was used (Figure 3).

The design of such a cooling system, using classic processing methods, was facilitated by the axisymmetric shape of the moulded part and the modular structure of the mould. In the case of the punch,

---

[1] Grupa Azoty, Tarnamid T-27 MCS 850 Poliamid 6 (PA6) – product data sheet

removing the replaceable modules (Figure 2) in no way modifies cooling channels, and in the case of the die, the removed module has its own cooling circuit

connected separately to the chiller. Such a system ensures even cooling of the moulded part and effective control of the heat transfer process.
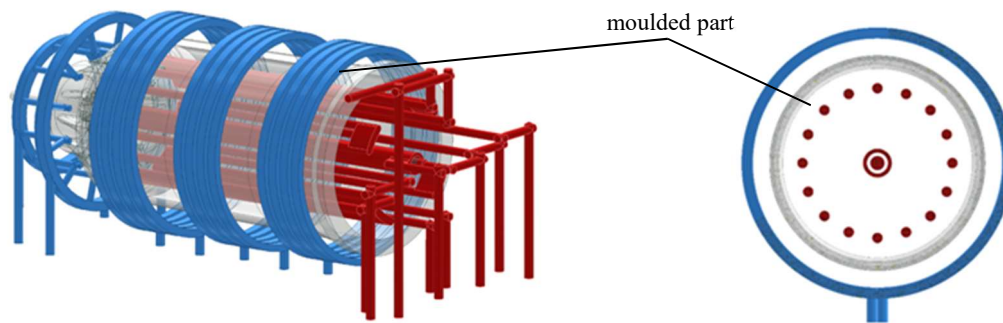

Fig. 3. 3D model of mould cooling: blue – cooling of the die; red – cooling of the punch

Numerical calculations of the injection moulding process of the designed product were done in Autodesk Moldflow Insight Ultimate 2021.2, which is based on the finite element method and allowed simulation of the cavity filling process, to obtain information about pressure and temperature distribution in the injection mould, and deformation of the injection moulded parts. The simulations were carried out for a 3D mesh of the housing. They included the filling, pressing, and cooling phases as well as the determination of the deformation of the moulded part as a result of the anisotropic plastic shrinkage. All calculations were made for PA6, Tarnamid T27.

Given the conformal cooling system used in the mould, a 3D cooling simulation module was required (Frenkler & Zawistowski, 1984; Jaskulski, 2020). It differs from the basic module in that it uses a 3D mesh instead of 1D beams to represent cooling channels, which allows the study of more complex flows. The 3D model of the injection mould contained 5.8 million tetrahedral elements, the cooling system – 2.2 million, and the moulded part – 0.8 million. The analysis of the injection mould cooling assumed averaging the mould temperature distribution during the cycle. The software used Fourier equation to determine the temperature distribution in the injection mould. On the other hand, the filling of the cavity using a 3D mesh as well as the injection mould cooling process using the conformal module were based on a Navier-Stokes equation.

Simulations were carried out for the following carefully calculated parameters:
- the temperature of the plastic: 270°C;
- the mould opening time: 5 s;
- the full cycle time (injection, packing, cooling): 90 s;

- the cavity filling time (calculated automatically): 8 s;
- the V/P-switch over (based on the value of pressure changes in the cavity, the algorithm automatically determines when to switch from the injection phase to the pressing phase in order to avoid a drastic pressure change as a result of uneven filling of the cavity): 99.9%;
- the packing profile: 80% of the maximum injection pressure for 10 s.

Figure 4 presents the result of the cavity filling simulation. The simulation showed the order in which the mould was filled and allowed the prediction of the filling time and evaluation of the correctness of the design of the channels through which the plastic is injected. The resulting mould filling time met the requirements of the adopted technological cycle. Figure 5 presents the result of the simulation of the coolant temperature distribution in individual circuits intended to transfer heat from the mould. The simulation allowed the assessment of the effectiveness and evenness of the moulded part cooling. The resulting coolant temperature distribution, the values of which were similar for each section, indicates the correct selection of cooling channel geometry and fluid flows. Figure 6 presents the plastic temperature distribution at the time of injection. The simulation enabled the identification of areas in which the temperature of the plastic could significantly increase as a result of, among other things, air compression in the closed parts of the mould cavity separated at the time of injection. The detection of such areas through simulation enabled the authors to introduce at the design stage channels to remove air from the mould during the plastic injection.
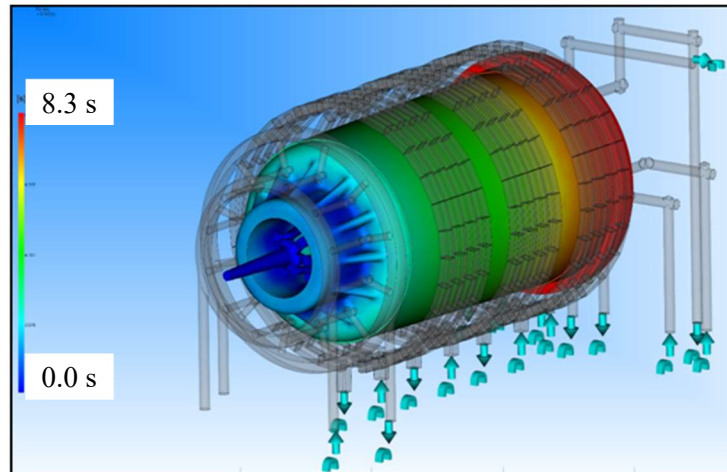
Fig. 4. Simulation of mould cavity filling as a function of time
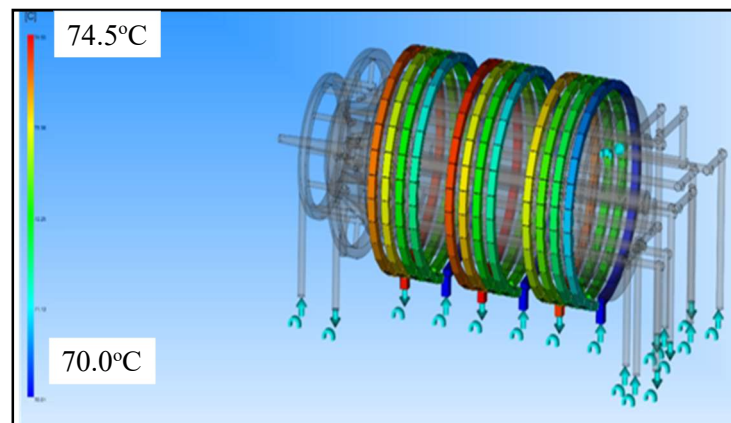
Fig. 5. Simulation of the cooling liquid temperature distribution in individual sections of the die
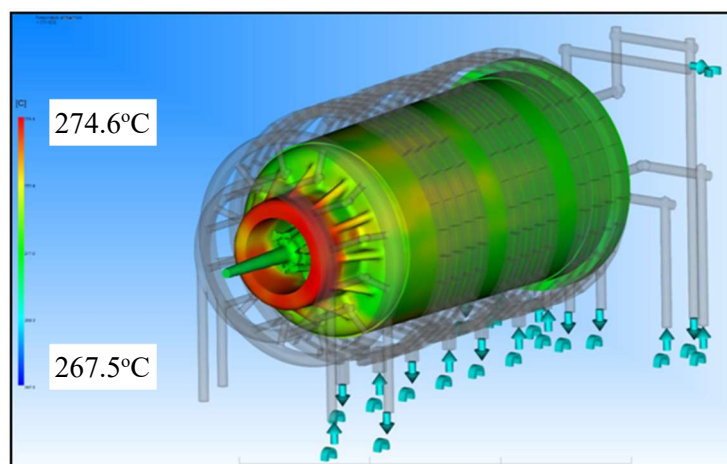
Fig. 6. Simulation of the plastic temperature distribution during the injection phase

Based on the results of calculations and numerical simulations presented in Figures 4, 5, and 6, the authors developed the technical documentation of the mould. All structural solutions were provisionally verified in the form of virtual 3D models, kinematic simulations, and on the basis of the thermal and flow processes during mould operation.

3. Manufacture of the injection mould and analysis of the pressing of the housing

The housing (Figure 7) was made based on the developed design documentation. The injection mould elements were made of dispersion-strengthened M261 BÖHLER (X13NiCuAlS4-1-1)[2] steel intended for such applications. The structural elements of the mould were made of tempered 40CrMnMoS86[3] steel supplied by FCPK Bytów in the form of finished machined semi-finished plates (Feldhausen et al., 2023). Additionally, typical structural elements (pillars, bushings, and locks) offered by FCPK Bytów were also used. The total weight of the mould amounted to 723 kg. In the housing there are areas which require a high degree of manufacturing precision, and which are important for the installation of the housing in the metal filter body and for the tightness of the hydraulic connections. Moulding surfaces were intentionally cut oversize to allow for dimensional changes after the verification of the dimensions of moulded parts and actual part shrinkage.
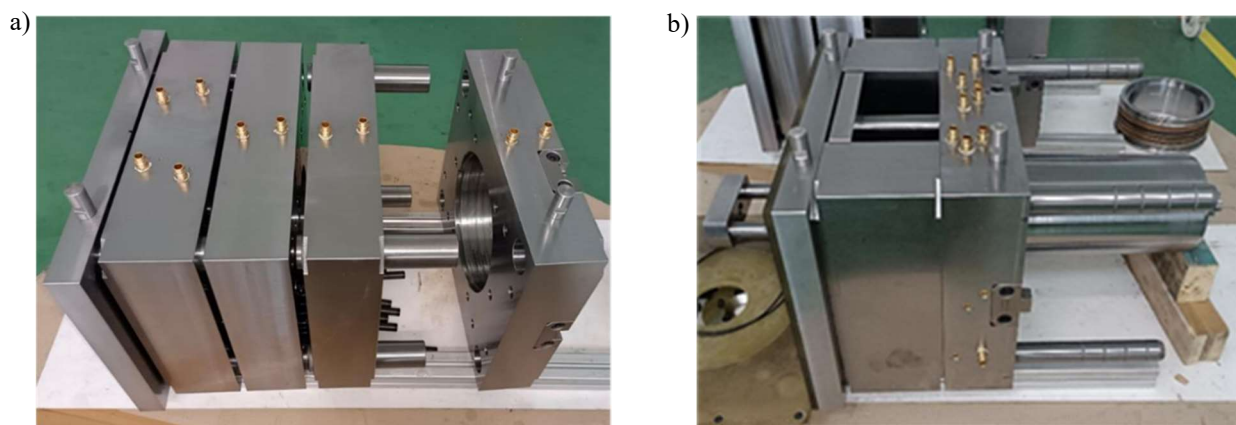
Fig. 7. Modular injection mould with a conformal cooling channel for the production of hydraulic filter housings: a) die (during assembly); b) punch

The technological performance tests of the mould involved producing a batch of several dozen of RF100 and RF150 filter housings. A TEDERIC TRX-650/8730 moulding machine was used for testing. During tests, the parameters of the injection moulding process (Table 1) were defined to achieve properly shaped and sized products. Images presented in Figure 8 show an example of a properly moulded part with visible directions of the plastic flow.

Table 1. Plastic injection parameters in the process of housing pressing

Parameter name	Calculated (assumed) values	Real values determined during tests	Unit
Injection temperature	251.1	250–270	[ºC]
Injection time	7.198	5	[s]
Cycle time	81.96	90	[s]
Injection pressure	131.66	160	[bar]
Clamp force (moulded part)	410	5,000	[kN]
Clamp force (mould)	3,140		
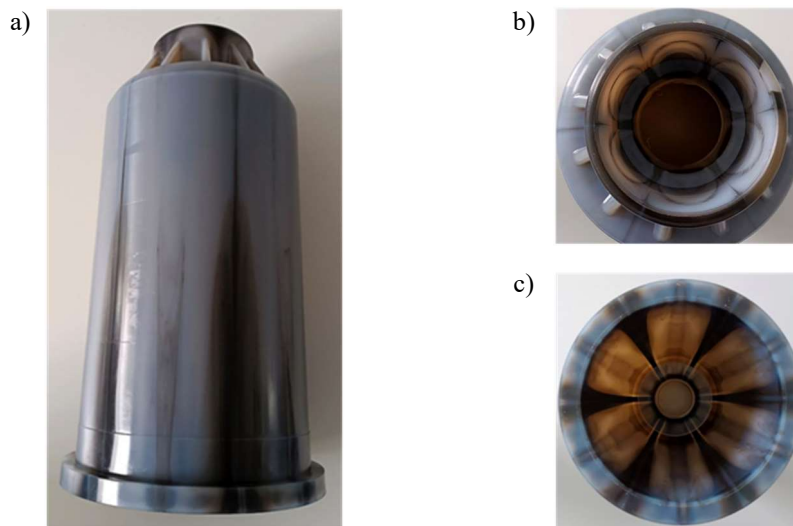
Fig. 8. Moulded filter housing: a) side view; b) external view, and c) internal view
(plastic flow directions visible)

T27 polyamide[4] has high humidity absorption (2.5–2.8%) impacting on the dimensions of the product – they increase when humidity is absorbed. To prevent uncontrolled and long-term humidity absorption, once removed from the mould, moulded parts are immediately dipped in a hot water bath (60–80ºC) for 1–2 h. They achieve the desired stable end shape after 24 hours. The trial batch of moulded parts made as described above was verified for dimensional accuracy (Table 2). The authors also calculated the real total plastic shrinkage value, which averaged between 0.9% and 1.14%, with the value declared by the manufacturer between 1.0% and 3.0%.

Table 2. Results of the dimensional inspection of a batch of 30 moulded parts

Dimension	Requirements			Dimensions of moulded parts		
	Nominal [mm]	Deviations [mm]		Minimum [mm]	Maximum [mm]	Average [mm]
Moulded part height	325	-1.8	0.0	323.63	324.96	324.65
Mounting diameter of the housing	165	-0.9	-0.2	164.22	164.82	164.35
Hydraulic seal diameter	68	-0.3	0.3	67.74	68.23	67.78

During technological performance tests, two dimensions of the moulded parts (i.e. diameters given in Table 2) were found to be outside the dimensional tolerance. To eliminate this problem and to adapt the shape to the dimensional requirements, the excess material was removed. The authors also found thermal discolouration ("burns") on the bottom surface of the moulded parts resulting from the insufficient deaeration of the cavity closed by the injected plastic. Additional deaeration channels were made on the contact surface of the end die modules.

Strength tests were performed on the manufactured filter housings and they involved the application of internal pressure to the hydraulic connection of a complete hydraulic filter. Pressure was applied to the inlet connection of the filter, with the outlet connection covered. During the test, pressure equal to the maximum working pressure (2 bar) and to the maximum non-destructive pressure (10 bar) was applied and the value of the destructive pressure was examined. The destructive load averaged 30 bar and its application resulted in the destruction of the aluminium body and lid of the filter (Figure 9). The described technological solution is now used for batch production of housings of filters by HYDROMEGA.

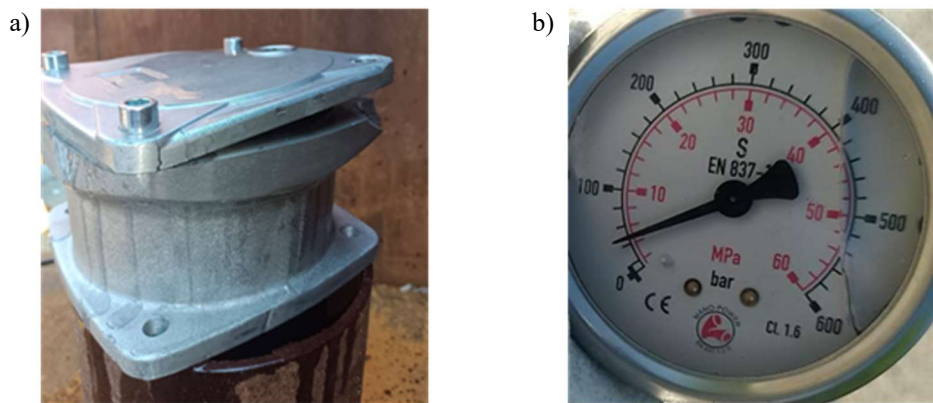[4] Grupa Azoty, Tarnamid T-27 MCS 850 Poliamid 6 (PA6) – product data sheet.

Fig. 9. Result of the pressure destructive test of the filter housing: a) image of the destruction of the housing, b) recorded value of the destructive pressure

4. Summary

The modular injection mould for the production of two types of large hydraulic filter housings was designed and developed at the Łukasiewicz – Institute for Sustainable Technologies in Radom, Poland. Changing the shape of the moulded part required removing or installing a replaceable structural module, which reduced the cost of manufacture and enabled cost-effective batch production. The mould uses a conformal cooling system that streamlines the heat transfer process and enables repetitive production of accurately shaped and sized polyamide moulded parts. In the mould design process, all available capabilities of structural modelling and simulation of thermal and flow processes in a virtual environment were used to eliminate costly and time-consuming corrections at the implementation stage. The design methodology used allowed direct and efficient implementation of the mould after the introduction of the planned adjustments to the moulding elements in compliance with tight dimensional requirements. The described technological solution is now used for batch production of housings of hydraulic filters by HYDROMEGA, a Gdynia-based company that commissioned the work described in the article.

References

1. Arman, S., Lazoglu, I. 2023. A comprehensive review of injection mold cooling by using conformal cooling channels and thermally enhanced molds. Int J Adv Manuf Technol 127, 2035–2106.

2. Dimla E., Miani F. 2005. Design and optimisation of conformal cooling channels in injection moulding tools. Journal of Materials Processing Technology (164–165): 1294–1300.

3. Feldhausen T., Paramanathan M., Heineman J., Hassen A., Heinrich L., Kurfess R., Fillingim K., Saleeby K., Post B. 2023. Hybrid Manufacturing of Conformal Cooling Channels for Tooling. Manufacturing Science Division, Oak Ridge National Laboratory, Knoxville, USA.

4. Gotlih J., Karner T., Belšak R., Ficko M., Berus L., Brajlih T., Pal S., Brezočnik M.. 2023. Design and Manufacturing of Conformal Cooling Channels for Injection Molding: A Review. New Technologies, Development and Application VI. NT 2023. Lecture Notes in Networks and Systems, vol 687. Springer, Cham.

5. Hassan H., Regnier N., Le Bot C., Defaye G. 2010. 3D study of cooling system effect on the heat transfer during polymer injection molding. International Journal of Thermal Sciences (49): 161–169.

6. Heneczkowski M. 2016. Symulacja wpływu parametrów wtrysku na jakość wyprasek w programie Autodesk Moldflow Insight. Mechanik, (4): 252–255.

7. Jaskulski A. 2020. Autodesk Inventor Professional. Helion.

8. Kazmer D. O. 2007. Injection Mold Desing Engineering. Monachium: Hanser.

9. Muszyński P., Mrozek K., Poszwa P. 2016. Wybrane metody chłodzenia form wtryskowych. Mechanik, (8–9): 996–1000.

10. Rosato D.V., Rosato M.G. 2000. Injection Molding Handbook. Nowy Jork: Springer Science+Business Media.

11. Sołtysik M., Moczała A. 2020. Rozwój sposobów chłodzenia form wtryskowych. Tworzywa Sztuczne w Przemyśle, (1): 14–18.

12. Strzelec S. 2020. Utrzymanie form wtryskowych z chłodzeniem konformalnym wykonanych w technologii druku 3D. Mysłowice: Voestalpine.

13. Strzelec S. 2020. Druk 3D w narzędziach wg voestalpine High Performance Metals. Mysłowice: Voestalpine.

14. Wang M. L., Zheng L. J., Bae S., Kang H.W. 2023. Comprehensive performance enhancement of conformal cooling process using thermal-load-based topology optimization. Applied Thermal Engineering.

15. Zawistowski H., Frenkler D. 1984. Konstrukcja form wtryskowych do tworzyw termoplastycznych. Warszawa: WNT.

16. Zbrowski A., Kozioł S., Kosowska P. 2012. Zastosowanie metod CFD w projektowaniu przepływowej komory kalorymetrycznej symulującej warunki klimatu wewnętrznego w budynku mieszkalnym. Energetyka, (XXIV): 64–67.

17. Zbrowski A., Kozioł S., Wojnar K. 2012. Zastosowanie metod CFD w projektowaniu przepływowej komory kalorymetrycznej symulującej zimowe warunki klimatyczne. Energetyka, (XXIV): 67-70.

DOCUMENT CREATED WITH

PDF COMBINER